Cleaner Engineering and Technology 24 (2025) 100891

Contents lists available at ScienceDirect

Cleaner Engineering and Technology

journal homepage: www.sciencedirect.com/journal/cleaner-engineering-and-technology

Soft computing approaches of direct torque control for DFIM Motor's

Zakariae Sakhri [a,**], El-Houssine Bekkour [a,f], Badre Bossoufi [a,*], Nicu Bizon [b], Mishari Metab Almalki [c], Thamer A.H. Alghamdi [d,e], Mohammed Alenezi [d,***]

[a] Laboratory of Engineering Modeling and Systems Analysis, SMBA University Fez, Morocco
[b] Faculty of Electronics, Communication and Computers, University of Pitesti, 110040, Pitesti, Romania
[c] Department of Electrical Engineering, Faculty of Engineering, Al-Baha University, Alaqiq, 65779-7738, Saudi Arabia
[d] Wolfson Centre for Magnetics, School of Engineering, Cardiff University, Cardiff, CF24 3AA, UK
[e] Electrical Engineering Department, Faculty of Engineering, Al-Baha University, Al-Baha, 65779, Saudi Arabia
[f] SMARTiLab, Moroccan School of Engineering Sciences (EMSI), Rabat, Morocco

ARTICLE INFO

Keywords:
DFIM
DTC
DTC-SVM
DTC-FL
DTC-ANN
DTC-GA
DTC-ACO
DTC-RTO DTC-SMC and P-DTC

ABSTRACT

Conventional Direct Torque Control (DTC) is widely used for torque and speed control in doubly-fed induction machines (DFIM). However, it has notable drawbacks, including high torque and flux ripples, which generate acoustic noise and reduce system performance. To address these limitations, several advanced approaches have emerged. This article provides a critical analysis of the following cutting-edge methods: DTC with Space Vector Modulation (DTC-SVM), DTC based on Fuzzy Logic (DTC-FL), DTC using Artificial Neural Networks (DTC-ANN), DTC optimized by Genetic Algorithms (DTC-GA), DTC with Ant Colony Optimization (DTC-ACO), DTC with rooted tree optimization (DTC-RTO), Sliding Mode Control (DTC-SMC), and Predictive DTC (P-DTC). Our evaluation focuses on various aspects: torque and flux ripple reduction, speed tracking improvement, switching losses minimization, algorithmic complexity simplification, and sensitivity reduction to parameter variations. Results show that DTC-ANN and DTC-SVM stand out for their ripple reduction performance, making them particularly suitable for applications requiring high precision. Additionally, DTC-FL and DTC-SMC excel in robustness against system parameter variations, a valuable asset for evolving industrial environments. Optimization approaches such as DTC-GA, DTC-ACO, and DTC-RTO contribute to reducing switching losses and improving energy efficiency, a crucial aspect for large-scale applications. Finally, P-DTC offers excellent dynamics and precise speed tracking, making it ideal for rapid response systems. These findings provide valuable insights for researchers and engineers seeking to optimize modern DTC system performance according to the specific needs of their applications.

1. Introduction

The origins of electric motors can be traced back to 1820, when Hans Christian Oersted made the groundbreaking discovery that electric currents create magnetic fields. This discovery set the stage for Michael Faraday's experiments in 1821, where he demonstrated electromagnetic rotation, the principle behind the first primitive direct current (DC) motor. Faraday's exploration continued, leading to his pivotal discovery of electromagnetic induction in 1831, which further spurred the development of electric motors (A review on Direct Torque, 2024). A significant advancement occurred in 1883 when Nikola Tesla developed the asynchronous alternating current (AC) motor, which represented a major milestone in motor technology. Today, the core types of electric motors, direct current (DC), asynchronous alternating current (AC), and synchronous, are still grounded in the foundational theories put forth by Oersted, Faraday, and Tesla more than a century ago. Among these, asynchronous machines, commonly known as induction motors, are particularly favored in industrial applications. Their popularity stems from several advantages: cost-effectiveness, robust construction, simplicity, and minimal maintenance needs. However, these motors necessitate more sophisticated internal structures and control mechanisms (A review on Direct Torque, 2024), (Herizi et al., 2023).

* Corresponding author.
** Corresponding author.
*** Corresponding author.
E-mail addresses: zakariae.sakhri@usmba.ac.ma (Z. Sakhri), badre.bossoufi@usmba.ac.ma (B. Bossoufi), AleneziM1@cardiff.ac.uk (M. Alenezi).

https://doi.org/10.1016/j.clet.2025.100891
Received 16 September 2024; Received in revised form 6 January 2025; Accepted 14 January 2025
Available online 22 January 2025

The Dual-Fed Induction Motor (DFIM) represents an evolution of the traditional induction motor. It is an asynchronous motor with a unique configuration where both the rotor and stator are supplied with alternating current, allowing for enhanced control and efficiency. The DFIM has gained attention due to significant strides in power electronics and innovative control strategies, making it a strong contender in high-power, variable-speed drive applications. One of the standout features of DFIMs is their capability to operate effectively at lower speeds. Moreover, these motors can be integrated with various control techniques and static converters, providing a flexible and dynamic response to changing load conditions. This adaptability, combined with the ability to maintain a constant frequency supply to the stator despite speed variations, positions DFIMs as a viable alternative to conventional synchronous machines in many modern electric drive systems (Herizi et al., 2023).

New developments in signal processing techniques opened the door to more sophisticated control structures in the mid-1980s. Proposed by Takahashi, Noguchi (Takahashi and Noguchi, 1986), and Depenbrock (1988), the term DTC (direct torque control) refers to the most recent developments made in this regard. The use of a hysteresis comparator offsets the benefits of the DTC approach, which include good dynamics, resilience, low sensitivity to parameter fluctuations, ease of implementation, and high performance. A pseudo-random overshoot of the hysteresis band is caused by the finite sampling frequency and, in theory, the comparator may lead to variable frequency operation (Krieger and Salmon, 2005). Consequently, the motor's behavior may be impacted by low-speed operation and changes in motor resistance. It is challenging to forecast the different output signals' harmonic composition (Fig. 1) (see Fig. 2).

Nevertheless, the DTC is associated with a number of significant drawbacks.

(a) The application of hysteresis controllers results in the generation of high flux and electromagnetic torque ripples, which in turn give rise to the production of unwanted mechanical vibrations and acoustic noises (Mahfoud et al., 2021a).
(b) Furthermore, the output power's quality is also negatively affected by switching losses and current distortions brought on by the changing switching frequency.
(c) Failure to account for the stator resistance can result in issues at low speeds.

Moreover, the Dual-Fed Induction Motor (DFIM) experiences torque oscillations when a traditional direct torque control (DTC) is applied. These oscillations can trigger mechanical resonances, which can result in vibrations and audible noise and premature machine aging (Comparison of the error; Direct torque control versus indirect).

Several approaches have been proposed to minimize the ripples and preserve a steady frequency. One such strategy is.

1. SVM based DTC

A Dual-Fed Induction Motor's enhanced direct torque control (DTC) technique employing space vector modulation (SVM) is presented in this study (Mahfoud et al., 2021a). The goal of the SVM-based control system is to replace hysteresis controllers with PI controllers in order to enhance DTC performance. With this replacement, the advantages of DTC control are maintained while reducing electro-magnetic flux and torque ripple, which minimizes mechanical vibration and acoustic noise.

2. DTC-PC

This article introduces a new innovative predictive direct torque control (DTC) technique for the Dual-Fed Induction Motor (DFIM) that is intended to run at a low switching frequency continuously is presented in this study (Venu Madhav et al., 2021). Even in variable-speed operating settings, the suggested DTC approach efficiently lowers torque and flux ripples at low switching frequencies. The study evaluates the suggested predictive DTC strategy's performance against the traditional DTC approach in a range of operating scenarios, including as step changes, continuous torque command variation, and DFIM performance close to synchronous speed. The findings demonstrate that, in comparison to the traditional DTC idea, the predictive DTC technique demonstrates superior dynamic responsiveness.

3. SMC based DTC

The outcomes demonstrate that the traditional DTC-Integral-Proportional approach is outperformed by the DTC-SMC (Direct Torque, 2024). The DTC-SMC exhibits a very quick torque response time, no steady-state error, and no overshoot. (Bekakra et al., 2018).

4. AI based DTC

At present, a great deal of research is devoted to solving these problems. Artificial intelligence (AI) has emerged as a crucial term in modern research fields. The main families of AI include fuzzy logic, neural networks, rooted tree optimization algorithms, ant colony optimization algorithms, and genetic algorithms. The authors of (Bekakra et al., 2018), (Bekakra et al., 2021a), (El Ouanjli et al., 2019a),

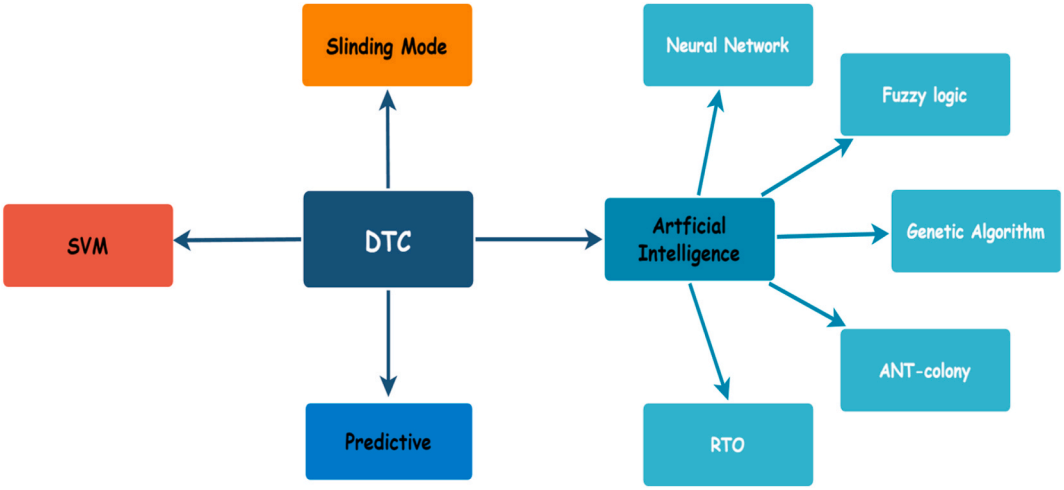

Fig. 1. Classification of DTC schemes for DFIM.

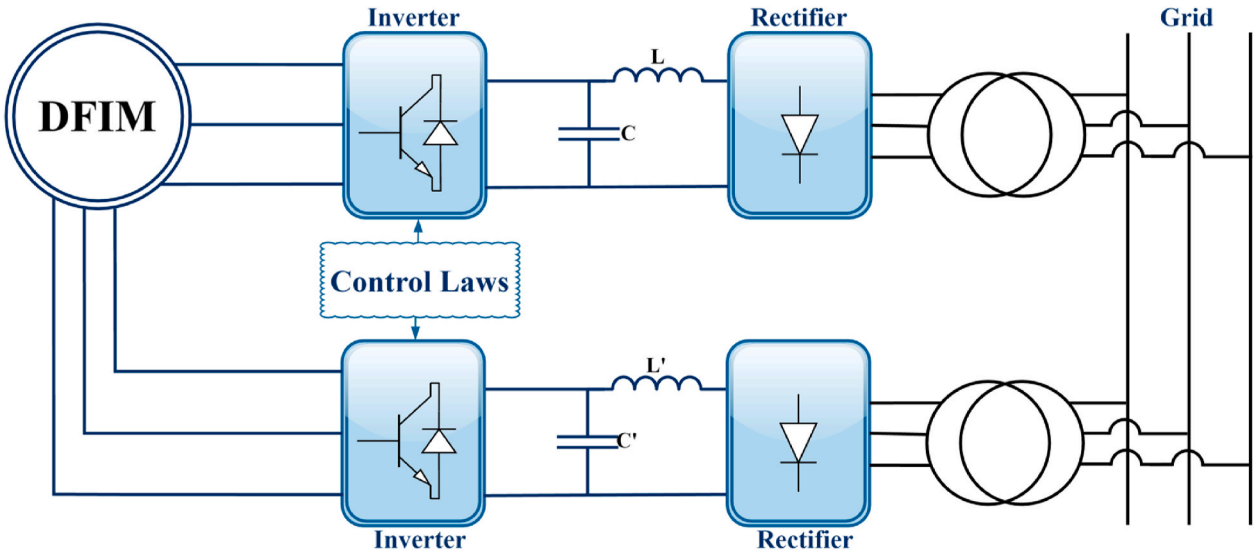

Fig. 2. Overview of DFIM drive System installation.

(Mahfoud et al., 2022a), and (Mahfoud et al., 2022b)recommend using AI methods to enhance DTC control's dynamic performance for DFIM. These control strategies seek to maximize performance in a range of operating environments, encompassing reduced torque and flux ripple, decreased THD, increased efficiency, and reduced energy consumption. The findings will be shown in the section that follows.

Many publications that examine DTC methods for dual-fed induction motor drives are available in the literature; however, these schemes are not subjected to a rigorous assessment. In addition to working on new research directions, the goal is to provide researchers with an understanding about the current state of the DTC method (Table 1).

2. Dual-fed induction motor (DFIM)

The power supply for the DFIM utilizes a chain of energy conversion with two converters, one on the stator and another on the rotor, as illustrated in **Erreur ! Source du renvoi introuvable.** A filter is positioned between the two converters (Cherifi and Miloud, 2018).

1. Model of the DFIM

The general equations of the double-fed induction motor in the three-phase reference frame are as follows (Bakou et al., 2019).

2.1. Electrical equations

By applying Faraday's law to each winding, we can write:

$$\begin{cases} [v_s] = [R_s].[i_s] + \dfrac{d\psi_s}{dt} \\ [v_r] = [R_r].[i_r] + \dfrac{d\psi_r}{dt} \end{cases} \quad (1)$$

2.2. Magnetic equations

Now, some of the assumptions made here are such that the relations of flux and currents are linear: in matrix form, they are thus expressed:

$$\begin{cases} [\psi_s] = [L_{ss}][i_s] + [M_{sr}][i_r] \\ [\psi_r] = [M_{rs}][i_s] + [L_{rr}][i_r] \end{cases} \quad (2)$$

the four inductor matrices are:

$$[L_{ss}] = \begin{bmatrix} L_s & M_s & M_s \\ M_s & L_s & M_s \\ M_s & M_s & L_s \end{bmatrix} \quad (3)$$

$$[L_{rr}] = \begin{bmatrix} L_r & M_r & M_r \\ M_r & L_r & M_r \\ M_r & M_r & L_r \end{bmatrix} \quad (4)$$

$$[M_{sr}] = [M_{rs}]^T = M \begin{bmatrix} \cos\theta & \cos\left(\theta + \frac{2\pi}{3}\right) & \cos\left(\theta - \frac{2\pi}{3}\right) \\ \cos\left(\theta - \frac{2\pi}{3}\right) & \cos\theta & \cos\left(\theta + \frac{2\pi}{3}\right) \\ \cos\left(\theta + \frac{2\pi}{3}\right) & \cos\left(\theta - \frac{2\pi}{3}\right) & \cos\theta \end{bmatrix} \quad (5)$$

2. Representation of the DFIM in two-phase reference frame $(\boldsymbol{\alpha},\boldsymbol{\beta})$

The two-phase model represented by the reference (α,β) is the most suitable model to examine the dynamic behavior and the control algorithm design of the DFIM. The machine's three-phase representation (a, b, and c) is made less difficult by this paradigm. In the reference frame (α, β), the electromagnetic equations of the DFIM are provided by (Mahfoud et al., 2021a), (Moussaoui et al., 2021), (El Ouanjli et al., 2017b), (Mahfoud et al., 2022h):

2.3. Electrical equations in αβ frame

The following equations express the stator and rotor voltages in the frame $\alpha\beta$:

$$\begin{cases} v_{s\alpha} = R_s.i_{s\alpha} + \dfrac{d\psi_{s\alpha}}{dt} \\ v_{s\beta} = R_s.i_{s\beta} + \dfrac{d\psi_{s\beta}}{dt} \\ v_{r\alpha} = R_r.i_{r\alpha} + \dfrac{d\psi_{r\alpha}}{dt} + \omega_m.\psi_{r\beta} \\ v_{r\beta} = R_r.i_{r\beta} + \dfrac{d\psi_{r\beta}}{dt} - \omega_m.\psi_{r\alpha} \end{cases} \quad (6)$$

With:

$$\omega_m = \omega_s - \omega_r \tag{7}$$

2.4. Magnetic equations in αβ frame

The fluxes of the rotor and stator are provided by:

$$\begin{cases} \psi_{s\alpha} = L_s.i_{s\alpha} + L_m.i_{r\alpha} \\ \psi_{s\beta} = L_s.i_{s\beta} + L_m.i_{r\beta} \\ \psi_{r\alpha} = L_r.i_{r\alpha} + L_m.i_{s\alpha} \\ \psi_{r\beta} = L_r.i_{r\beta} + L_m.i_{s\beta} \end{cases} \tag{8}$$

2.5. Mechanical equations in αβ frame

The following expression provides the electromagnetic torque equation as a function of stator flux and current:

$$T_{em} = p.\left(\psi_{s\alpha} i_{s\beta} - \psi_{s\beta} i_{s\alpha}\right) \tag{9}$$

$$J\frac{d\Omega}{dt} + f\Omega = T_{em} - T_r \tag{10}$$

The Concordia transformation (El Ouanjli et al., 2019d) can be utilized to convert a three-phase reference $(a, b, and\ c)$ into a two-phase reference (α, β). The transformation can be expressed as follows:

$$\begin{bmatrix} X_\alpha \\ X_\beta \end{bmatrix} = \sqrt{\frac{2}{3}}.\begin{bmatrix} 1 & -\frac{1}{2} & -\frac{1}{2} \\ 0 & \frac{\sqrt{3}}{2} & -\frac{\sqrt{3}}{2} \end{bmatrix}.\begin{bmatrix} X_a \\ X_b \\ X_b \end{bmatrix} \tag{11}$$

Where **(X)** can represent current, voltage, or machine flux. This conversion is essential for implementing control strategies that can dynamically adjust to changes in the motor's operational states, thereby enhancing the DFIM's performance in various applications.

This two-phase model greatly simplifies the complex interactions within the motor by reducing the three-dimensional problems into two dimensions, where advanced control strategies like vector control can be more easily implemented to improve the performance and efficiency of the DFIM. The use of the Concordia transformation is particularly advantageous in scenarios where precise control of torque and speed is required, making it a cornerstone in modern DFIM control algorithms (El Ouanjli et al., 2019e), (El Mahfoud et al., 2021a).

3. Model of a two-level voltage source inverter (VSI)

The dual-level voltage source inverter (VSI) is a key technology that has become a standard in the domain of energy efficiency applications (Kouro et al., 2010), (Rodriguez et al., 2002). The inverter creates an output phase voltage from a rectifier (U_{dc}), which delivers the input voltage. By manipulating controlled transistors, this voltage is turned into a three-phase AC voltage signal, characterized by changeable amplitude and frequency (Holmes and Lipo, 2003), (Kaźmierkowski et al., 2002). The selection of switching components, generally IGBT transistors combined with antiparallel diodes, depends on the inverter's power rating and the required switching frequency (Baliga, 2010).

1. Two-level voltage source inverter (2L-VSI) mathematical model

The dual-fed induction motor (DFIM) in this work is supplied by a dual-level voltage source inverter (2L-VSI), as shown in Fig. 3. There are just two complimentary, each output arm the topology incorporates controllable power semiconductor switches, resulting in eight distinct switching states. The array of seven unique voltages generated by these eight inverters' switching configurations can be observed in Fig. 4. Table 2 provides a detailed breakdown of the eight possible voltage vectors along with their corresponding voltage states (Sami et al., 2020).

Of the eight vectors, six $(V_1 - V_6)$ are active vectors, and the other two $(V_0\ and\ V_7)$ are zero vectors.

A coordinate system (abc) with three axes is commonly employed for the purpose of delineating the voltage and current parameters within a three-phase configuration:

$$v_{abc} = [\,v_a \quad v_b \quad v_c\,]^T \tag{12}$$

$$i_{abc} = [\,i_a \quad i_b \quad i_c\,]^T \tag{13}$$

Additionally, the relationship between the inverter output voltage applied to the DFIM and the DC-link voltage, V_{dc}, (Evangelista et al., 2010), (Matraji et al., 2015), along with the switching functions, S_a, S_b, and S_c, is elucidated in Equation (14) as follows:

$$v_{abc} = [\,v_a \quad v_b \quad v_c\,]^T \frac{V_{dc}}{2} \tag{14}$$

The voltage in the two-dimensional $\alpha\beta$ stationary reference frame (Zaid and Ro, 2019), is expressed in equation (15):

$$v_{\alpha\beta} = \begin{bmatrix} v_\alpha \\ v_\beta \end{bmatrix} = \begin{bmatrix} \frac{3}{2} & -\frac{1}{3} & -\frac{1}{3} \\ 0 & \frac{\sqrt{3}}{3} & \frac{\sqrt{3}}{3} \end{bmatrix} \begin{bmatrix} v_a \\ v_b \\ v_c \end{bmatrix} \tag{15}$$

In the $\alpha - \beta$ reference frame, the stator voltages (U_{dcs}) and rotor voltages (U_{dcr}) are determined by the switching states (S_a, $S_b$and S_c), derived from the switching Table 2 (Fig. 4) (Sutikno et al., 2014):

$$\begin{cases} V_\alpha = \frac{U_{DC}}{3}(2.S_a - S_b - S_c) \\ V_\beta = \frac{\sqrt{3}U_{DC}}{3}(S_b - S_c) \end{cases} \tag{16}$$

Table 1
Categorization of DTC control methods with literature references.

Control bases DTC	References
Conventional DTC	(Bekakra et al., 2021a), (Moussaoui et al., 2021), (El Ouanjli et al., 2017a), (Zarean Shahraki and Kazemi, 2012), (Ouanjli et al., 2017a), (Ouanjli et al., 2017b), (Rafajlovski and Digalovski, 2018), (El Ouanjli et al., 2019b), (Aroussi et al., 2020)
SVM based DTC	(Mahfoud et al., 2021a), (Boukadida et al., 2014), (Sutikno et al., 2014), (Habetler et al., 1992), (Ozkop and Okumus, 2008), (Hiba et al., 2013), (Casadei et al., 2000), (Ahmed et al., 2020a), (Kumar and Das, 2017), (Tripathi et al., 2004)
SMC based DTC	(Bekakra et al., 2018), (Ali et al., 2019), (Kati, 2011), (Bekakra et al., 2020), (Jaladi, 2019), (Boumaraf et al., 2021)
DTC-MPC	(Venu Madhav et al., 2021), (Zhang et al., 2011), (Abad et al., 2006), (Aghasi et al., 2012), (Mohammed et al. et al., 2022), (Amiri et al., 2018), (Abad et al., 2008), (Agustin et al., 2019)
Fuzzy based DTC	(Bouhoune et al., 2017), (Ouanjli et al., 2018), (El Ouanjli et al., 2019c), (Brahim et al., 2020), (Kruselj, 2017), (Department of Electrical Engineering et al., 2010a)
ANN based DTC	(Mondal et al., 2002a), (Hamidia et al., 2013), (Ahmed et al., 2020b), (Mahfoud et al., 2022c), (Zemmit et al., 2016), (Mahfoud et al., 2022d)
GA based DTC	(Mahfoud et al., 2022e), (Mahfoud et al., 2021c), (Zemmit et al., 2018), (Mahfoud et al., 2022f), (Singh et al., 2016), (Jayachitra and Vinodha, 2014), (Whitley, 1994), (Tabassum, 2014)
ACO based DTC	(Mahfoud et al., 2022b), (Mahfoud et al., 2022g), (Li et al., 2022), (Varol and Bingul, 2004), (Rezvanian et al., 2023), (Wang et al., 2023), (A. Colorni), (Skackauskas et al., 2022), (Chiha et al., 2012)
RTO based DTC	(Bekakra et al., 2021b), (Wadood et al., 2018), ('Improving the search pattern of)

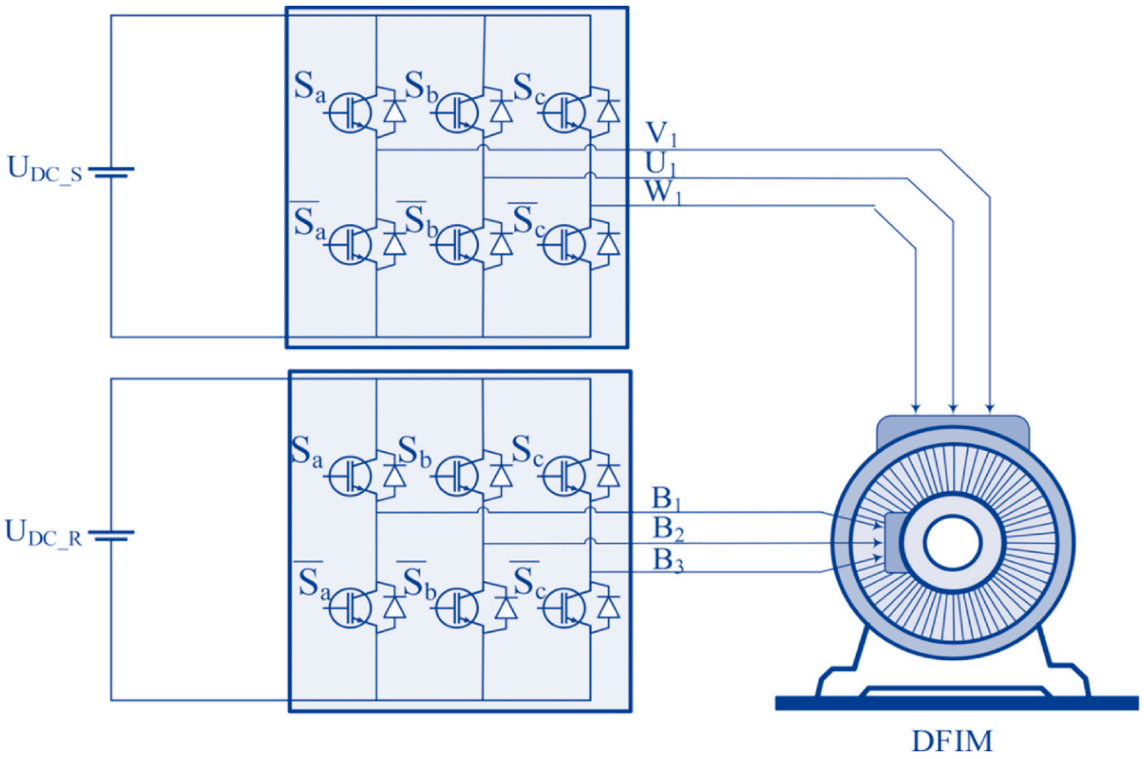

Fig. 3. Representation of the 2L-VSI circuit.

4. Direct torque control

1. Historical Development of Direct Torque Control

Introduced in the late 1980s by Takahashi and Noguchi (1986), the advent of Direct Torque Control (DTC) brought about a revolution in motor control as it enabled direct manipulation of both torque and flux, rendering the need for a speed sensor obsolete. Subsequently, DTC underwent a series of continuous enhancements in order to overcome its initial drawbacks, particularly in relation to torque ripple and switching frequency. The progress made in power electronics, digital signal processing, and computing has also played a significant role in optimizing the efficiency and precision of DTC. It is imperative to comprehend the historical evolution of DTC in order to fully grasp its current state and evaluate its potential for future advancements in engine control technology (Rafajlovski and Digalovski, 2018).

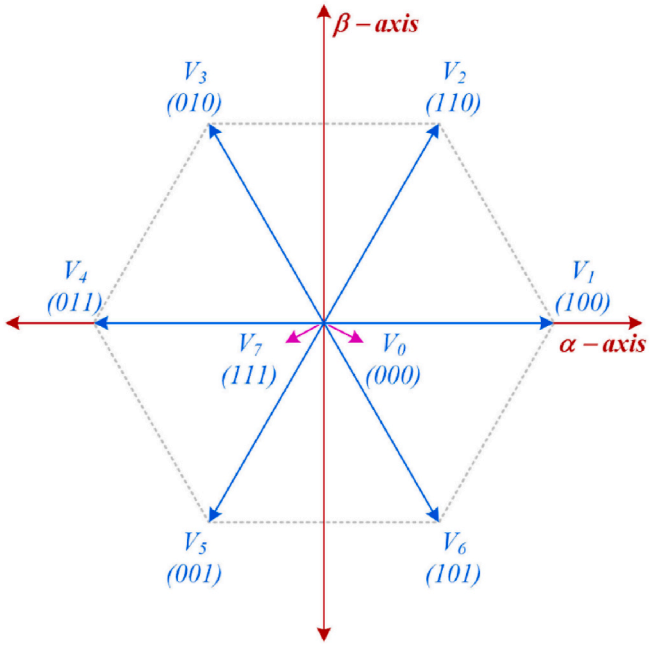

Fig. 4. Schematic representation of the voltage vectors in a 2-level Voltage Source Inverter (2L-VSI).

Table 2
Voltage vector and switching state Configurations for a two-level inverter in $\alpha\beta$ frame.

Voltage Vectors	Voltages in $\alpha\beta$ Frame		Switching States		
	v_α	v_β	S_a	S_b	S_c
V_0	0	0	0	0	0
V_1	$\frac{2}{3}V_{dc}$	0	1	0	0
V_2	$\frac{1}{3}V_{dc}$	$\frac{1}{\sqrt{3}}V_{dc}$	1	1	0
V_3	$-\frac{1}{3}V_{dc}$	$\frac{1}{\sqrt{3}}V_{dc}$	0	1	0
V_4	$-\frac{2}{3}V_{dc}$	0	0	1	1
V_5	$-\frac{1}{3}V_{dc}$	$-\frac{1}{\sqrt{3}}V_{dc}$	0	0	1
V_6	$\frac{1}{3}V_{dc}$	$-\frac{1}{\sqrt{3}}V_{dc}$	1	0	1
V_7	0	0	1	1	1

2. Principe of the DTC control (DTC Modelling)

The DTC works by directly activating switches in the drive to adjust the actual frequency according to the reference speed. The flux and torque hysteresis controllers play an essential role in keeping these quantities within predefined bands. When the flux or torque reaches the limits of these hysteresis bands, the controller generates a signal to change the switching state of the drive, thereby changing the voltage vector applied to the motor. The voltage vector is selected using a

commutation table based on the outputs of the hysteresis comparators and the position of the stator flux. There are eight possible voltage vectors (six active and two zero) that can be applied. Abrupt transitions between these vectors, caused by changes in the switching state of the hysteresis controllers, result in sudden changes in the magnetic flux and electromagnetic torque, causing undesirable ripple (Mahfoud et al., 2022h).

4.1. Estimation of the flux and electromagnetic torque

The system regulates the flux and torque without needing to directly measure them. Instead, the flux and torque are estimated and compared against reference values. The control system then adjusts the inverter output to maintain the desired flux and torque (El Ouanjli et al., 2019d), (Belay et al., 2024).

a. Control of stator and rotor fluxes

Stator and rotor flux vectors are estimated based on Dual-Fed Induction Motor (DFIM) voltage and current measurements. The stator and rotor flux expression is written as (Zarean Shahraki and Kazemi, 2012), (Mahfoud et al., 2022h):

$$\begin{cases} \widehat{\psi}_{s\alpha} = \int (v_{s\alpha} - R_{s\alpha}.i_{s\alpha})dt \\ \widehat{\psi}_{s\beta} = \int (v_{s\beta} - R_{s\beta}.i_{s\beta})dt \end{cases} \quad (17)$$

$$\begin{cases} \widehat{\psi}_{r\alpha} = \int (v_{r\alpha} - R_{r\alpha}.i_{r\alpha})dt \\ \widehat{\psi}_{r\beta} = \int (v_{r\beta} - R_{r\beta}.i_{r\beta})dt \end{cases} \quad (18)$$

The inverter switches are managed over a control period (Te), during which the states (S_a,S_b *and* S_c) of each inverter are maintained constant. A two-level hysteresis comparator facilitates flux control within two concentric circles of close radii (see Fig. 5a). The bandwidth of the hysteresis is determined by the switching frequency of the inverter (see Fig. 5b and c).

b. Torque estimation

The torque generated by the DFIM is calculated using the cross, product of the stator flux and current magnitudes. The estimated torque is given by (Mahfoud et al., 2022c):

$$\widehat{T}_{em} = p.\left(\widehat{\psi}_{s\alpha}.i_{s\beta} - \widehat{\psi}_{s\beta}.i_{s\alpha}\right) \quad (19)$$

c. The objective is to control the flux of the stator and rotor.

Hysteresis controllers maintain the stator and rotor fluxes within predefined two-level bands (Fig. 5c). In the event that the estimated flux exceeds the band limits, the controller adjusts the voltage vector to return the flux to within the specified limits. This mechanism results in frequent switching of the inverter.

d. The genesis of flux and torque ripples

The occurrence of flux and torque ripples is predominantly attributable to the discrete nature of voltage vector switching in conventional DTC. Hysteresis controllers precipitate abrupt alterations in the applied voltage vector upon the flux or torque reaching the limits of the hysteresis bands. These precipitous transitions give rise to precipitous changes in magnetic flux and electromagnetic torque, resulting in the generation of sharp ripples (Fig. 5b).

e. Elaboration of the Switching Table

The selection of voltage vectors *Vs and Vr* is guided by the required torque and flux levels, which vary based on industry requirements and the dynamic characteristics of torque and flux. Table 3 provides details on flux errors ($\Delta\Psi s$ *and*$\Delta\Psi r$), torque errors (ΔTem), and the positions of

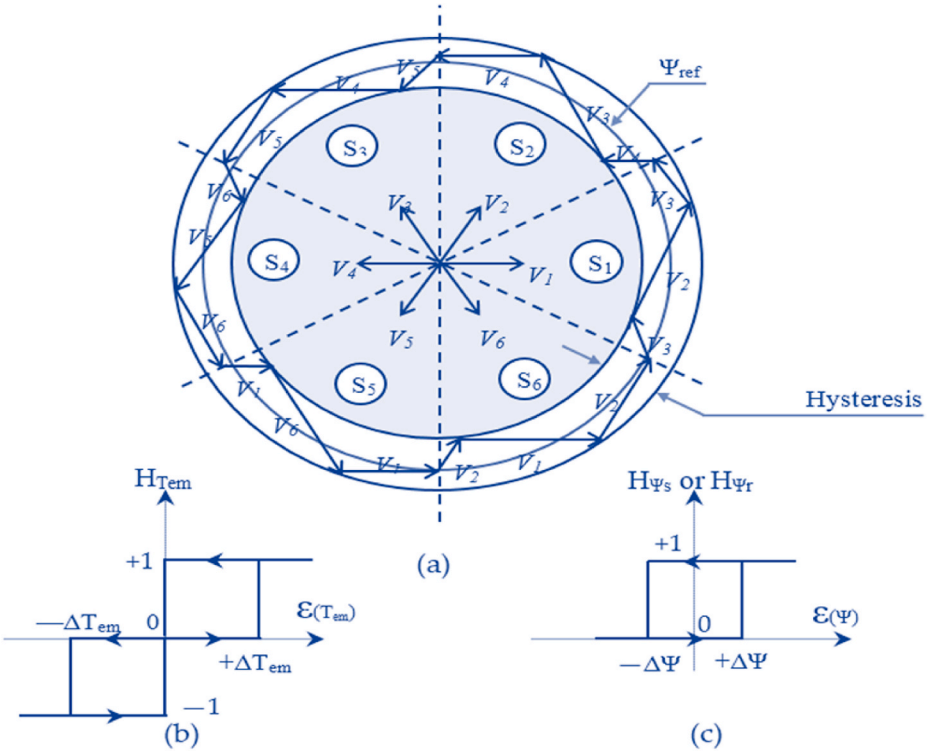

Fig. 5. (**a**) trajectories of the fluxes, (**b**) three-level torque hysteresis comparator, and (**c**) two-level flux comparators.

the flux vectors (i = 1 through 6), allowing for appropriate vector selection to regulate the fluxes and electromagnetic torque of a fed induction motor (Mahfoud et al., 2021b), (Mahfoud et al., 2022h) (Fig. 5).

4.2. Synthesis technique for calculating speed PI parameters in DTC

a. Overview of PI Controller in DTC

The DFIM's speed is controlled in DTC by use of the PI controller. It is stated to be achieved when the speed reference signal matches the real observed speed value. In this situation the speed PI regulator uses a comparison mistake as input. From mechanical Equation (5), the speed is expressed as a function of the torque, as given by: $(1/f)/(1+sj/f)$, one deduces the transfer function TF of the process.

Furthermore, applied for controller gain determination is the pole positioning method. Fig. 6 shows the speed PI controller graphic block.

b. Calculation of Controller Gains

The initial step involves determining the gain (G_0) by intersecting the −45-degree line on the Bode diagram of gain with the phase curve (refer to Fig. 7b for details). Subsequent to this, the gains for the PI regulator are computed for the closed-loop speed transfer function. Assuming a time constant τ of 0.1 seconds, the value of (G_0) obtained from the Bode diagram is used in Equation (20) to calculate K_p. This K_p value is then utilized to determine K_i using the same equation. The resulting values for the speed control loop are $K_p = 0.776$ and $K_i = 28.74$.

c. Equation for PI Controller

The PI controller's equation in the Laplace domain is:

$$PI(s) = \frac{T}{G_0 \times \tau}\left(1 + \frac{1}{T_i s}\right) = K_P + K_i\frac{1}{s}$$

$$\begin{cases} K_P = \dfrac{T}{G_0 \times \tau} \\ K_I = \dfrac{K_P}{0.1 \times \dfrac{I}{f}} \end{cases} \quad (20)$$

where:

$T = J/f$ *and* $G_0 = 1/f$ *and* τ time constant.

d. Stability Analysis Using Nyquist Criterion

To ascertain system stability, the closed-loop transfer function is plotted on a Nyquist diagram. The stability criterion requires that the contour encircles the point $(-1, 0)$ on the left, which is confirmed as per Fig. 7a. This indicates that the system maintains stability under the given settings.

Fig. 8 depicts the speed transfer function's step response after correction. The measured speed response closely tracks the setpoint with a small deviation and fast reaction time, indicating the programmed PI controller's effectiveness in maintaining desirable speed levels.

5. DTC for DFIM

Direct Torque Control (DTC) is increasingly recognized for its effective application in induction motor drives, particularly in Doubly Fed Induction Motors (DFIM). Its appeal lies in the rapid dynamic response and resilience to variations in system parameters, all without the necessity for advanced controllers (Takahashi and Noguchi, 1986), (Aarniovuori et al., 2012), (Abdul Kadir et al., 2007), (Idris and Yatim, 2002), (Lee et al., 2005), (Reza and Mekhilef, 2013). This method is valued for its straightforward implementation process as it does not require coordinate transformations.

In the standard DTC framework (see Fig. 9), errors in electromechanical torque and both stator and rotor fluxes are identified and processed using hysteresis comparators for digitization. A pre-defined switching table is then employed to regulate the inverter switches, which in turn determines the positioning of the voltage vector (V_s) based on the flux angles of the stator and rotor. While this strategy enhances the speed of torque response, it may also lead to torque ripple and variations in the inverter switching frequency. To improve the precision in voltage vector selection, techniques involving voltage zone subdivisions have been introduced (Kumar et al., 2006), albeit with limited success in reducing torque ripple due to sector transitions.

The evolution of DTC has led to the categorization of various schemes into Traditional and Modern DTC approaches (refer to Fig. 10), with further details provided in subsequent sections. At its core, DTC directly manipulates motor torque and flux through the control of voltage supply inverter switches (Bascetta et al., 2010). This is principally achieved using hysteresis controllers that manage system states, particularly the flux amplitudes (both stator and rotor) and electromagnetic torque, to maintain them within preset error boundaries.

The outcomes derived from these controllers, in combination with flux position information, dictate the selection of the most favorable voltage vectors. The VSI has the capability to reach seven distinct phase-plane positions, each corresponding to one of the eight possible sequences of inverter output voltage vectors (Bose, 2009), (Reza et al., 2014). The foundational model of DTC for a DFIM consists of two control pathways dedicated to overseeing flux and torque. These pathways are governed by three hysteresis regulators, two of which are specifically assigned to managing the fluxes of the stator and rotor, while one is tasked with overseeing torque regulation. Depending on the operational mode, the system is supplied with either reference fluxes or feedback from a speed controller, which acts as the torque reference. Subsequently, the estimation and regulation modules compute parameters such as produced torque, flux levels, and flux positions. By comparing predicted values against reference values, the hysteresis controllers generate digital signals, which are then utilized to make decisions regarding adjustments to the VSI based on the primary position. The DFIM ultimately receives the output voltages produced by the inverters (El Ouanjli et al., 2017a).

1. Space Vector Modulation based Direct Torque Control (DTC-SVM)

Habetler et al. (1992) introduced the concept of Direct Torque Control with Space Vector Modulation (DTC-SVM) (Habetler et al.,

Table 3
The inverter sequences.

H_{ψ_s} or H_{ψ_r}	H_{Tem}	Sector S_i					
		S_1	S_2	S_3	S_4	S_5	S_6
1	1	$v_2(110)$	$v_3(010)$	$v_4(011)$	$v_5(001)$	$v_6(101)$	$v_1(100)$
	0	$v_7(111)$	$v_0(000)$	$v_7(111)$	$v_0(000)$	$v_7(111)$	$v_0(000)$
	−1	$v_6(101)$	$v_1(100)$	$v_2(110)$	$v_3(010)$	$v_4(011)$	$v_5(001)$
0	1	$v_3(010)$	$v_4(011)$	$v_5(001)$	$v_6(101)$	$v_1(100)$	$v_2(110)$
	0	$v_0(000)$	$v_7(111)$	$v_0(000)$	$v_7(111)$	$v_0(000)$	$v_7(111)$
	−1	$v_5(001)$	$v_6(101)$	$v_1(100)$	$v_2(110)$	$v_3(010)$	$v_4(011)$

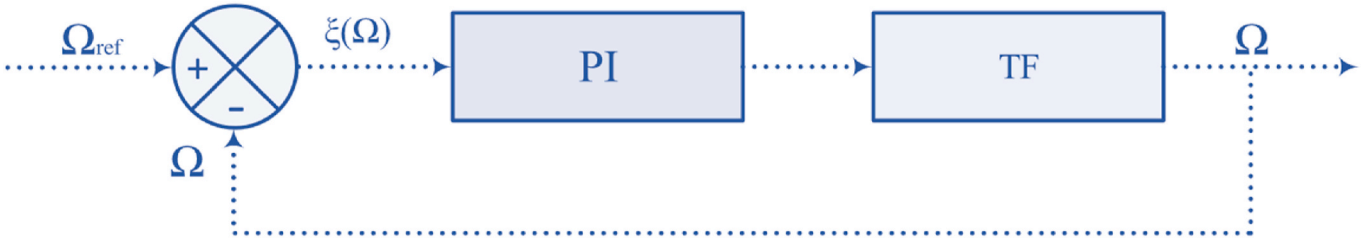

Fig. 6. Speed PI controller diagram block.

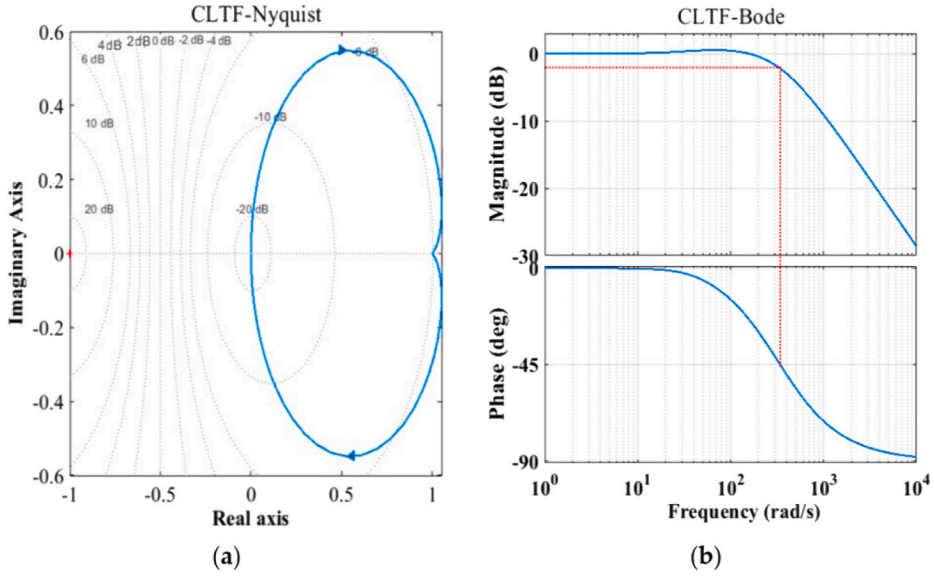

Fig. 7. Closed Loop Function Transfer (CLFT) bode responses (b) and circular Nyquist response (a) diagrams.

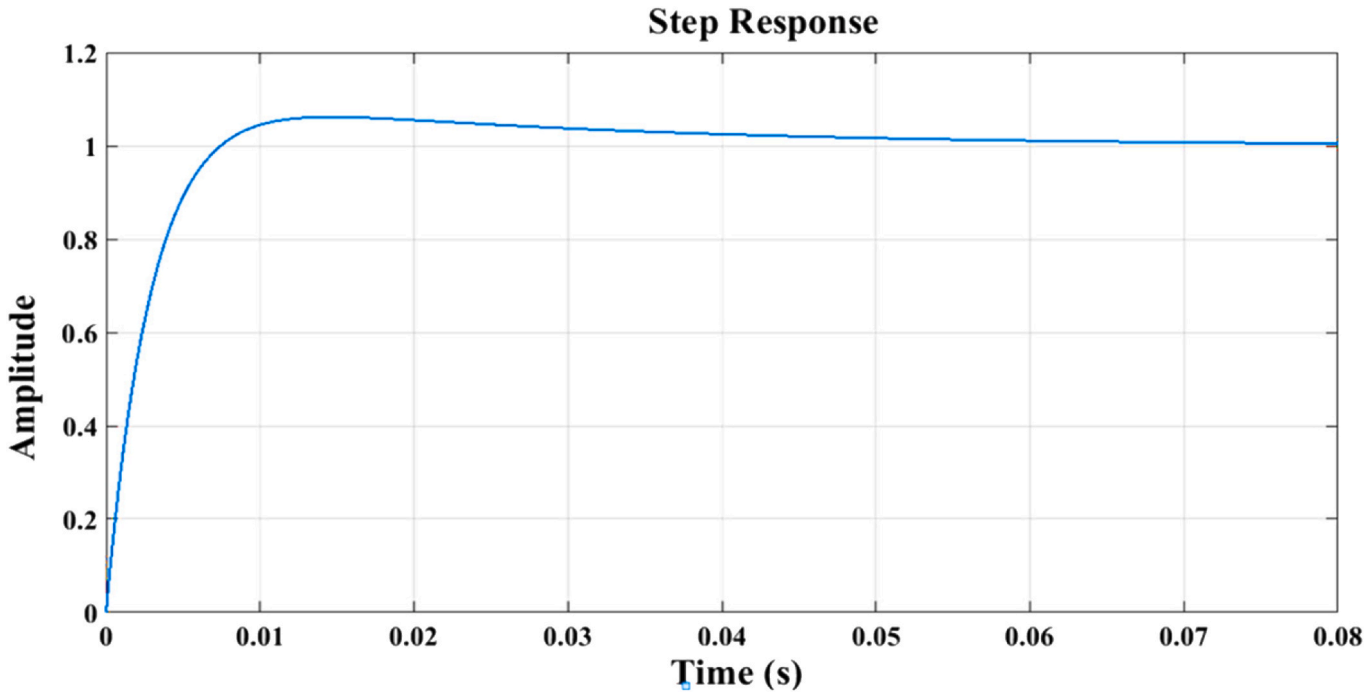

Fig. 8. The process step response after regulation.

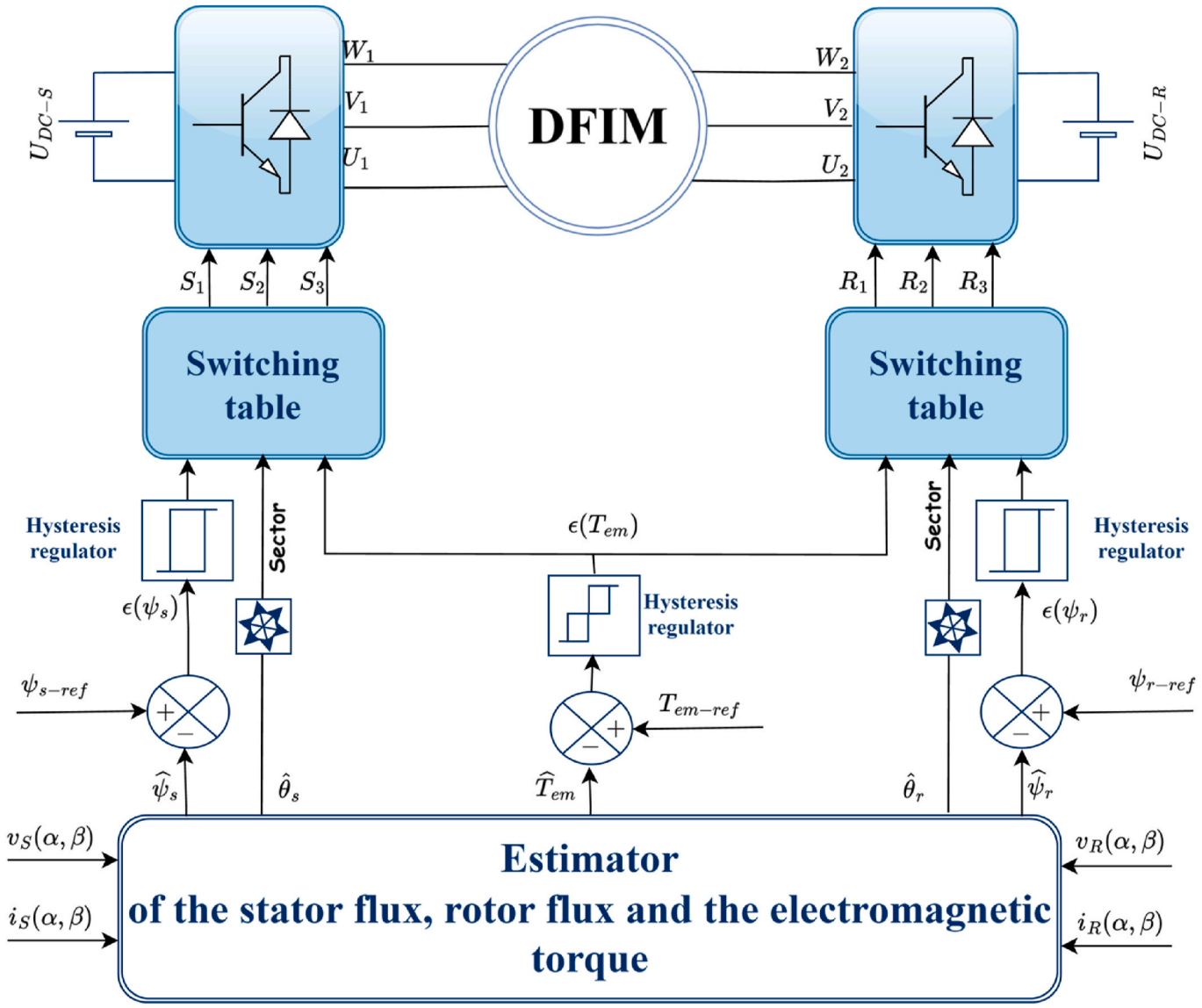

Fig. 9. General structure of DTC of the DFIM.

1992), aimed at manipulating the flux speed in order to control the electromagnetic torque of Dual-Fed Induction Motors (DFIM). By incorporating zero voltage vectors to regulate torque, DTC-SVM presents considerable advantages over hysteresis-based DTC by effectively addressing its inherent limitations (Casadei et al., 2000), (Tripathi et al., 2004). In hysteresis-based DTC, the determination of stator and rotor voltage relies on selecting voltage vectors from a lookup table, which is based on torque and flux requirements analyzed by hysteresis comparators. In contrast, DTC-SVM computes the reference vector of stator and rotor voltage within a sampling period and generates it through the employment of a space vector modulator (Habetler et al., 1992), (Ozkop and Okumus, 2008). The calculation of the reference vector of stator and rotor voltage in DTC-SVM is predicated upon torque and flux requirements, enabling a higher level of precision in motor operation control. (Sutikno et al., 2014).

5.1. General structure of the control DTC-SVM

Three PI controllers handle the torque, stator flux, and rotor flux in the DTC-SVM for DFIM control, which has two inverters. The torque PI controller calculates the quadratic stator and rotor voltages, abbreviated as v_q. The other two PI controllers in the flux loop generate direct voltages, which are represented as v_d. After obtaining the values of v_d and v_q, they are converted into a stable reference frame (α, β) before being inputted into the SVM. The Support Vector Machine (SVM) produces the switching signals $S_a, S_b,$ *and* S_c for the power transistors of the inverter (Controller design for direct torque, 2024).

5.2. Application of DTC control with SVM on DFIM

Space Vector Modulation (SVM) is separate from typical pulse-width modulation (PWM) approaches. It employs a vectorial spatial representation of the inverter's output, avoiding the requirement for discrete phase modulators. Instead, the reference voltages are defined by the components of the spatial voltage vector inside the intricate plane (Energies; Five-Phase Induction Motor DTC; Improving the search pattern; Mossa and Bolognani). SVM works on the premise of estimating the inverter voltage vector by projecting the reference vector (V_{ref}) between two neighboring vectors, which indicate non-zero switching states (Abu-Rub et al., 2013).

The switching vector diagram is constructed as a hexagon split into six 60° sectors for two-level inverters, as seen in Fig. 11.

The duration to which each vector is applied can be precisely calculated, with any remaining time within the cycle allocated to the

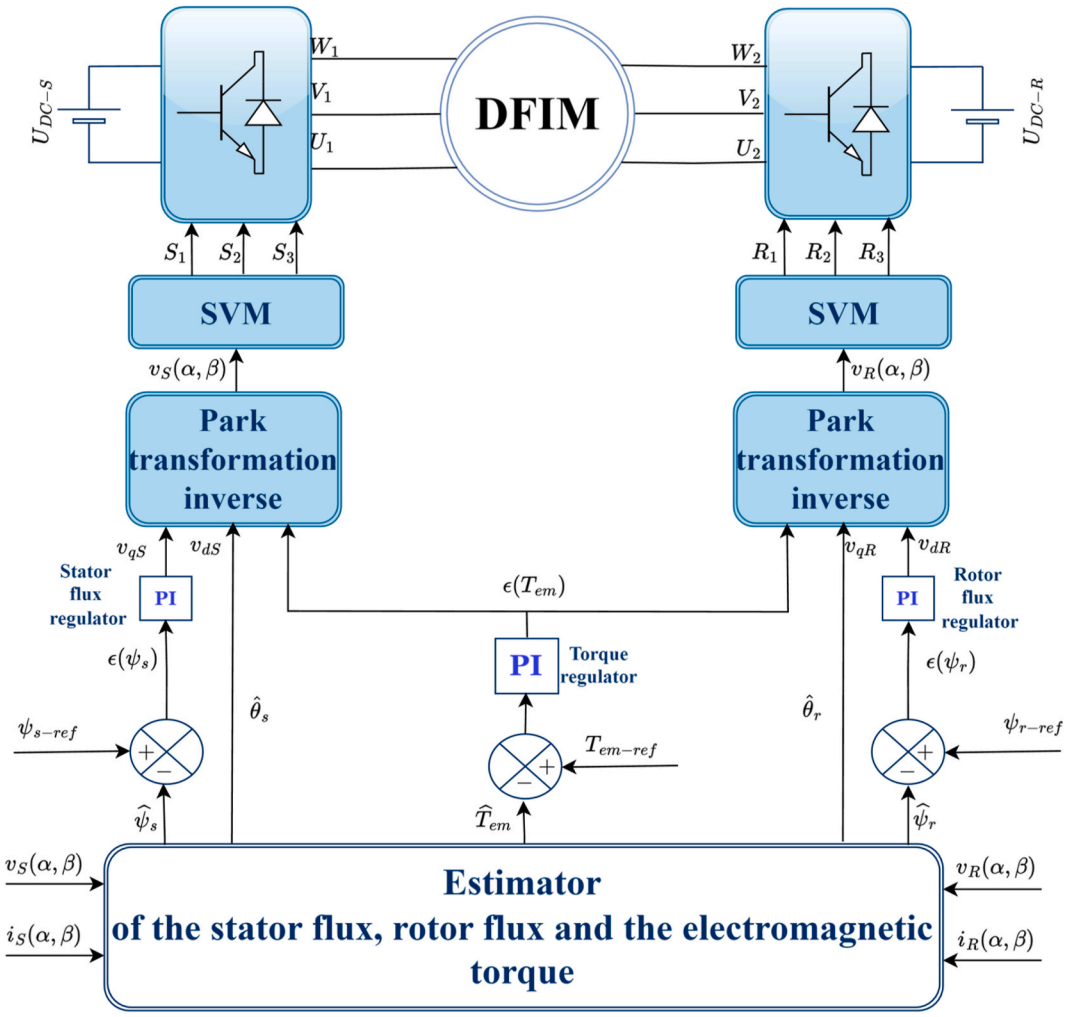

Fig. 10. Block diagram DTC-SVM scheme for DFIM.

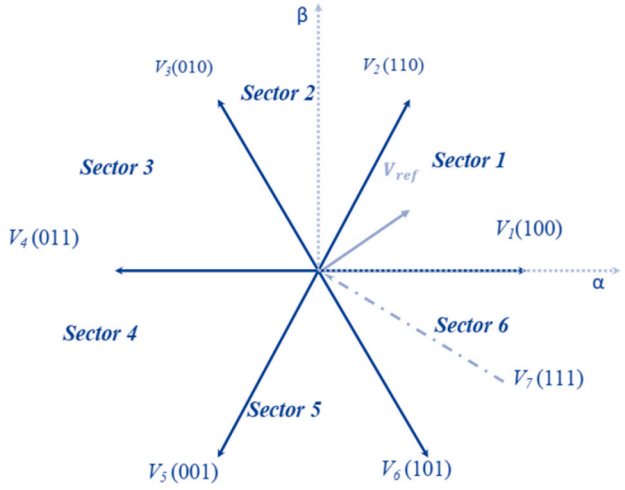

Fig. 11. Illustrates the schematic representation of a voltage space vector.

zero vector (Kim and Sul, 1996). Table 4 details the control signals for inverter switches across various sectors, exemplifying the configurations required for each sector's specific needs.

In sector 1, for instance, the reference voltage is synthesised using vectors V_1, V_2 and V_0 (the zero vector), as seen in Fig. 12. The

Table 4
inverter switches across various sectors.

Sector 1	$T_1 = -Z, T_2 = X$
Sector 2	$T_2 = Y, T_3 = Z$
Sector 3	$T_3 = X, T_4 = -Y$
Sector 4	$T_4 = Z, T_5 = -X$
Sector 5	$T_1 = -Y, T_6 = -Z$
Sector 6	$T_6 = -X, T_1 = Y$

application of the volt-second principle for this sector is described by the following equation:

$$V_{ref} T_e = V_1 T_1 + V_2 T_2 + V_0 T_0 \tag{21}$$

$$T_e = T_1 + T_2 + T_0 \tag{22}$$

Here, T_1, T_2 and T_0 represent the times allocated to each of the voltage vectors.

Simple projections are used to derive the timings T_1 and T_2, which correspond to the voltage vectors:

$$X = \frac{T_e}{V_{dc}} \sqrt{2} V_\alpha \tag{23}$$

$$Y = \frac{T_e}{2V_{dc}} \left(\sqrt{6}\, V_\beta + \sqrt{2}\, V_\alpha \right) \tag{24}$$

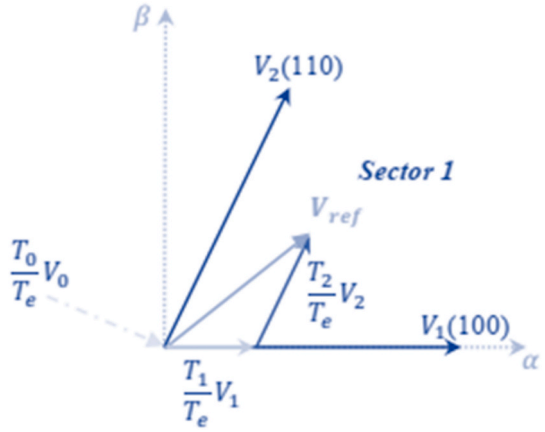

Fig. 12. Demonstrates the reference vector composed by merging adjacent vectors within sector 1.

$$Z = \frac{T_e}{2V_{dc}}\left(\sqrt{2}\,V_\beta - \sqrt{6}\,V_\alpha\right) \tag{25}$$

The following is a representation of the switching times (duty cycles) computation:

$$T_{aon} = \frac{T_e - T_1 - T_2}{2} \tag{26}$$

$$T_{bon} = T_{aon} + T_1 \tag{27}$$

$$T_{con} = T_{bon} + T_2 \tag{28}$$

Fig. 13 depicts the calculation of switching periods or duty cycles for sector 1. The symmetrical carrier wave produced by the SVM model is presented, with an example period (T_e) in sector 1. Fig. 10 next displays the total structure of DTC-SVM control for the DFIM, which is coupled by two voltage inverters.

2. Fuzzy Logic based Direct Torque Control (DTC-FL)

In 1994, Mir proposed the first fuzzy-based direct torque control (FDTC) controller, which replaced hysteresis controllers and commutation tables with fuzzy logic for space vector selection in the conventional DTC-DFIM drive. The fuzzy controller takes into account torque and flux errors, as well as stator and rotor flux positions. Each of the 601 sectors has been divided into two subsets, resulting in a large number of fuzzy rules. This approach has since become a promising method for improving the performance of variable speed drives, particularly in the context of dual-feed induction machines (DFIM). By using fuzzy logic

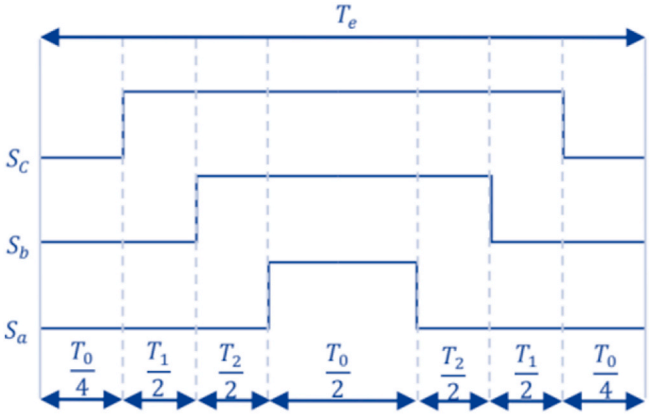

Fig. 13. Switching times of sector 1.

controllers (FLC) instead of traditional elements, FDTC provides improved dynamic response and increased resilience to parameter variations. The FLC uses inputs such as stator and rotor flux error, electromagnetic torque error and stator and rotor flux vector positions to generate optimal switching states for the inverter arms. This efficient control of flow and torque relative to their setpoints is achieved by taking advantage of linguistic variables and fuzzy sets, enabling precise control with a minimum of rules and better adjustment to changing operational circumstances. Research has demonstrated the effectiveness of fuzzy logic in resolving the drawbacks of conventional DTC, notably the reduction of torque ripples and improved robustness. Despite the difficulties associated with parameter tuning and the complexity of implementation, the advantages offered by fuzzy logic in DTC underline its potential for improving the performance and robustness of DFIM control systems (Bouhoune et al., 2017), (Ouanjli et al., 2018), (El Ouanjli et al., 2019c).

5.3. General structure of the control DTC-FL

The conventional hysteresis controllers and switching tables are replaced with two fuzzy logic controllers in this setup to enhance system performance and reduce fluctuations in electromagnetic torque and flux. Within this system, inputs such as flux error, torque error, and flux angle are fed into each fuzzy logic controller to optimize control responses (Department of Electrical Engineering et al., 2010b).

$$\varepsilon_{\psi s} = \psi_{s-ref} - \widehat{\psi}_s = \Delta\psi_s \tag{29}$$

$$\varepsilon_{\psi r} = \psi_{r-ref} - \widehat{\psi}_r = \Delta\psi_r \tag{30}$$

$$\varepsilon_{Tem} = T_{em-ref} - \widehat{T}_{em} = \Delta T_{em} \tag{31}$$

The error functions employed in this context are formed from the disparities between commanded and estimated magnitudes. Each input variable is separated into numerous fuzzy sets, which permits more efficient management with a limited set of rules (El Ouanjli et al., 2019c). Fig. 14 displays the block design for the fuzzy DTC implementation on a DFIM.

The control process utilizing fuzzy logic generally develops in three separate phases: fuzzification, rule-based output determination, and defuzzification, as explained by (Akın et al., 2003).

5.4. Fuzzification of inputs

The objective of the fuzzification procedure is to turn deterministic input variables into linguistic variables using predetermined membership functions. One significant input variable is the flux location, which refers either to the stator or rotor flux. The range of this variable is partitioned into six fuzzy sets, called $\theta 1$ through $\theta 6$. Each of these sets is represented by a triangle membership function, as depicted in Fig. 15.

The fuzzification procedure aims to convert the deterministic input variables into linguistic variables by establishing membership functions for each input variable.

The first input variable is the location of the flux, which may either be in the stator or the rotor. The variable's discourse universe consists of six fuzzy sets (θ_1 to θ_6) with their membership functions shown in Fig. 15.

A triangular function of membership has been chosen for all angle variables θi.

The second input variable, the error in electromagnetic torque, is categorized into three fuzzy sets within its discourse universe.

- Positive torque error is denoted as (P);
- Zero torque error is denoted as (Z);
- Negative torque error is denoted as (N).

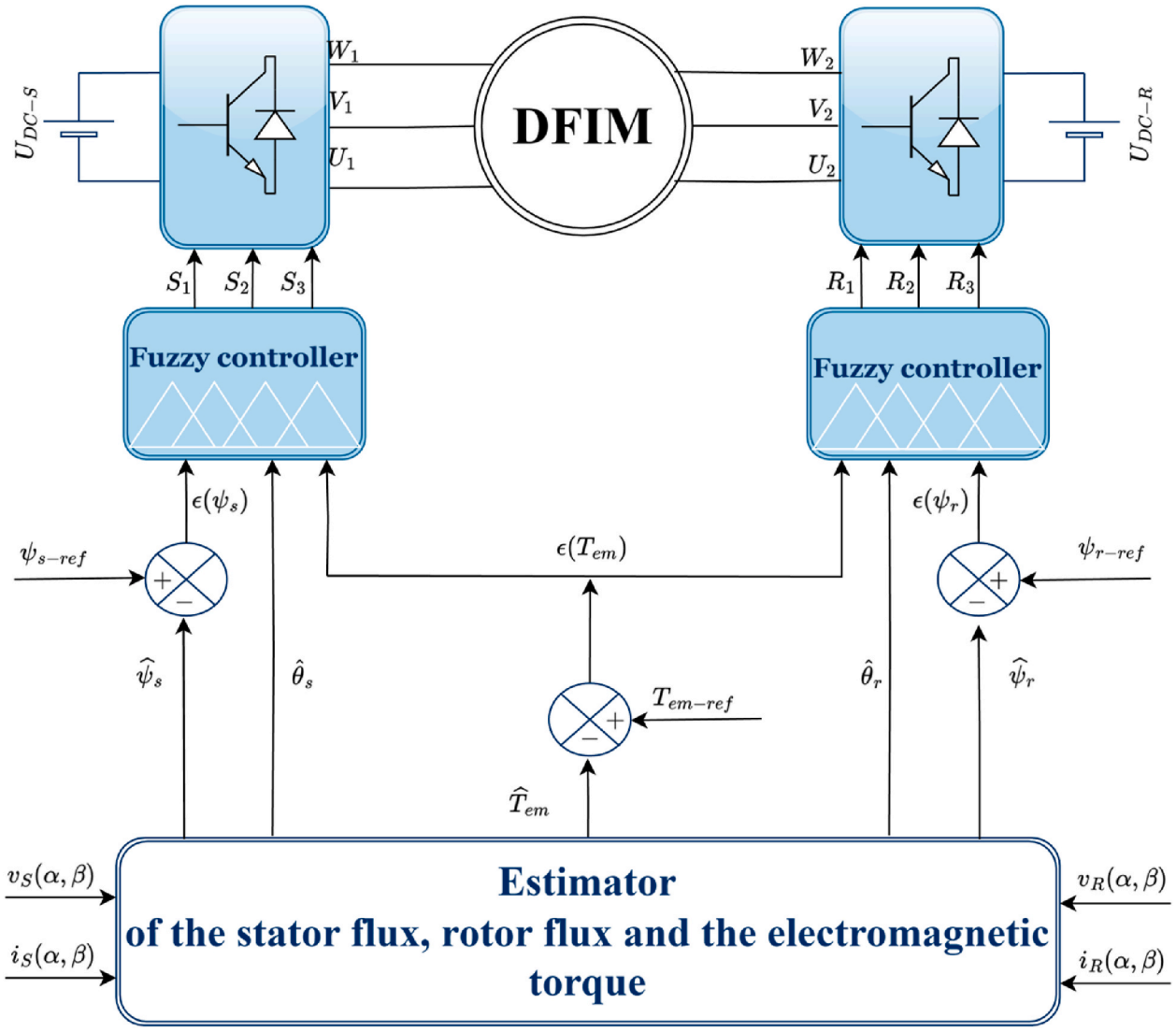

Fig. 14. Conceptual framework of fuzzy logic-based DTC.

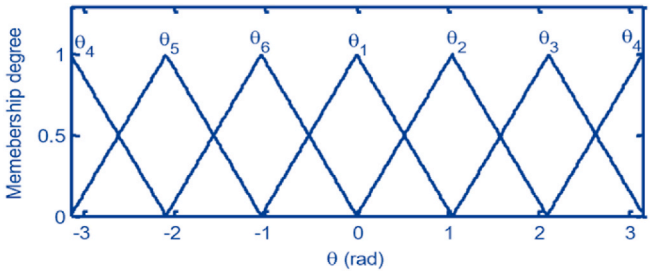

Fig. 15. Membership functions for flux position variables.

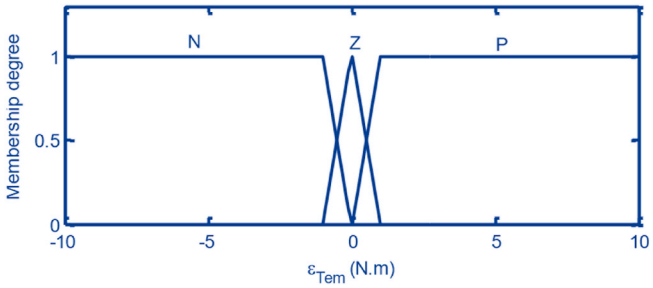

Fig. 16. Electromagnetic torque error membership function.

Fig. 16 illustrates the membership functions for these sets, employing trapezoidal functions for the 'P' and 'N' sets and a triangular function for the 'Z' set.

The third input variable, flux error, is segmented into two fuzzy sets within its universe of discourse.

- Flux error is categorized as positive (P).
- Flux error is categorized as negative (N).

As depicted in Fig. 17, trapezoidal membership functions are used for both fuzzy sets.

5.5. Outputs defuzzication

The defuzzification process entails converting the fuzzy data supplied by the inference system into a tangible physical or numerical value that informs the operation's control rule. For the inverter switches, the output variable consists of three sub-outputs, each reflecting a switching magnitude (S_1, S_2, S_3). The discourse universe for each output is separated into two fuzzy sets, denoted as zero and one. As illustrated in

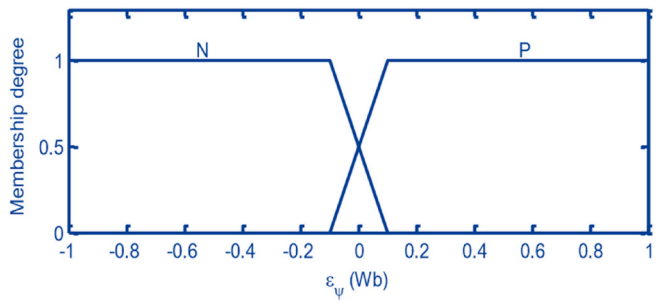

Fig. 17. The flux linkage error membership function.

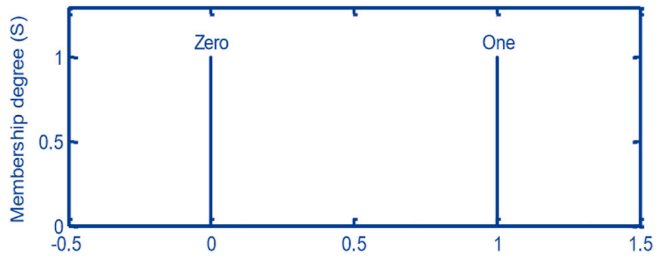

Fig. 18. Functions that determine membership for output variables.

Fig. 18, Trapezoidal membership functions are applet for these sets.

5.6. Control regulations

The formulation of control rules is dictated by the relationship between the output and input variables utilized in the conventional direct torque control switching table. Fig. 19 presents the layout of a fuzzy logic controller. Additionally, the methodology for determining the output variables from the given input variables is systematically arranged in Table 5.

The control algorithm consists of 36 rules and utilizes the Mamdani technique with Max-Min decision for inference. This approach is chosen for its ease of implementation and superior performance. This technique is articulated as:

$$\mu_{Ri} = min(\mu_{Xi}(\varepsilon_\theta), \mu_{Yi}(\varepsilon_{Tem}), \mu_{wi}(\varepsilon_\psi)) \quad (32)$$

The Mamdani minimum method yields results via the use of fuzzy reasoning.

$$\mu_{N'i} = min(\mu_{ri}, \mu_{Ni}(n)) \quad (33)$$

The output's membership function μ_N is determined as follows:

$$\mu_N(n) = max(\mu_{N'i}(n)), i = 1, 2, ...36. \quad (34)$$

Control rules are articulated as mathematical functions linking input variables to output variables in a fuzzy logic system. The general form of a control rule can be expressed as:

If (θ is X) and ($\varepsilon_{\mathrm{Tem}}$ is Y) and (ε_ψ is W) then (V is V_i).

Here X, Y and W represent the fuzzy sets of the input variables, and $V_i(S_1, S_2, S_3)$ denotes the fuzzy sets of the output variables. Below are examples of the control rule:

- If (is θ_1) and ($\varepsilon_{\mathrm{Tem}}$ is P) and (ε_ψ is P) then (S_1 is 0) and (S_2 is 1) and (S_3 is 0).
- If (is θ_2) and ($\varepsilon_{\mathrm{Tem}}$ is N) and (ε_ψ is P) then (S_1 is 1) and (S_2 is 0) and (S_3 is 1).

3. Artificial Neural Network based Direct Torque Control (DTC-ANN)

Artificial Neural Networks (ANNs) are widely applied across numerous technological and scientific sectors, solving complicated issues unresolvable using rigid mathematical approaches. ANNs play a vital role in various applications such as classification, image and audio processing, estimation, process identification, and the control of electrical systems, among others. (Chegwidden and Watts, 1975), (Lin et al., 2001), (Mondal et al., 2002b), (Stein, 1975).

ANNs are valued in research owing to their resilience and efficiency. Research (Esen et al., 2008) emphasized the usefulness of ANNs and Adaptive Neuro-Fuzzy Inference Systems (ANFIS) in correctly simulating ground-coupled heat pump (GCHP) systems. The 2008 study applied a combination technique of ANNs and Statistical Weighted Preprocessing (SWP) to estimate the performance of GCHP systems, primarily concentrating on horizontal layouts. The appropriateness of ANNs for this purpose was proved by their study.

More, modeling research assessed a novel solar air heater (SAH) system utilizing ANN and wavelet neural network (WNN) models, with the findings reported in (Esen et al., 2009). According to research reported in (Esen et al., 2017), ANFIS and ANN are efficient in estimating the performance of solar ground-source heat pump systems. Another unique use of ANNs was in modeling a robotic system meant to traverse across environments with obstacles (V. M). Additionally, a unique strategy integrating the Gravitational Search Algorithm (GSA) with

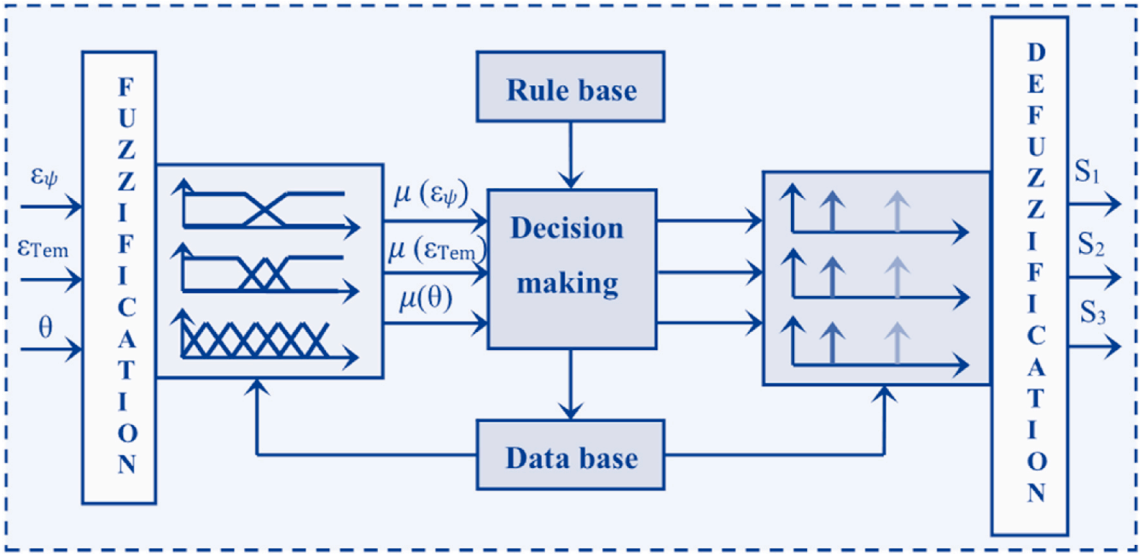

Fig. 19. The architecture of the fuzzy controller designed for the two-level inverter.

Table 5
Displays a group of fuzzy rules.

θ_1			
e_{Tem} / e_ψ	N	Z	P
N	v_5	v_0	v_3
P	v_6	v_7	v_2

θ_2			
e_{Tem} / e_ψ	N	Z	P
N	v_6	v_7	v_4
P	v_1	v_0	v_3

θ_3			
e_{Tem} / e_ψ	N	Z	P
N	v_1	v_0	v_5
P	v_2	v_7	v_4

θ_4			
e_{Tem} / e_ψ	N	Z	P
N	v_2	v_7	v_6
P	v_3	v_0	v_5

θ_5			
e_{Tem} / e_ψ	N	Z	P
N	v_3	v_0	v_1
P	v_4	v_7	v_6

θ_6			
e_{Tem} / e_ψ	N	Z	P
N	v_4	v_7	v_2
P	v_5	v_0	v_1

ANNs for selecting initial weight and bias values has been presented (Zamfirache et al., 2022). This strategy dramatically boosts performance in reference-tracking jobs.

5.7. ANN-based comparators, regulation speed, and switching tables controls

A neural network may be conceptualized as a mathematical framework for distributed processing that displays properties analogous to those seen in biological brain networks. It is made of multiple nonlinear computational units, referred to as neurons, which act simultaneously and are interconnected by connections represented by numerical parameters known as weights (Mahfoud et al., 2022c), (Mahfoud et al., 2022d), (Menghal and Laxmi, 2018).

ANNs are constructed of densely linked basic processors that work in parallel. One of the major components of ANNs is their training data, which is necessary for learning and enhancing performance (V. M). The neuron, key to the ANN design, has summing junctions and activation functions. The mathematical formulas that explain a neuron's function are described given by (Mahfoud et al., 2022c):

$$y_i = F_1(s)^*\left\{\sum_{i=1}^{N}(x_i{}^*w_i + b)\right\} \tag{35}$$

$$O_i = F_2(s)^*\left\{\sum_{i=1}^{N}(y_i{}^*w_i + b)\right\} \tag{36}$$

In this section, xi, wi, b and y denote the input signals, the corresponding synaptic weights of these input signals, a bias parameter, and the neuron's output signals, respectively. The hyperbolic tangent function $F_1(s)$, a nonlinear activation function, is defined by the equation:

$$F_1(s) = \frac{e^{\alpha s} - e^{-\alpha s}}{e^{\alpha s} + e^{-\alpha s}} \tag{37}$$

as depicted in Fig. 20. Furthermore, a linear activation function, $F_2(s)$, is defined by:

$$F_2(s) = \beta s \tag{38}$$

where α and β are the respective gains. This function is differentiable, bipolar, and exhibits monotonic behavior, achieving its highest gain at zero. The Neural Network undergoes training through the feedforward backpropagation method until the Mean Squared Error (*MSE*) between the desired output patterns and the actual outputs is minimized.

$$MSE = \frac{1}{N}\sum_{i=1}^{N}(d_i(k) - O_i(k))^2 \tag{39}$$

where.

- $d_i(k)$: is the target output,
- $O_i(k)$: is the network's actual output,
- N: represents the dataset size, and
- k: denotes the iteration count.

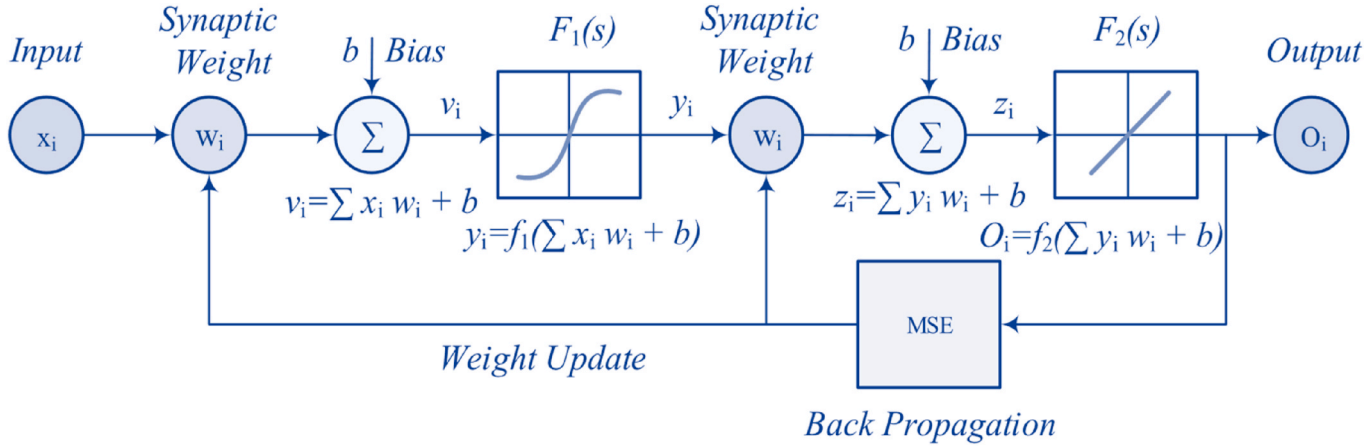

Fig. 20. ANN for DTC: a schematic framework.

The weight update formula is:

$$w_{ji}(k+1) = w_{ji}(k) - \eta \frac{\partial MSE(k)}{\partial w_{ji}(k)} \tag{40}$$

where $w_{ji}(k+1)$ and $w_{ji}(k)$ represent the updated and previous weights between the *ith* and *jth* neurons, and η is the learning rate.

It is recommended to use neural network-based controllers for speed, stator and rotor flux, and torque, as illustrated in Fig. 21a, b, 22c, and 22d. These ANNs function as hysteresis comparators and play a crucial role in developing an on-off switching model for the switching tables depicted in Fig. 23a and b. This model assists in creating a switching pattern for inverter switches. The inputs, ξ_i, to each ANN's comparator are the differences between the reference setpoints and the estimated setpoints.

$$\begin{aligned} \xi_{\Omega} &= \Omega_{\text{ref}} - \Omega \\ \xi_{\psi s} &= \psi_{S\_ref} - \psi_{S\_\text{est}} \\ \xi_{\psi r} &= \psi_{r\_ref} - \psi_{r\_est} \\ \xi_{T} &= \psi_{T\_\text{ref}} - \psi_{T\_\text{est}} \end{aligned} \tag{41}$$

In the hidden layer of the network, each controller trains a specified number of neurons. The input ξ_i is multiplied by the weight *wi*, and the hidden layer's output is calculated as $v_i = \sum_{i=1}^{N} e_a w_i + b$, where b represents the bias. Both a hyperbolic tangent nonlinear activation function and a linear activation function are employed for error backpropagation. Since the outputs $y_i = f\left(\sum_{i=1}^{N} e_a w_i + b\right)$ of the artificial neural network (ANN) are not exactly 0 or 1, a comparator without a hysteresis band is used until the desired output is reached. Weights are continuously adjusted via the backpropagation algorithm using Equation (40) to reduce the error defined in Equation (39). Fig. 24's schematic arrangement illustrates the suggested ANN-DTC strategy for implementation on both ends of DFIM.

5.8. Selection of artificial neural network (ANN) parameter technique

a. Preparation of training data (input-output pairs).

The training dataset preparation necessitates comprehensive information regarding the operation modes of the variable speed drive system, encompassing all four quadrants (including both acceleration and deceleration in two rotational directions), as well as scenarios with and without load torque application. By conducting extensive practical experiments utilizing DTC-ANN control through the MATLAB toolbox, the optimal parameters for each ANN controller were selected after multiple trials, aiming to achieve the most effective controllers for the application of DTC-ANN control to the DFIM.

In the process of preparing the training dataset, 70% of the data is allocated for supervised learning, 15% for network validation, and the remaining 15% for learning assessments. The validation and testing data play crucial roles as criteria for halting and evaluating performance, which are integrated into the MATLAB toolbox. The first criterion focuses on assessing generalization quality, terminating the algorithm when generalization no longer improves to prevent overfitting. While not impacting the learning process, the second criterion offers an independent evaluation of network performance during and after learning. The sampling interval was established at 0.00013 s.

b. Selection of Neural Network Topology

The lack of a definitive methodology for specifying the number of hidden layers and neurons within each layer renders the determination of the neural network architecture a complex process. Consequently, we employed a trial-and-error methodology. Initially, we considered structures with a single hidden layer and a minimal number of neurons, gradually increasing the neuron count until the desired performance level was attained. Following a period of extensive experimentation, the use of 10 neurons for the speed controller, 16 neurons for the torque and flux controllers, and 20 neurons for the switch table controllers yielded suboptimal outcomes. This observation indicated that solely adjusting the number of neurons was inadequate for enhancing performance. Consequently, we proceeded to utilize 10, 16, and 20 neurons in the hidden layers corresponding to each controller. For the activation functions, tangent-sigmoid functions (tansig in MATLAB) were employed for the hidden layer neurons, while linear activation functions (purelin) were utilized for the network outputs.

c. Selection of the Learning Algorithm.

The final phase of the process involved the selection of the learning algorithm. The Backpropagation Error Learning Method was chosen as the most appropriate algorithm for this task. The MATLAB toolbox offers a variety of algorithms, including the gradient descent algorithm (traingd), gradient descent with momentum (traingdm), and the Levenberg-Marquardt algorithm (trainlm), all of which employ the batch technique. The toolbox provides performance metrics, including the mean squared error (MSE) for minimization and the regression value (R), which is used to measure the correlation between outputs and

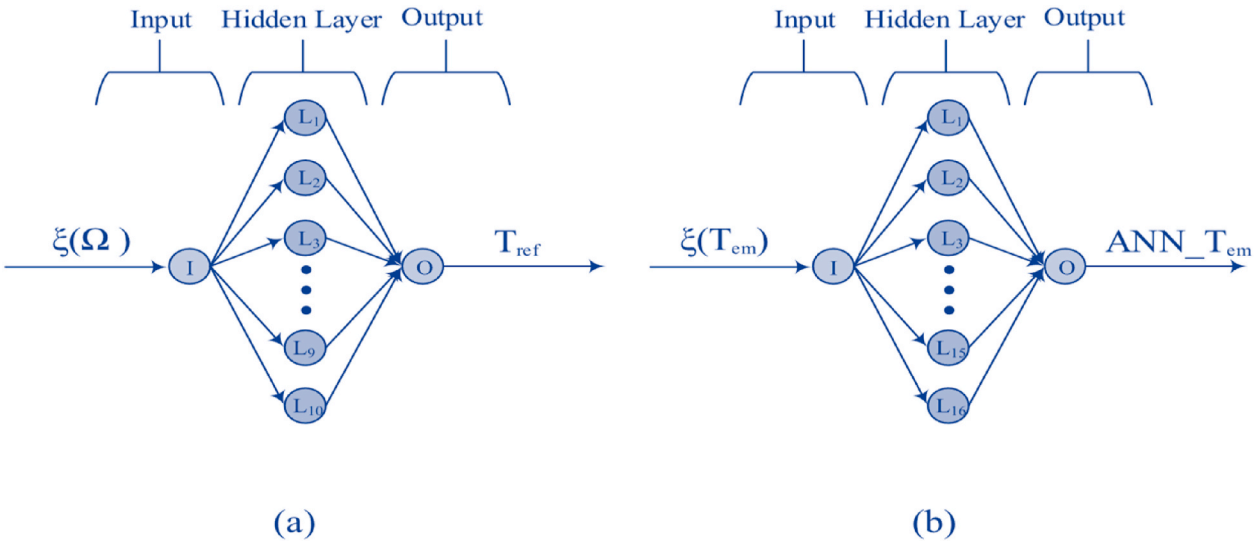

Fig. 21. Feed-forward ANNs for speed controller (a) torque controller (b).

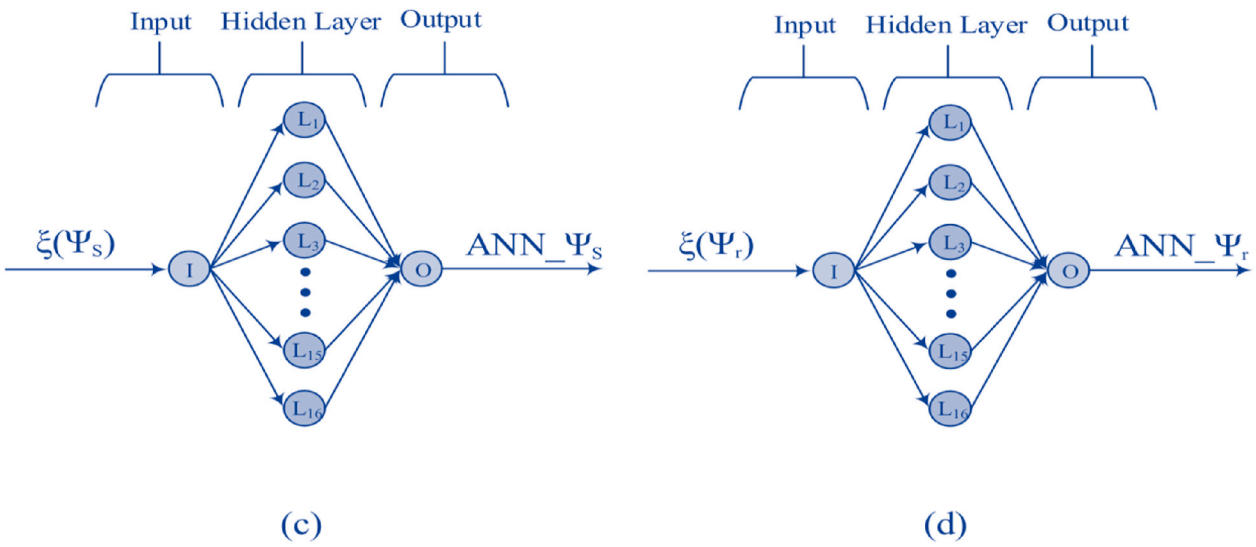

Fig. 22. Feed-forward ANNs for stator flux controller (c) rotor flux controller (d).

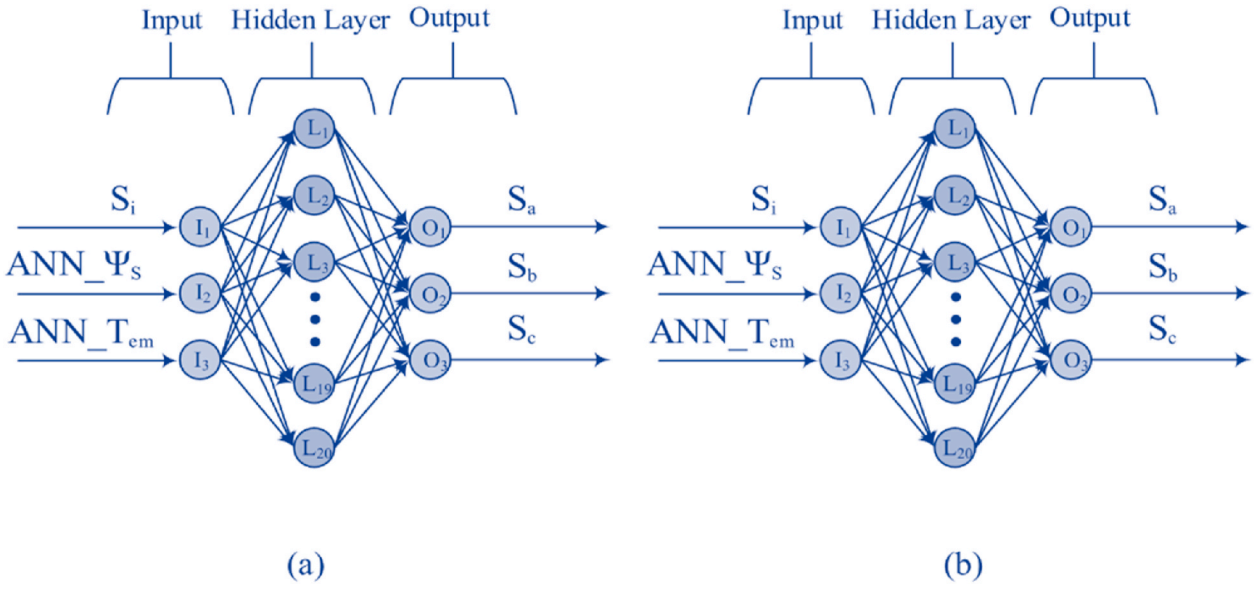

Fig. 23. Feed-forward ANNs for switching tables on the stator (a) and rotor (b).

targets. R = 1 indicates a strong relationship. A notable indicator of potential overfitting is when the learning performance is satisfactory, yet the testing performance is significantly suboptimal. Once all

parameters for the neural regulators have been configured, the learning phase commences. Fig. 25 illustrates the error backpropagation learning algorithm employed for the construction of the neural network (Mahfoud et al., 2022c).

4. Genetic Algorithm based Direct Torque Control (DTC-GA)

According to Whitley (1994) (Whitley, 1994), the Genetic Algorithm (GA) is a stochastic global adaptive search optimization technique based on the principles of natural selection. An objective function evaluates each chromosome in the population that starts this method, representing a different solution to the problem (Singh et al., 2016). Moreover, GA is utilized in contemporary applications to determine the ideal parameter values of rational functions (Irshad et al., 2016). It is utilized in an electric distribution network's control system (Storti et al., 2015). Furthermore, GA is used with MPPT to improve a PV system's ability to capture energy (Daraban et al., 2014). Moreover, it is utilized to improve distribution systems' power quality and dependability (Gupta et al., 2014). But GA has its limitations. In addition to taking a long time to reach convergence and adjust every parameter, such as the mutation rate, elitism percentage, crossover parameters, and so forth, it is unable to ensure the identification of the global minimum. Moreover, GA requires the normalization of fitness because it is a trial-and-error process (Tabassum, 2014), (Hannan et al., 2018).

5.9. General structure of the control DTC-GA

Genetic algorithms are a particular type of evolutionary algorithm that employ techniques derived from evolutionary biology, including selection, crossover, and mutation (Jayachitra and Vinodha, 2014). Fig. 27 illustrates the sequence of actions performed in a GA, shown as a flowchart that follows a GA's evolutionary principles. Fig. 28's schematic arrangement illustrates the suggested DTC- GA strategy for implementation on both ends of DFIM.

Fig. 26 illustrates the streamlined configuration of the genetic

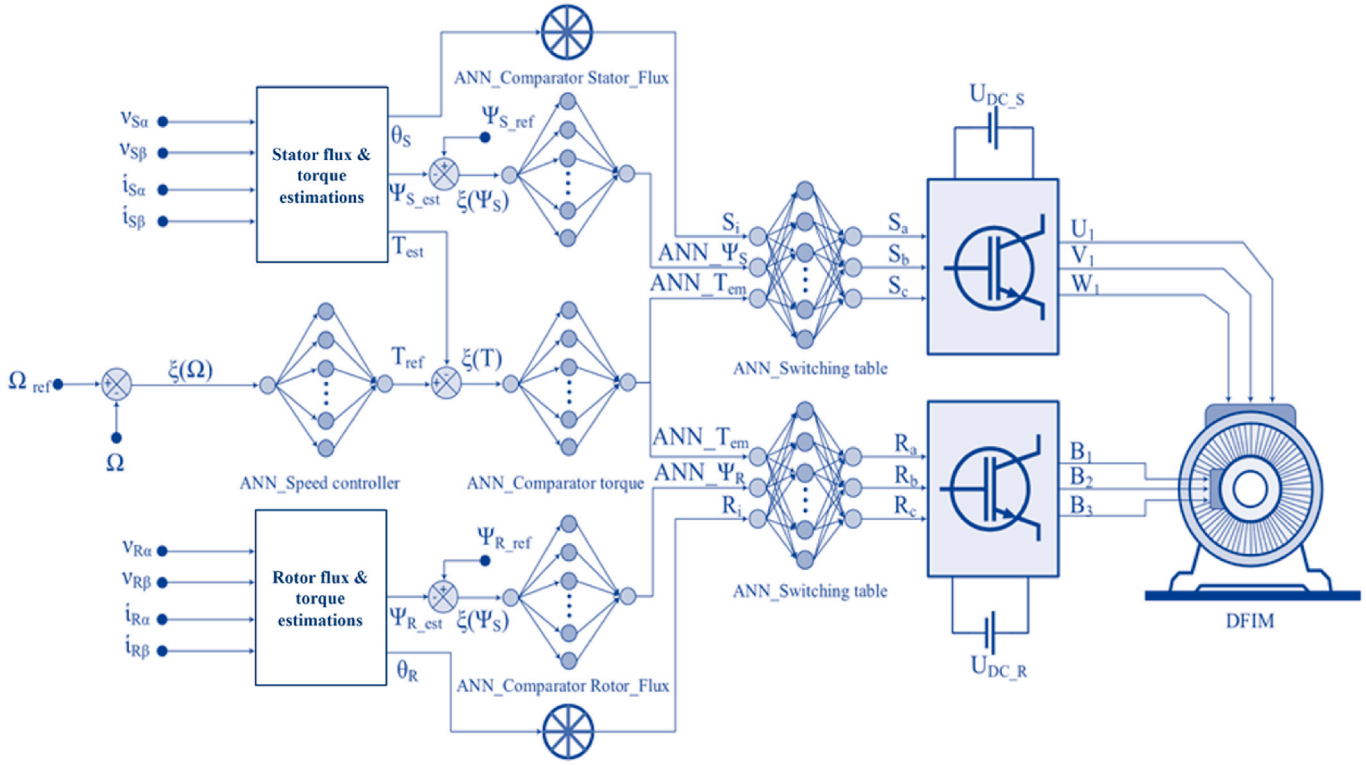

Fig. 24. Application of the ANN-DTC to a doubly-fed induction motor (DFIM).

algorithm optimization approach.

5.10. Operators and parameters of GA

The success of a GA is contingent upon the efficacy of its operators. These operators, which include selection, crossing, and mutation, are fundamental to the functioning of the GA. While the underlying principles of each operator are relatively straightforward, Explaining the importance of each operator in the overall performance of a GA can be challenging. This is partly due to the fact that each operator operates according to its own set of criteria, including the selective value of the individuals, the probability of activation of the operator, and so forth (Mahfoud et al., 2022f).

5.11. Chromosome coding

The method starts by encoding solutions in binary format, represented as chromosomes in the logical framework (El Mahfoud et al., 2021b). Genetic algorithms (GAs) use coding methods, which sets them apart from other search optimization procedures. Typically, a genetic algorithm utilizes binary coding (Soleimani and Kannan, 2015). Due to the variability of circumstances, it is not possible to definitively determine the optimal coding strategy. Real numbers often prove practical, though their applicability is confined to specific issues. It's crucial to identify the performance boundaries of the PID controller before setting its coefficients. The discussed method stipulates that the minimum value for PID coefficients is zero. Addressing encoding problems requires more than just using a Genetic Algorithm (GA). Hence, the effectiveness of the GA depends significantly on the chosen encoding format. In this approach, each PID parameter is considered a gene, with each gene encoded as a distinct chromosome (Shukla et al., 2019).

5.12. Fitness

The choice of the objective capacities considered to evaluate each chromosome's fittingness could be a pivotal stage in GA execution. Execution files were utilized in a few distributions (Bekakra et al., 2021c) as objective capacities. Whereas utilizing ISE, IAE, and ITAE in (El Ouanjli et al., 2017a), the creators of (Lyu and Lin, 2022) utilized mean squared blunder (MSE), fundamentally time outright mistake (ITAE), coordinates outright mistake (IAE), and necessarily square blunder (ISE). In this work, the speed mistake flag $e(t) = \Omega_{ref}(t) - \Omega(t)$ was minimized and compared utilizing the execution records IAE, ITAE, and ISE, as well as a combination of the three records, to decide which was most suitable. The taking after depiction of the execution files is required (Optimization of PID Tuning Using, 2021):

$$IAE = \int_0^t |e(t)|dt \tag{42}$$

$$ISE = \int_0^t e(t)^2 dt \tag{43}$$

$$ITAE = \int_0^t t \cdot |e(t)|dt \tag{44}$$

$$F_w = \omega_1 \times IAE + \omega_2 \times ISE + \omega_3 \times ITAE \tag{45}$$

where F_w is the weighted work, $e(t)$ is the mistake flag, and ω_1, ω_2, and ω_3 are the weights. The hereditary calculation was utilized in this work to play down the blunder between the reference and the genuine speed of the engine. This operation is carried out by expanding the wellness esteem spoken to by equation (46), which naturally diminishes the mistake. For each emphasis of the controller, picks are produced in such a way as to maximize wellness. Optimal arrangements are defined as gains that allow for a significant error (Amirjanov, 2015).

$$\boldsymbol{Fitness\_Value} = \frac{\mathbf{1}}{\boldsymbol{Objecitves\_Functions}} \tag{46}$$

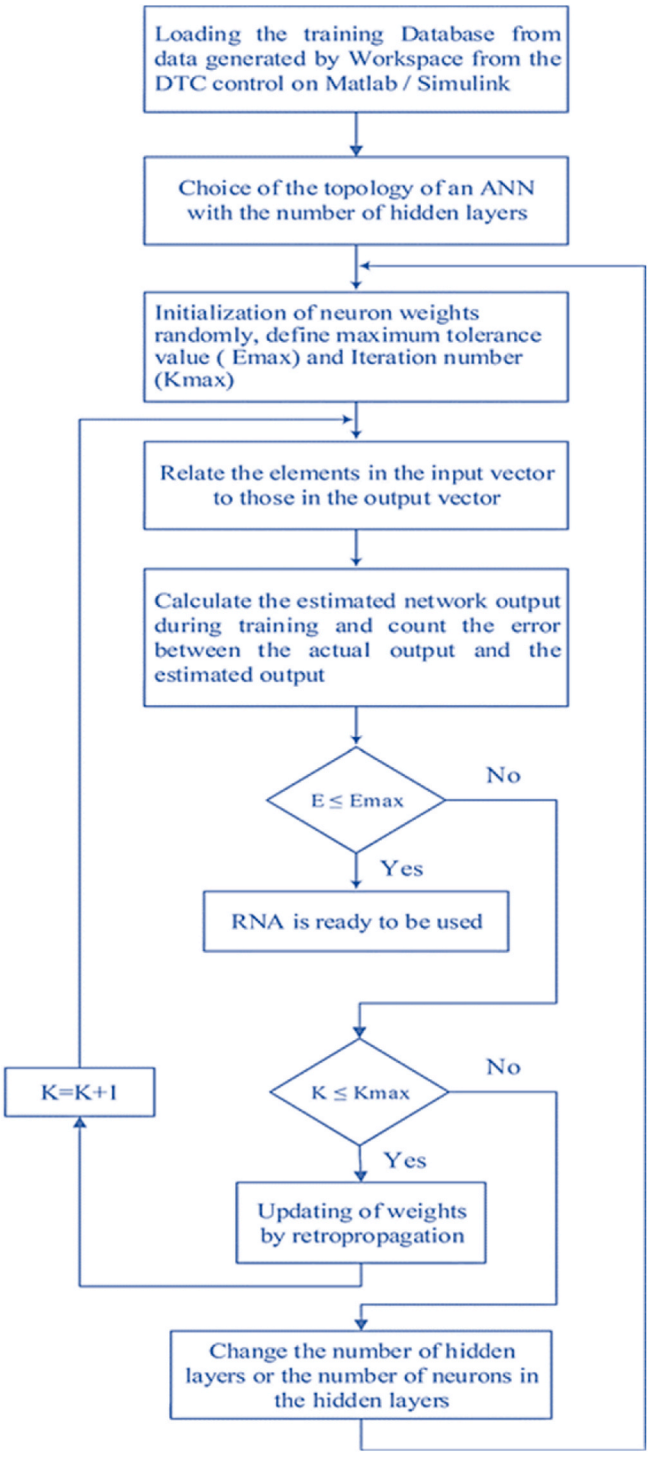

Fig. 25. The error backpropagation learning algorithm is utilized to construct a neural network.

5.13. Population initialization

After selecting the coding scheme, it is necessary to establish an initial population consisting of valid solutions to the issue. Various methods have been used in previous studies to create the initial population (‘Sustainability | Free Full). The user’s understanding of the issue determines the initialization selection. If there is no specific information available, the most appropriate approach is to randomly initialize the system in a way that evenly covers the whole search space, thereby promoting maximal exploration. Nevertheless, in other scenarios, it is feasible to use alternative techniques. Furthermore, this stage presents a primary

challenge, namely the population size selection. A population that is too large can significantly increase computational time and require substantial memory, while a population that is too small may only lead to the identification of local optima. Grefenstette observed that genetic algorithms exhibit optimal performance when the population size is within the range of 10–160 (Meena and Devanshu, 2017). Nevertheless, studies have demonstrated that the interactions between crossover, mutation, and population size are non-linear. Odeyato proposed a population size between 100 and 400, while Robertson investigated sizes up to 8000 (‘Systems | Free Full). In separate studies, Goldberg evaluated the optimal population sizes for both sequential and parallel GA. The initial choice of population size has a significant impact on the algorithm’s speed. In this study, the optimal population size was determined to be 20 individuals. This figure was arrived at following extensive testing and subsequent validation as an effective parameter.

5.14. Selection operator

During each generation ’i’, an intermediate population is created using the selection operator. This population is then combined and modified to form the population for the next generation ’$i+1$’. The selection of chromosomes is based on the adaptability levels of the individuals. There are various methods for selecting candidates, with the focus on the most effective ones:

1. The "ranking" method is the simplest form of selection. It involves organizing the n chromosomes of the population in order of their evaluations, either ascending or descending depending on the objective. The top **M** individuals are selected, ensuring that only the most elite individuals are retained.
2. Selection via a roulette wheel entail assigning a segment to each chromosome in proportion to its fitness. These segments are consolidated on a normalized axis ranging between 0 and 1 (uniform distribution between 0 and 1); subsequently, the selected segment and corresponding chromosome are identified. This method ensures that favorable chromosomes are chosen more frequently than unfavorable ones, allowing for the possibility of multiple selections of the same chromosome. However, the accurate mathematical expectation of selection may be challenging to obtain in small populations due to the limited number of draws, resulting in varying degrees of selection bias based on population size.
3. Tournament selection involves randomly selecting two or more individuals from the population, with the most robust individual being chosen, i.e., the one with the highest fitness level.
4. Random selection, as the name implies, involves choosing chromosomes based on a uniform distribution.

For this investigation, tournament selection was chosen, as it is commonly preferred by numerous researchers (gai Ye et al., 2017), (Comparison of the error; Direct torque control versus indirect).

5.15. Crossover operator

Crossover permits the fusion of genetic material from two parents to produce two children. The underlying assumption is that the resulting children acquire the most desirable qualities from their parents. The crossover approach entails combining the beneficial regions of the chromosomes belonging to the parents, labeled P1 and P2, to create two children, E1 and E2, with increased attributes. For instance, in a binary setting, the merger of two strings, 00000000 and 11111111, at the fifth bit position might give birth to two unique children, namely 11110000 and 00001111, each with a chance of 0.5, reflecting fifty percent of the genetic material (Colorni et al; Aparanji et al; A novel optimal PID controller). It is proposed to restrict the occurrence of crossover

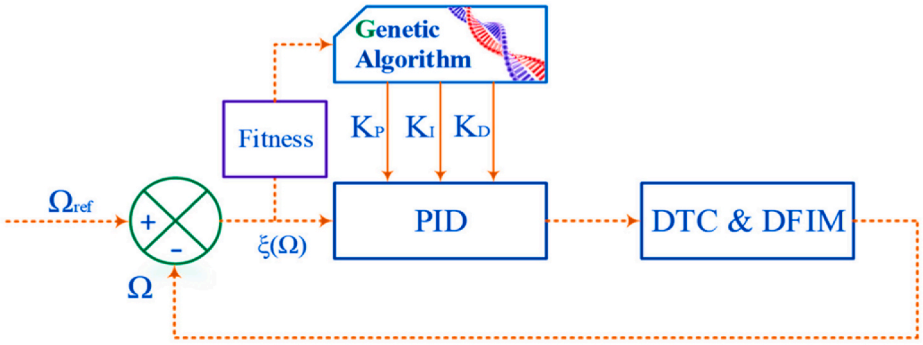

Fig. 26. Genetic algorithm (GA) is used to optimize the settings of the PID controller.

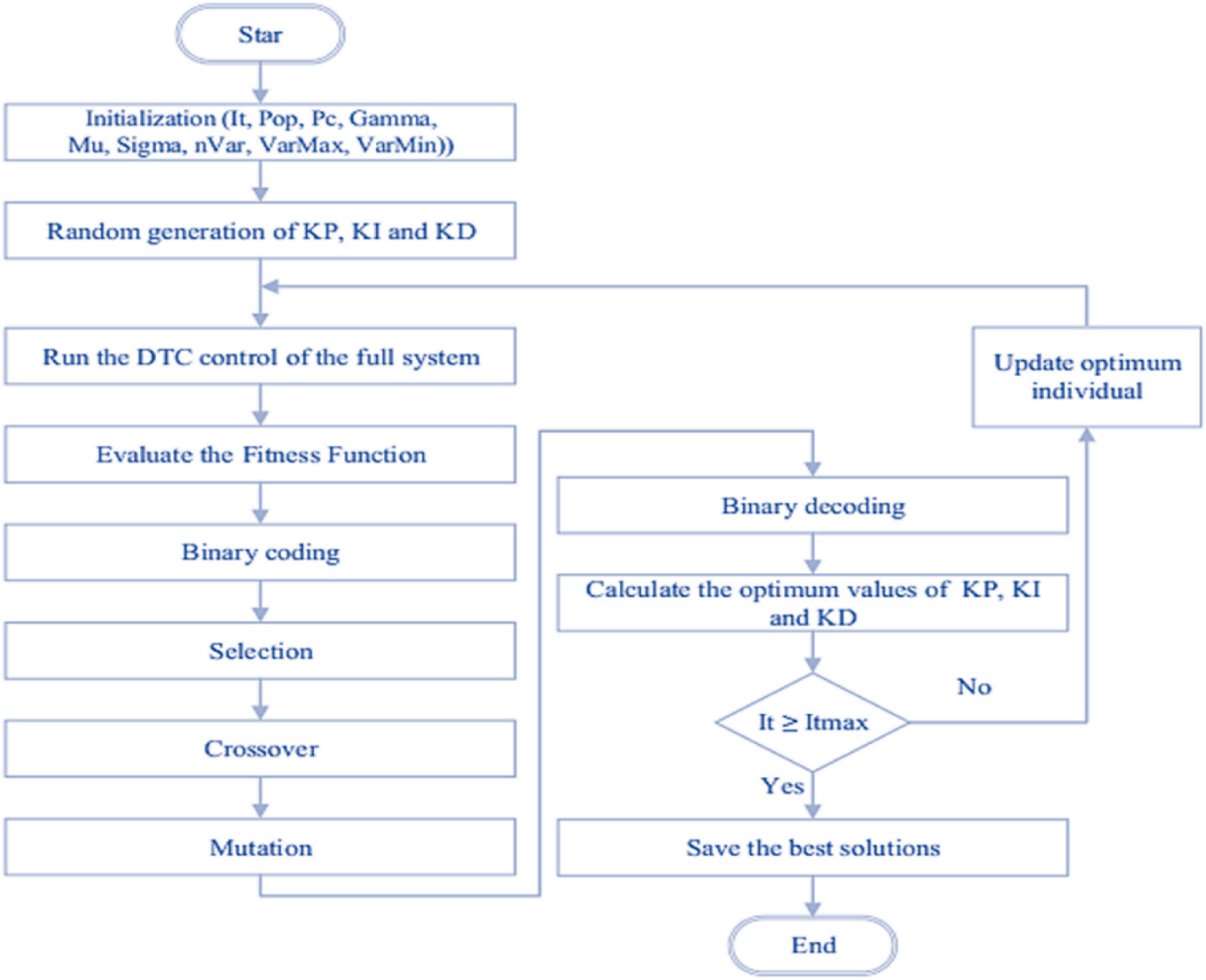

Fig. 27. Diagram illustrating the sequence of steps in the Genetic Algorithm.

occurrences by defining a probability value ranging from 0.6 to 0.99 ('Tuning PID Controller for Inverted). In the current experiment, a crossover probability of 0.8 was selected based on its usefulness as an appropriate parameter for the crossover operator.

5.16. *Mutation operator*

Fig. 27 displays a flowchart that conforms to the evolutionary principles of genetic algorithms (GA), while distinguishing the procedural processes required in a GA. In a GA, the algorithm delineates the sequence of operations. The function of mutation is to inhibit quick convergence to a local optimum, hence encouraging exploration of the

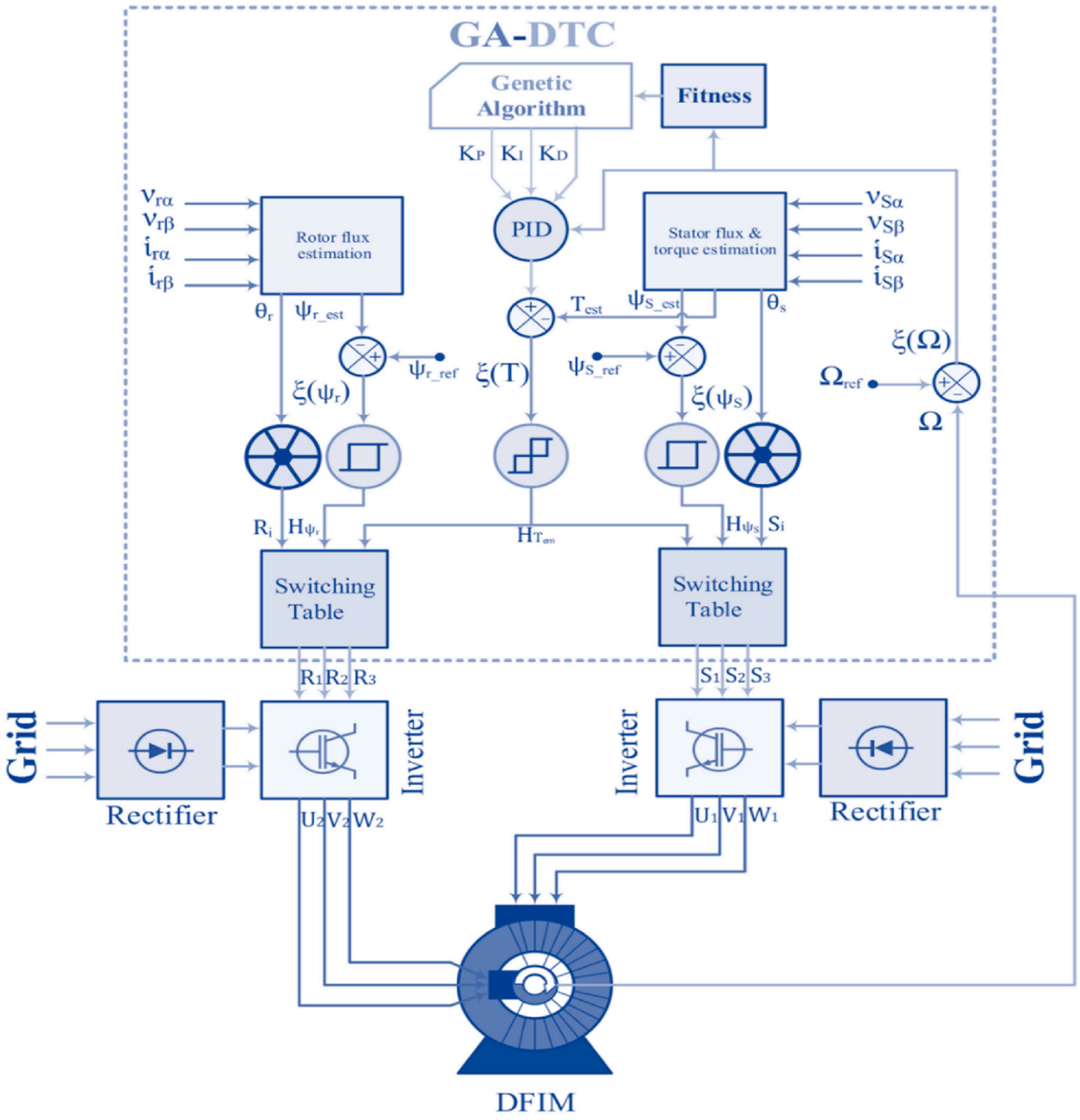

Fig. 28. The schematic diagram of DTC- GA control applied to DFIM.

search space. Mutation entails changing a chromosome to investigate a potentially more intriguing location within the search space. Despite endowing GA with ergodic qualities, mutation is typically seen as a supplemental operator that assures accessibility to all locations in the search space. Hence, the value of this operator cannot be over-emphasized. The mutation rate must lie between the ranges of $[0.001, 0.01]$ ('Energies | Free Full) to add unique information to the genetic chromosome and prevent the population from drifting towards a local optimum under specified conditions. In the cited research, the probability value (P_m) was fixed at 0.001 ('Energies | Free Full).

5. Ant Colony Optimization based Direct Torque Control (DTC-ACO)

Heuristically, the ant colony Optimization algorithm (ACO) has effectively simulated this ant foraging behavior in nature (A. Colorni). Nevertheless, of course, this algorithm became well-known for its global optimization ability without a problem description. Furthermore, its features include internal parallelism, positive feedback, and robustness. The ACO matches, most prominently, better than other algorithms in terms of higher reliability, more robust search capabilities, and ease of implementation, particularly on combinatorial optimization problems. These have interested many and have been tried in different disciplines. As a result, ACO has significantly advanced as a multidisciplinary topic. ACO has effectively solved the traveling salesperson problem (TSP) and numerous other problems, demonstrating reasonably good results. More research reveals that ACO can deal with NP-hard problems such as quadratic assignment, vehicle routing, and job shop scheduling primarily because of its improved learning system, which includes distributed computing, strong robustness, and an easy-to-integrate structure, making it collaborate with other optimization algorithms. It suffers from long search times and sometimes stalls, known as the pause phenomenon (Wang et al., 2023). Fig. 29's synoptic form describes the

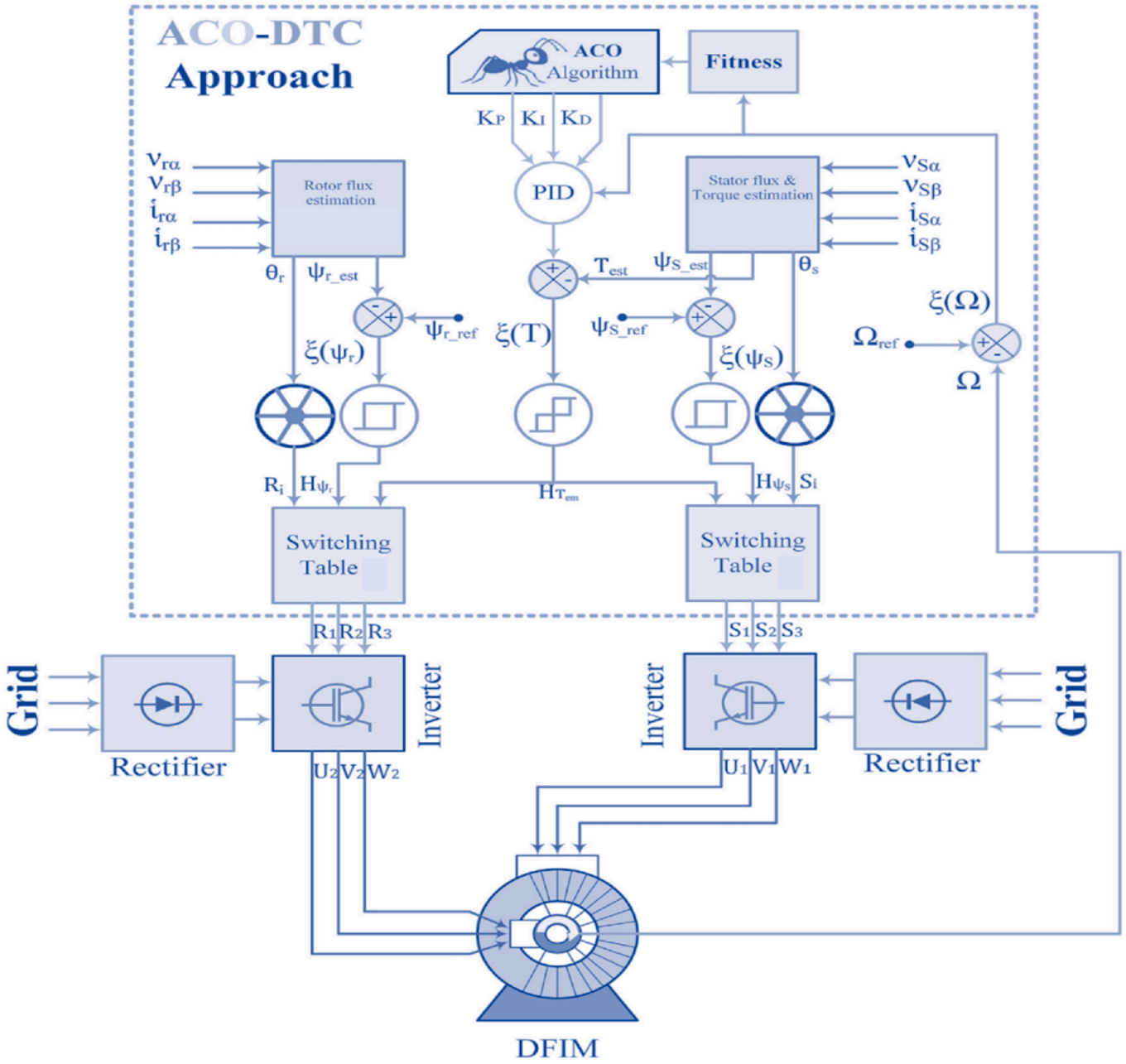

Fig. 29. The schematic diagram of DTC-ACO control applied to DFIM.

newly proposed DTC-ACO strategy, which is applied on both sides of the DFIM.

5.17. *Operating principle*

The ACO technique is a metaheuristic that draws inspiration from the foraging behavior of ants. Initially, ants move randomly within their environment. When they locate food (ND), they trace their way back to their colony (NS), depositing a pheromone trail along the route (Rezvanian et al., 2023), (Chiha et al., 2012). If other ants encounter this trail, they may cease their random search and follow the pheromone-marked path, thereby reinforcing it if it indeed leads to food. Consequently, the shortest route to the food source becomes increasingly popular and reinforced, making it the most attractive path. Less traveled paths weaken over time, leading all ants to eventually converge on the shortest, most efficient route. Fig. 30 illustrates this process, showing how ants select the shortest branch.

The Ant Colony Optimization (ACO) approach designates an ant as an autonomous agent capable of constructing potential solutions. There are two fundamental factors in deciding when an ant will be employed to build a solution.

(a) Visibility factor: Also known as the gluttonous force, it is represented by ηij, where $''ij''$ indicates the decision under consideration.
(b) Pheromone factor: represented by τij, where $''ij''$ represents the decision in question again. The higher the value of τij, the more historically beneficial it has proven to make this decision.

These factors influence the probability that a particular decision $''ij''$ will be selected by an ant, guiding its path-building activity in the solution space. This relationship underscores the probability that a particular decision will be favored based on past successes and immediate visibility or attractiveness.

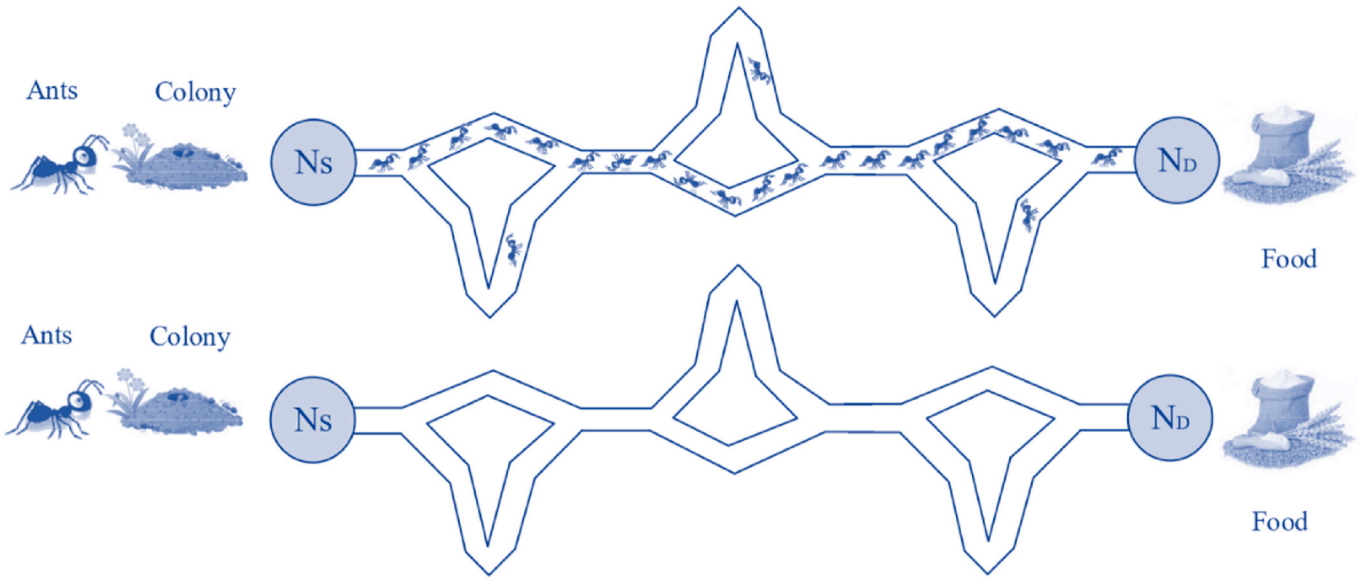

Fig. 30. The structure of the experiment concerning how a colony of ants selects the smallest branches.

$$p_{ij}^{k}(t)=\begin{cases}\dfrac{\left[\tau_{ij}(t)\right]^{\alpha}\cdot\left[\eta_{ij}(t)\right]^{\beta}}{\sum_{s\in J(i)}\left[\tau_{ij}(t)\right]^{\alpha}\cdot\left[\eta_{ij}(t)\right]^{\beta}}, \boldsymbol{j}\in J_i\\ 0, \boldsymbol{j}\notin \boldsymbol{J_i}\end{cases} \tag{47}$$

$\tau ij(t)$ is the pheromone amount on edges of node i to j at time t. $\eta ij(t)$ displays the visibility, or attractiveness, between nodes i and j, which varies according to conditions that help to solve the problem. The parameter α is the level of importance that gives the pheromone trail in making decisions, and β gives the importance weight of the visibility term. *Ni* is the set of unselected nodes.

5.18. Development of the integrated ACO and PID controller

So far, academics have investigated the optimization of PID controllers using the ACO algorithm, using various ways to improve the ACO's effectiveness. The use of ACO for parameter tuning of a Proportional-Integral-Derivative (PID) controller in a second-order process with multiple cost functions is described in reference (Varol and Bingul, 2004). The study demonstrates significant improvements compared to traditional tuning approaches. Fig. 31 depicts the optimization of the PID controller using the ACO block structure.

The problem of designing a PID controller using the ACO algorithm may be seen as a network problem similar to that shown in Fig. 32. In the network, every feasible value for each of the PID parameters, that is, K_P, K_I *and* K_D, is represented by three different vectors. These vectors can be thought of as paths that connect various nests in the network.

In such a scenario, an ant must move through three nests, making decisions at various nodes from the origin to the destination. In this scenario, the ACO's most preferred goal is to find a route with the minimum cost function in Equation (53) that connects the three found nests. At each step of movement, the ants drop pheromones on the chosen routes. These pheromone levels are then adapted by the reinforcement rule, wherein the trail strength is enhanced by the solution quality for a particular solution. More specifically, after it has finished an assigned tour, each ant updates pheromones on the path constructed through the local pheromone update rules as given in Equation (48). This enables fitter paths to acquire denser pheromone concentrations, guiding successive ants toward potentially optimal solutions.

$$\tau_{ij}(k)=\tau(k-1)+\frac{0.01\theta}{J} \tag{48}$$

The symbol $\tau_{ij}(k)$ represents the pheromone value between nest i and j at the k_{th} iteration.

The symbol θ represents the coefficient used for updating pheromones in a generic manner.

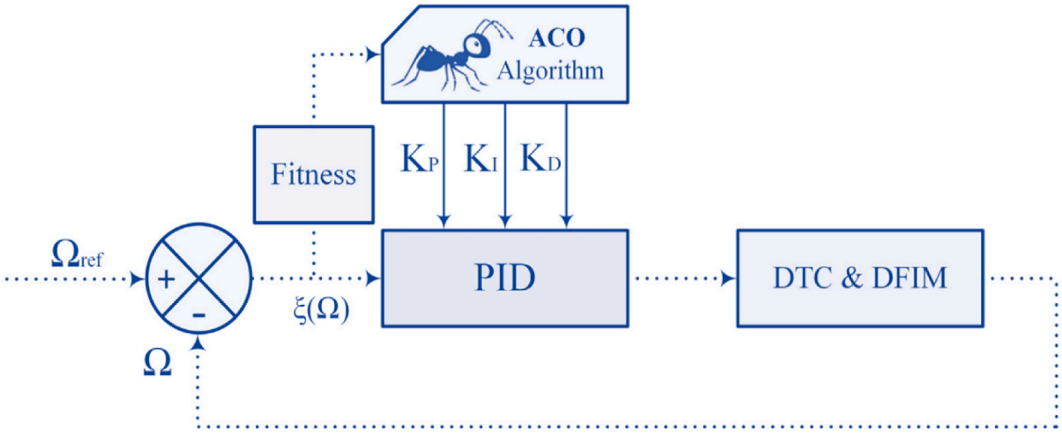

Fig. 31. Enhancing the PID controller using ant colony optimization.

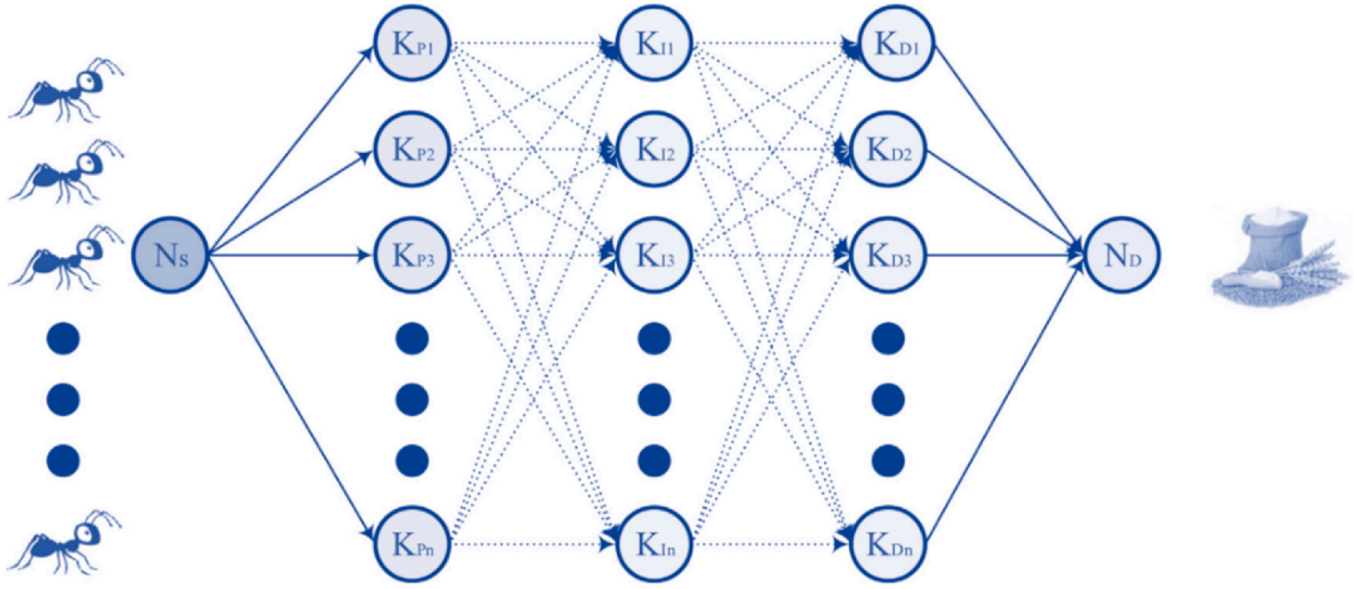

Fig. 32. Shows a graph of the ACO for the PID tuning process.

J represents the cost function associated with the trip taken by the ant.

The global pheromone updating rule adjusts the pheromone levels on paths belonging to the most successful ant colony tour Equation (49) and the least successful ant colony tour Equation (50):

$$\tau_{ij}(k)^{best} = \tau(k)_{ij}^{best} + \frac{\theta}{J_{bset}} \tag{49}$$

$$\tau_{ij}(k)^{worst} = \tau(k)_{ij}^{worst} - \frac{0.3\theta}{J_{worst}} \tag{50}$$

In this context, τ^{best} and τ^{worst} denote the pheromone concentrations on the routes traversed during the tours, with the minimum cost (J^{best}) and maximum cost (J^{worst}) correspondingly, inside a single iteration. The concentrations of pheromones on the pathways of the most successful tour are greatly elevated, whereas those on the paths of the least successful trip are diminished. Subsequently, pheromone evaporation, as detailed in Equation (51), allows the ant algorithm to essentially "forget" its prior activities, enabling the ACO to explore new options and avoid being constrained to local optima.

$$\tau_{ij}(k) = \tau(k)_{ij}^{\lambda} ij + \left(\tau(k)_{ij}^{worst} ij + \tau(k)_{ij}^{best} ij\right) \tag{51}$$

where λ is the evaporation constant (Zemmit et al., 2018), (Varol and Bingul, 2004).

5.19. Fitness

A crucial aspect of implementing the ACO is selecting appropriate cost functions to assess the fitness of each node. Various studies, such as those by (Particle Swarm Optimization; PDF, 2024; Sliding mode based DTC of, 2024) and (An enhanced ACO and PSO, 2024), utilize performance indices as cost functions. Specifically, in (Particle Swarm Optimization), the authors evaluate three distinct cost functions, Integral Time Absolute Error (ITAE), Integral Absolute Error (IAE), and Integral Square Error (ISE), both individually and in a weighted combination. Among these, the ISE has been demonstrated to be particularly effective in enhancing performance. Consequently, in this work, a weighted combination of these cost functions is employed to boost the efficacy of the ACO, thereby improving the overall system performance. This approach to performance indices is outlined by (Kanojiya and Meshram, 2012).

$$ISE = \int_0^t e(t)^2 dt \tag{52}$$

The PID controller is employed to minimize the error signal $e(t)$, thereby reducing the values of specific performance indices and, in turn, minimizing the equivalent value represented by knots. This reduction leads to the formation of knots. The adequacy of each node is determined as follows:

$$Fitness\ Value = \frac{1}{ISE} \tag{53}$$

5.20. ACO parameters

The method of PID optimization utilizing Ant Colony Optimization (ACO) is outlined in the following algorithm, with the matching flowchart displayed in Fig. 33.

This approach encodes PID controller parameters using 5000 nodes, each representing a possible solution for the parameters (K_P, K_I and K_D). Increasing the number of nodes boosts the accuracy of the solution updates. After extensive tests, the best ACO parameters were found to be $=$ 0.06 and $\lambda = 0.95$. Selecting adequate ACO parameters is critical for swiftly converging to optimum values. This paper presents a technique to assess optimum values and decreased convergence time. The initial parameters of the ACO algorithm

$(Var\ Pmax, VarPmin, VarImax, VarImin, VarDmax, VarDmin, and\ n\_iter))$ should be set to high values $(VarPmax = VarImax = VarDmax = 100, VarPmin = VarImin = VarDmin = -100, n\_iter = 100)$ to increase the likelihood of obtaining the best values for K_P, K_I and K_D. However, the system only converges after a specific duration. After this first phase, the algorithm parameters should be changed closer to the optimum gains discovered before to decrease the number of rounds and minimize execution time.

6. Rooted Tree Optimization Algorithm based Direct Torque Control (DTC-RTO)

The implementation of the Rooted Tree Optimization (RTO) method for optimizing DTC responses in DFIM has been investigated throughout various research studies. Bekakra et al. (2021b) provided a strategy where RTO was applied to tune integral-proportional (IP) controller

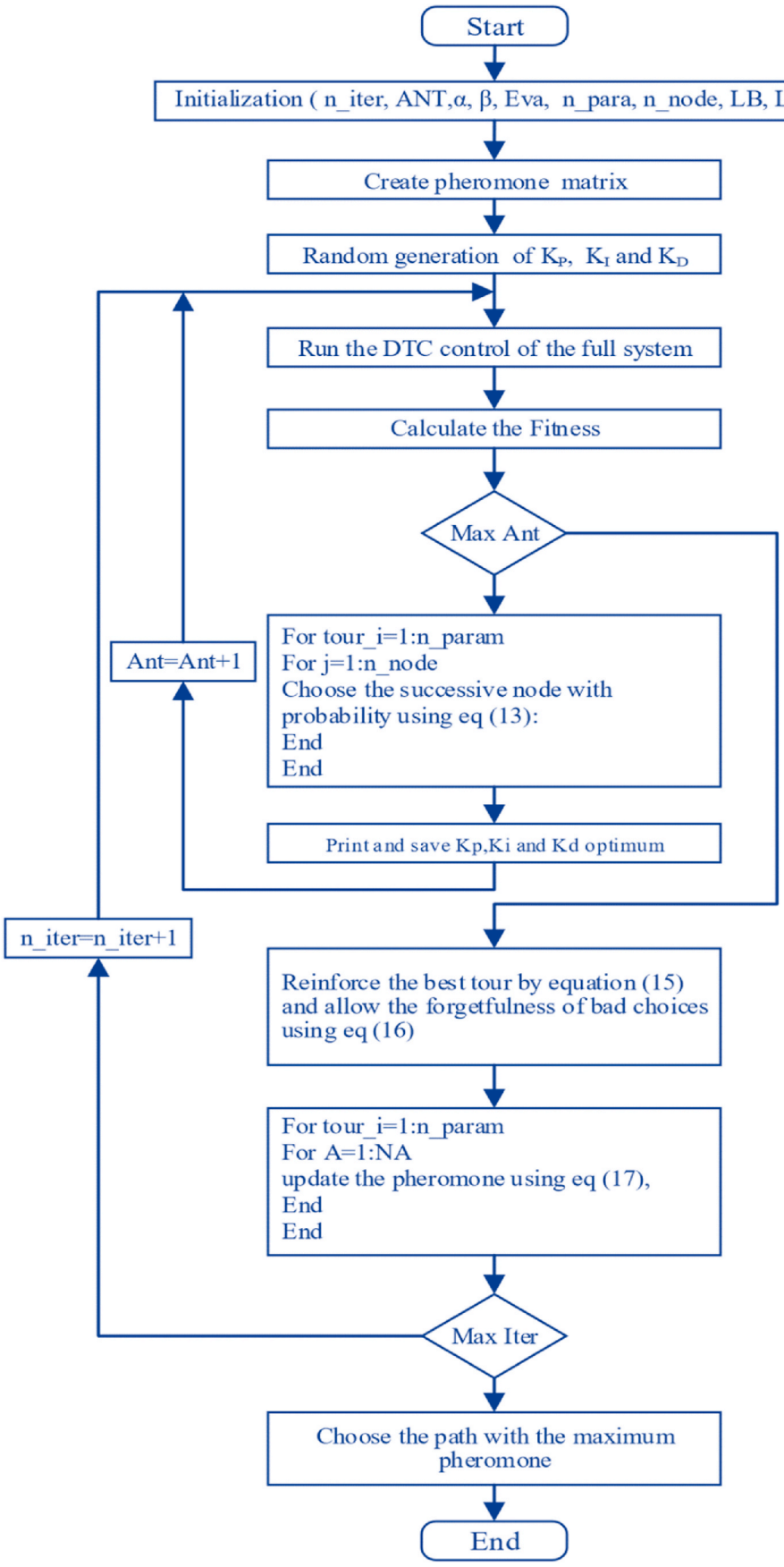

Fig. 33. Diagram illustrating the sequence of steps in the ACO algorithm.

settings in the speed loop control of DTC for DFIM, exhibiting increased performance over typical tuning approaches like Ziegler-Nichols and pole placement. The research revealed superior speed responsiveness and resilience against parameter alterations compared to conventional approaches and other optimization techniques such as fuzzy-PID and iterative feedback tuning (Bekakra et al., 2021b)

Edagbami et al. ('Improving the search pattern of) improved the RTO method by introducing Lateral Growth Rooted Tree Optimization (LGRTO), which removes the impact of the best root to avoid premature convergence. Edagbami et al. ('Improving the search pattern of) evaluated the LGRTO on benchmark functions and real-world applications, demonstrating competitive performance compared to other sophisticated optimization approaches.

5.21. Rooted tree optimizations

The Rooted Tree Optimization (RTO) algorithm, introduced in 2016 (Labbi et al., 2016), is inspired by the way desert plant roots search for water. Initially, roots start from the top of the stalk and extend into the first soil layer (initial generation). These roots explore randomly for moisture, and the root closest to the moisture source becomes the node for the next generation of roots, continuing the search for the optimal location (best solution) to access water, as shown in Fig. 34 (A novel rooted tree optimization).

5.22. Equations of RTO

The RTO technique, like to other algorithms, starts by generating an initial population at random. Within the RTO framework, each "root" signifies a possible solution, while the "Wetness Degree (D_w)" serves as the assessment measure, showing the fitness of a candidate relative to the rest of the population.

a. Rate of the nearest root to water (Rn)

The rate in question specifies the percentage of candidates from the whole population that should converge towards the wettest place, which is the ideal answer. The new population that congregates closest to the water supply is defined as follows:

$$x^{new}(k, iter+1) = x^{best}(iter) + c_1.D_w(k).randn.upper/(N.iter) \quad (54)$$

Where, *iter*: iteration step, $x^{new}(k, iter+1)$: new candidate for the iteration $(iter+1)$, $x^{best}(iter)$: best solution from the previous generation, *k*: candidate number, *N*: population scale, *upper*: upper limit of the parameter, *randn*: normal random number between $[-1, 1]$.

b. Rate of the continuous root in its orientation (Rc)

This rate signifies the proportion of members who continue the previous path as they are positioned near the water source. The new population originating from a randomly selected root is given by:

$$x^{new}(k, iter+1) = x(k, iter) + c_2.D_w(k).rand.\left(x^{best}(iter) - x(k, iter)\right) \quad (55)$$

Where, $(k,iter)$: Represents the candidate from the previous iteration *iter*, *rand*: Is a random number between $[0, 1]$.

c. Random Root Rate (Rr)

This measures the ratio of selected candidates to the entire population, dispersed randomly across the search space to increase the chances of discovering the global solution. Furthermore, roots from the prior generation that exhibit a low wetness degree are substituted. A new set of random roots is then established for the population.

$$x^{new}(k, iter+1) = x_r(iter) + c_3.D_w(k).randn.upper/iter \quad (56)$$

Where:

$x_r(iter)$: Represents a randomly selected individual from the previous generation,

c_1, c_2 and c_3 are adjustable parameters that can be tuned as needed. The rates R_n, R_r *and* R_c are determined experimentally based on the specific problem being addressed. These rates are considered variables that influence the rate of convergence (Labbi et al., 2016).

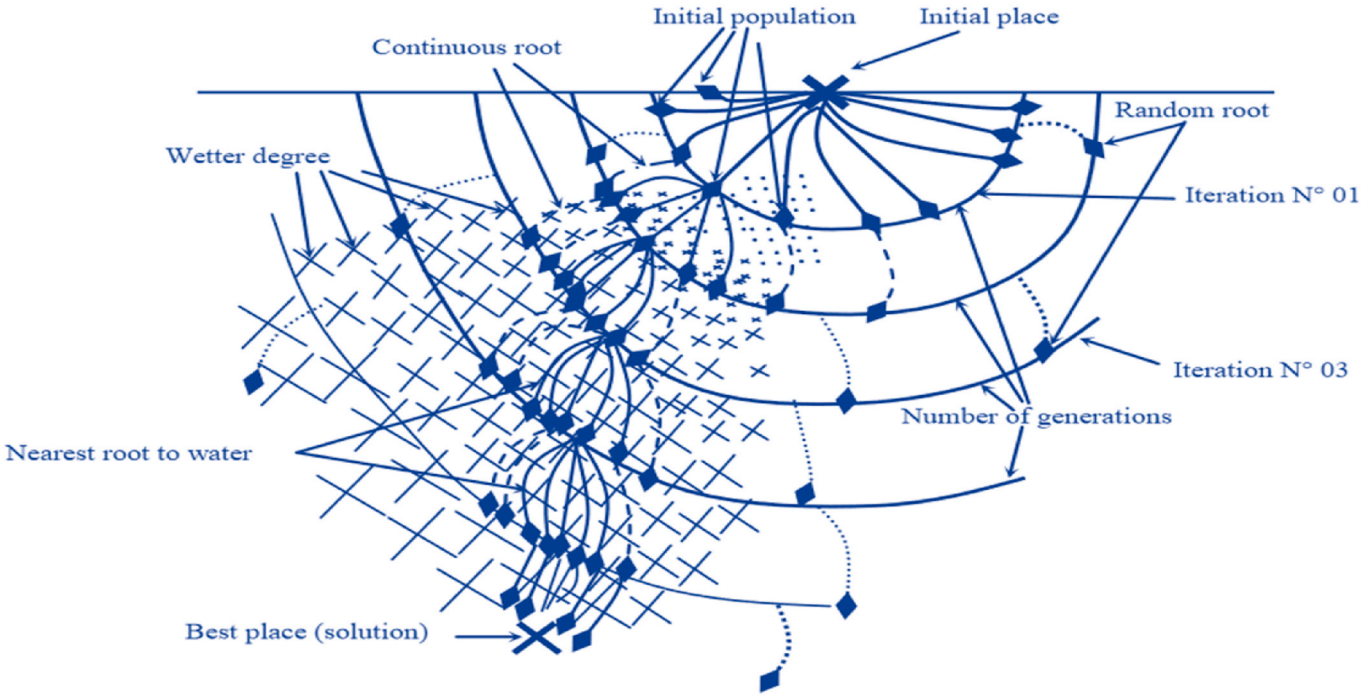

Fig. 34. Root behavior of desert plants in their search for water.

5.23. RTO algorithm

The RTO algorithm progresses through the following steps.

Step 1: Initialize the Population

Create an initial set of N candidates, each randomly positioned within the variable limits of the research space. At this initial phase, establish numerical values for the rates R_n, R_r and R_c.

Step 2: Evaluate the Population

Assess all members of the population by calculating their objective function, known as the wetness degree D_w, which is defined as:

$$D_w(k)=\begin{cases}\dfrac{f_k}{max(f_k)} & \text{for the maximum objective function}\\ 1-\dfrac{f_k}{max(f_k)} & \text{for the minimum objective function}\end{cases},k=1,2,\ldots,N \tag{57}$$

Step 3: Reproduction and Replacement

Generate a new population by rearranging the current population according to the wetness degree D_w. Replace individuals based on the rates R_n, R_r and R_c using the designated equations (Eqs. (54)–(56)).

Step 4: Iteration

Repeat Step 2 unless the predefined stopping criteria are met, indicating either convergence or the fulfillment of other specified conditions.

These steps provide a clear and systematic approach to the process from initialization to potential convergence. They guide through evaluation, adaptation, and iterative improvement based on the simulated behaviour of root systems in nature.

5.24. RTO applied to PID controller

The responses of several simulated systems to a unit step in reference input are examined to demonstrate the proposed method's effectiveness in a control system. The systems considered for the PID controller problem are of different orders (second, third, and fourth) (Fuzzy gain scheduling of PID controllers, 2024) as follows:

$$G_1(s)=\frac{e^{-0.5s}}{(s+1)^2} \tag{58}$$

$$G_2(s)=\frac{4.228}{(s+0.5)(s^2+1.64s+8.456)} \tag{59}$$

$$G_3(s)=\frac{27}{(s+1)(s+3)^3} \tag{60}$$

Additionally, the proposed algorithm, along with the IFT method, has been rigorously tested on three additional simulated systems (Lequin et al., 2003).

$$G_4(s)=\frac{e^{-5s}}{20s+1} \tag{61}$$

$$G_5(s)=\frac{1}{(10s+1)^8} \tag{62}$$

$$G_6(s)=\frac{(1-5s)e^{-3s}}{(10s+1)(20s+1)} \tag{63}$$

A block diagram of a simplified control system demonstrating this setup is shown in Fig. 35. These configurations allow for a comprehensive evaluation of the control strategy across a variety of system dynamics.

In practical applications, the output of the PID controller is defined by the following formula:

$$u(t)=K_P\left[e(t)+\frac{1}{K_I}\int_0^t e(t)+K_D\frac{de(t)}{dt}\right] \tag{64}$$

For the PID controller, the transfer function that goes with it is:

$$G_{PID}(s)=K_P\left[1+\frac{1}{K_I s}+K_D s\right] \tag{65}$$

where:

K_P represents the proportional gain, K_I is the integral action time, K_D is the derivative action time and $e(t)$ is the error between the input and the output of the process at time ' t '.

The fundamental objective of multi-objective optimization is to achieve equilibrium between contending objectives. Multiple solutions that concurrently optimize all considered objectives are frequently presented in such problems, with no single solution being clearly superior. In general, no single solution is superior in all respects. Performance criteria for control system applications frequently include a weighted combination of various characteristics, such as overshoot and settling time. The optimal system response should minimize the settling time (T_s) while maintaining a low or nonexistent level of overshoot (O_{sh}). As a result, the objective function *Obj* is established by:

$$Obj=min\ (F) \tag{66}$$

Where.

$F=[f_1 \quad f_2]^T$: vector of the objective functions,
f_1: settling time (T_s)
f_2: overshoot (O_{sh})

The objective function can be formulated as:

$$Obj=\alpha_1 f_1+\alpha_2 f_2 \tag{67}$$

where:

α_1 and α_2 are adjustable parameters.

In Equation (67), the primary focus of the objective function is on settling time and overshoot, as these are crucial for ensuring the system's response is both quick and stable. A faster settling time and minimal overshoot reduce the area between the input and output, minimizing error in a closed-loop system.

The study investigates the use of a PID controller, optimized with Rooted Tree Optimization (RTO), for managing various linear systems with constant time delays, specifically $G_1(s), G_4(s)$ and $G_6(s)$. It is important to highlight that if the time delay fluctuates, the controller may need frequent re-tuning to adjust its gains in response to changes in the system model. This adaptation is vital for maintaining stability and enhancing performance, as the controller utilizes fixed gains that have been optimized through offline tuning with RTO.

5.25. Adjustment of the PI speed controller using the pole placement technique and RTO

In speed control loops, an PI controller is favored for its effective response, especially in rejecting disturbances (Comparison of Proportional, 2024). This section examines two tuning methods for an PI speed controller: the classical pole placement method and the optimization of a multi-objective function (Equation (67)) using Rooted Tree Optimization (RTO). The RTO algorithm iteratively adjusts the gains *Ki* and *Kp* based on feedback from the closed-loop speed transfer function, as

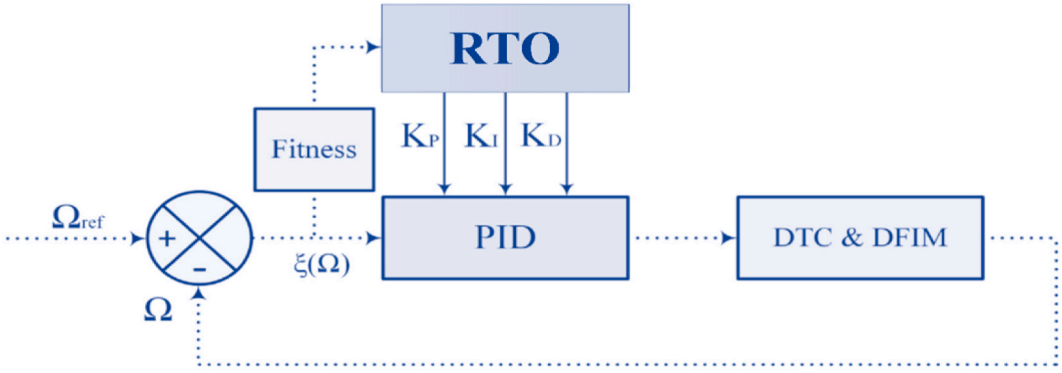

Fig. 35. Shows a block design of a PID controller built on a simpler control system.

shown in Fig. 36.

a PI speed controller tuned by pole placement method

The closed-loop speed transfer function, as illustrated in Fig. 36, is expressed as:

$$\frac{\Omega_r(s)}{\Omega_r^*(s)} = \frac{1}{\frac{J}{K_P K_I}s^2 + \frac{K_P+f}{K_P K_I}s + 1} \tag{68}$$

This function can be compared to a standard second-order system given by:

$$F(s) = \frac{1}{\frac{1}{\omega_n{}^2}S^2 + \frac{2\xi}{\omega_n}S + 1} \tag{69}$$

From this comparison, the following relationships are derived:

$$\begin{cases} \dfrac{J}{K_P K_I} = \dfrac{1}{\omega_n{}^2} \\ \dfrac{K_P+f}{K_P K_J} = \dfrac{2\xi}{\omega_n} \end{cases} \tag{70}$$

These equations lead to the solutions for the controller gains:

$$\begin{cases} K_P = 2J\xi\omega_n - f \\ K_I = \dfrac{J\omega_n{}^2}{K_P} = \dfrac{J\omega_n{}^2}{2J\xi\omega_n - f} \end{cases} \tag{71}$$

and K_P is proportional gain, K_I is integral gain, ξ is damping factor and ω_n is natural frequency.

b Stability Conditions for the PI Speed Controller

Stability is essential for the optimal performance of control systems. Referring to Equation (68), which defines the closed-loop speed transfer function with an PI controller, the denominator of this function is expressed as:

$$D(s) = \frac{J}{K_P K_I}s^2 + \frac{K_P+f}{K_P K_I}s + 1 \tag{72}$$

The roots of the denominator $(D(s) = 0)$ equation (68) describes the poles of the system. The calculations yield:

$$\begin{cases} s_1 = -\dfrac{1}{2J}\left[K_P + f - \sqrt{(K_P)^2 + 2K_P f - 4JK_I K_P + f^2}\right] \\ s_2 = -\dfrac{1}{2J}\left[K_P + f + \sqrt{(K_P)^2 + 2K_P f - 4JK_I K_P + f^2}\right] \end{cases} \tag{73}$$

Substituting the values of the DFIM parameters, J and f into Equation (72), we obtain:

$$\begin{cases} s_1 = -\dfrac{5}{2}\left[K_P - \sqrt{(K_P)^2 - \dfrac{4}{5}K_I K_P}\right] \\ s_2 = -\dfrac{5}{2}\left[K_P + \sqrt{(K_P)^2 - \dfrac{4}{5}K_I K_P}\right] \end{cases} \tag{74}$$

For stability, all system poles must reside in the left-half of the complex plane (ScienceDirect), meaning their real parts must be purely negative. Defining the poles as:

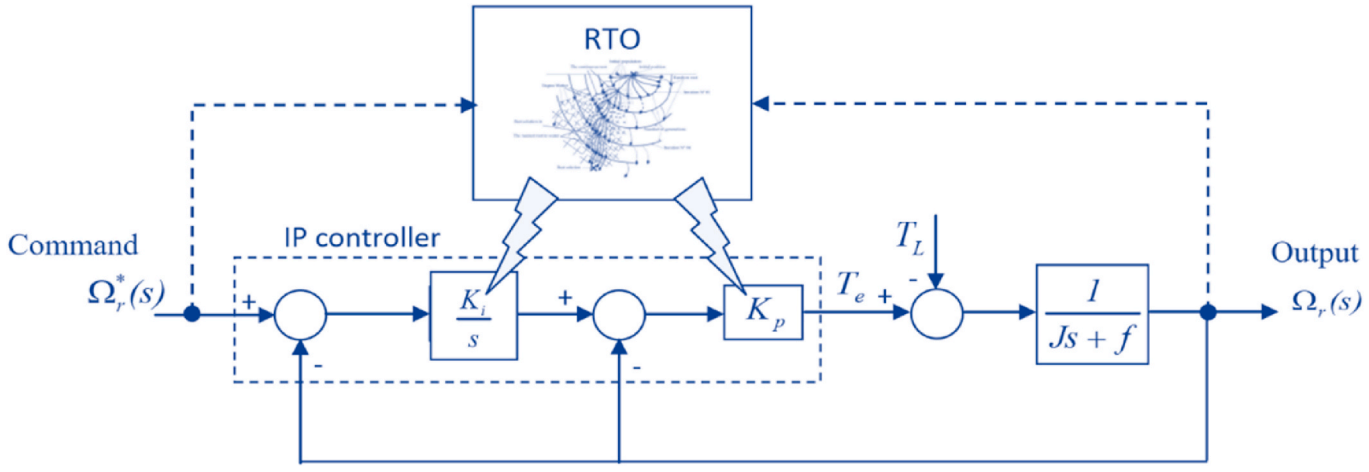

Fig. 36. Tuning of PI speed controller.

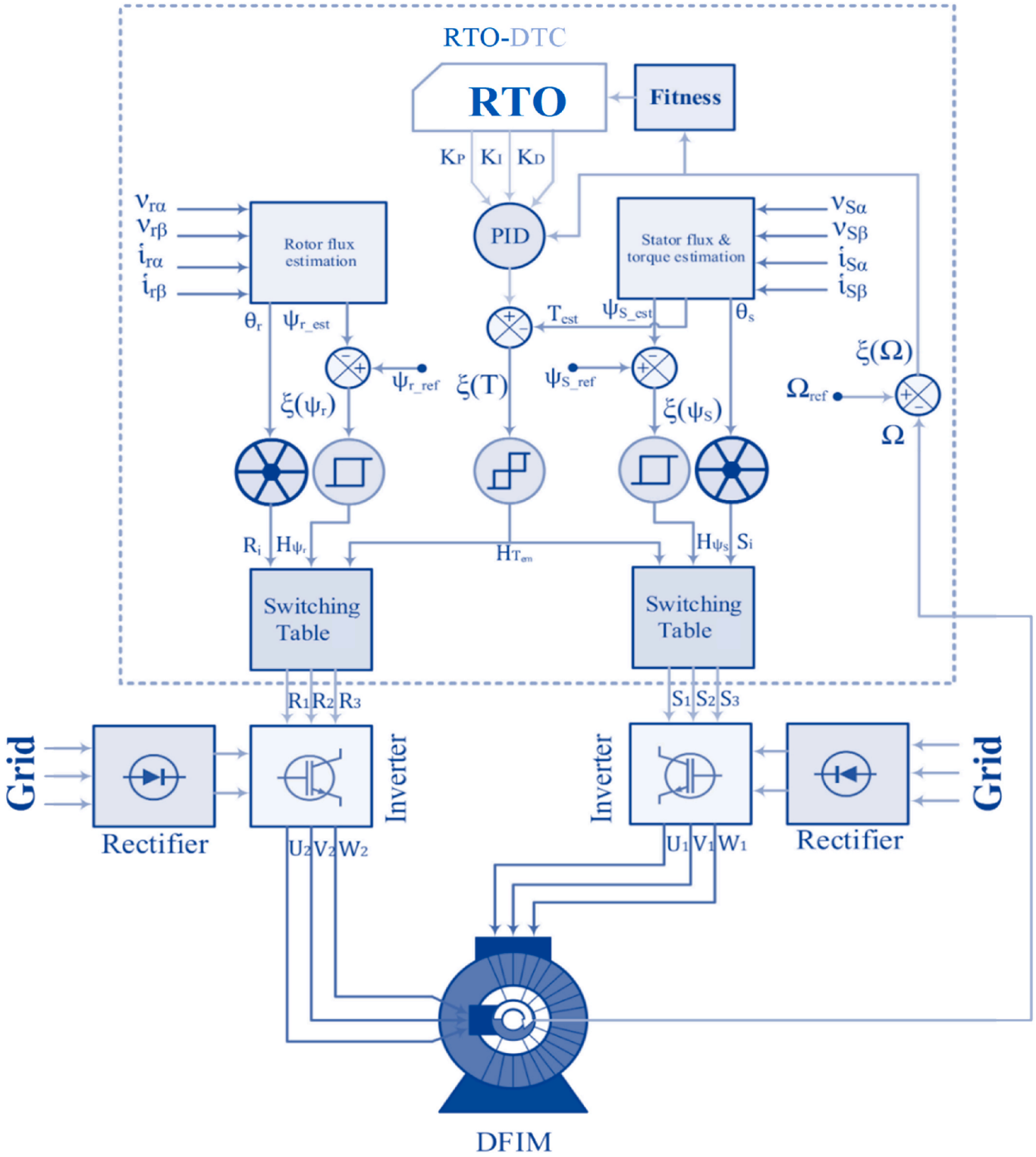

Fig. 37. The schematic diagram of DTC- RTO control applied to DFIM.

$$\begin{cases} s_1 = A_1 + jB_1 \\ s_2 = A_2 + jB_2 \end{cases} \tag{75}$$

where: A_1 and A_2 are the real parts of the poles s_1 and s_2, respectively, B_1 and B_2 are the imaginary parts of the poles s_1 and s_2, respectively. and,

$$\begin{cases} A_1 = -\frac{5}{2}\left[K_P - \sqrt{(K_P)^2 - \frac{4}{5}K_P K_I}\right] \\ B_1 = 0 \\ A_1 = -\frac{5}{2}\left[K_P + \sqrt{(K_P)^2 - \frac{4}{5}K_P K_I}\right] \\ B_2 = 0 \end{cases} \tag{76}$$

Hence, the system is considered stable if:

$$\begin{cases} A_1 \langle 0 \\ and \\ A_2 \langle 0 \end{cases} \Longrightarrow \begin{cases} -\frac{5}{2}\left[K_P - \sqrt{(K_P)^2 - \frac{4}{5}K_P K_I}\right] \langle 0 \\ and \\ -\frac{5}{2}\left[K_P + \sqrt{(K_P)^2 - \frac{4}{5}K_P K_I}\right] \langle 0 \end{cases} \tag{77}$$

Thus, according to Equation (76), the system remains stable under the condition that:

$$K_i > 0 \; and \; K_p > 0 \tag{78}$$

5.26. PI speed controller tuned by RTO

The PI speed controller, tuned by the RTO, aims to improve the dynamic response and either minimize or eliminate steady-state errors in the system. We look at transient response indices like settling time (*Ts*), overshoot (*Osh*), integral absolute error (*IAE*), integral square error (*ISE*), and integral time absolute error (ITAE) to figure out how well the PI-controlled system works. Fig. 37 displays the complete DTC diagram for a DFIM with an PI controller adjusted via RTO. The primary objective is to fine-tune the gains of the PI controllers, K_I and K_P, using the system illustrated in Fig. 37. The optimization of these parameters is achieved by the RTO method, which starts with an initial population and aims to minimize the objective function outlined in Equation (68). Each gain, K_I and K_P, is represented by a number of roots, determined experimentally to yield optimal results, with a single root in two dimensions symbolizing the best values for K_I and K_P. Fig. 38 presents a flowchart of the RTO-based tuning method for the PI controller within the DFIM's DTC system. The process begins with a randomly selected initial population for the two dimensions (gains K_I and K_P). The DTC-DFIM model then evaluates the objective function for each population member as per Equation (68). Throughout each iteration, a single minimum objective function value is recorded, preserving the optimal K_I and K_P values associated with this minimum. The algorithm concludes once it reaches the preset maximum number of iterations, solidifying the best values found for the objective functions across all iterations (see Fig. 39).

7. Predictive based Direct Torque Control (P-DTC)

Predictive-based Direct Torque Control (P-DTC) is an advanced control strategy designed for managing complex industrial systems. It works by predicting the system's future behavior using a dynamic model within the controller, allowing for the calculation of optimal control parameter values (Camacho, 1993). The use of Model Predictive Control (MPC) in digital control systems has proven to enhance both speed and precision ('Model Predictive Control | SpringerLink).

Applying a predictive control strategy to Direct Torque Control (DTC) has gained recognition for its ability to minimize the switching frequency of the voltage inverter and reduce torque and flux ripples. In P-DTC setups, the conventional DTC switching table is replaced by an online optimization algorithm that selects vectors based on a predefined cost function ('[PDF] Model Predictive Direct Torque, 2024), (Zeinaly et al., 2011), (Papafotiou et al., 2009). Predictive models for stator flux, torque, and angular velocity are used to forecast the future states of these control variables.

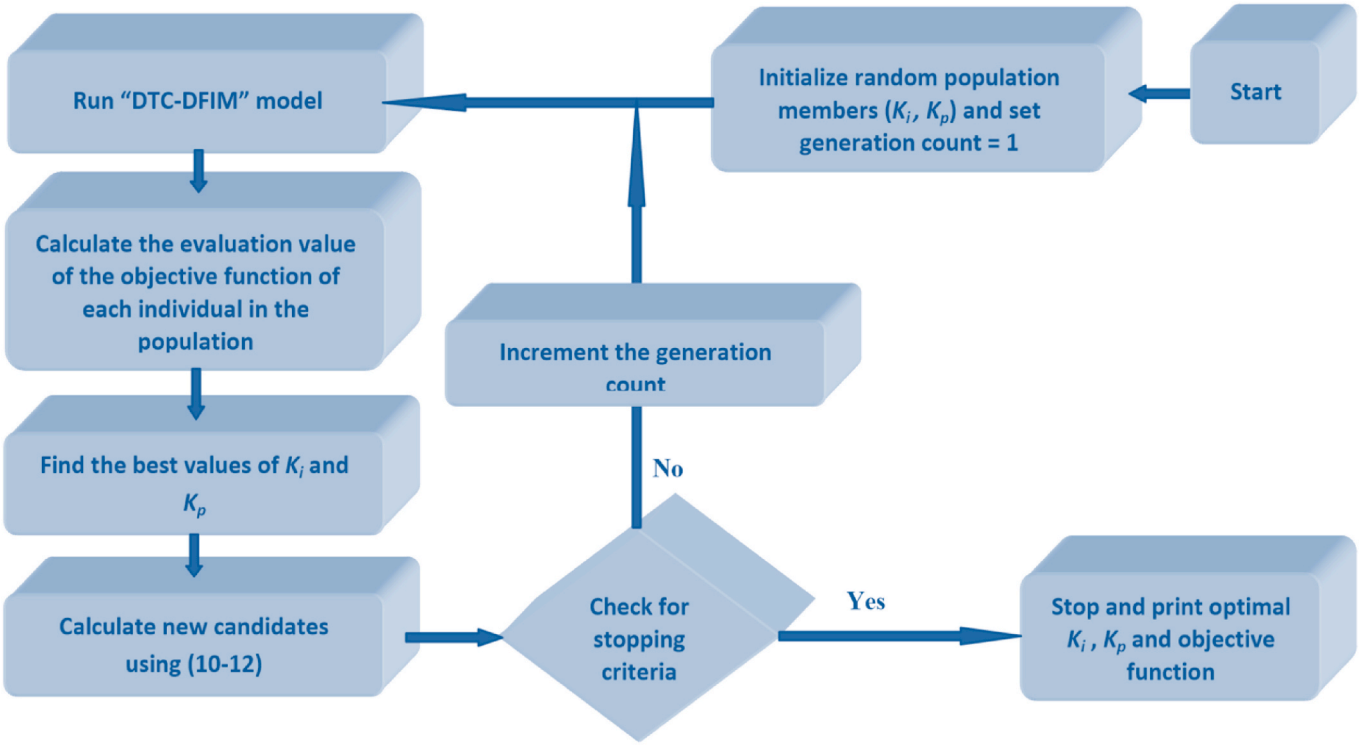

Fig. 38. Flowchart of the DTC-RTO.

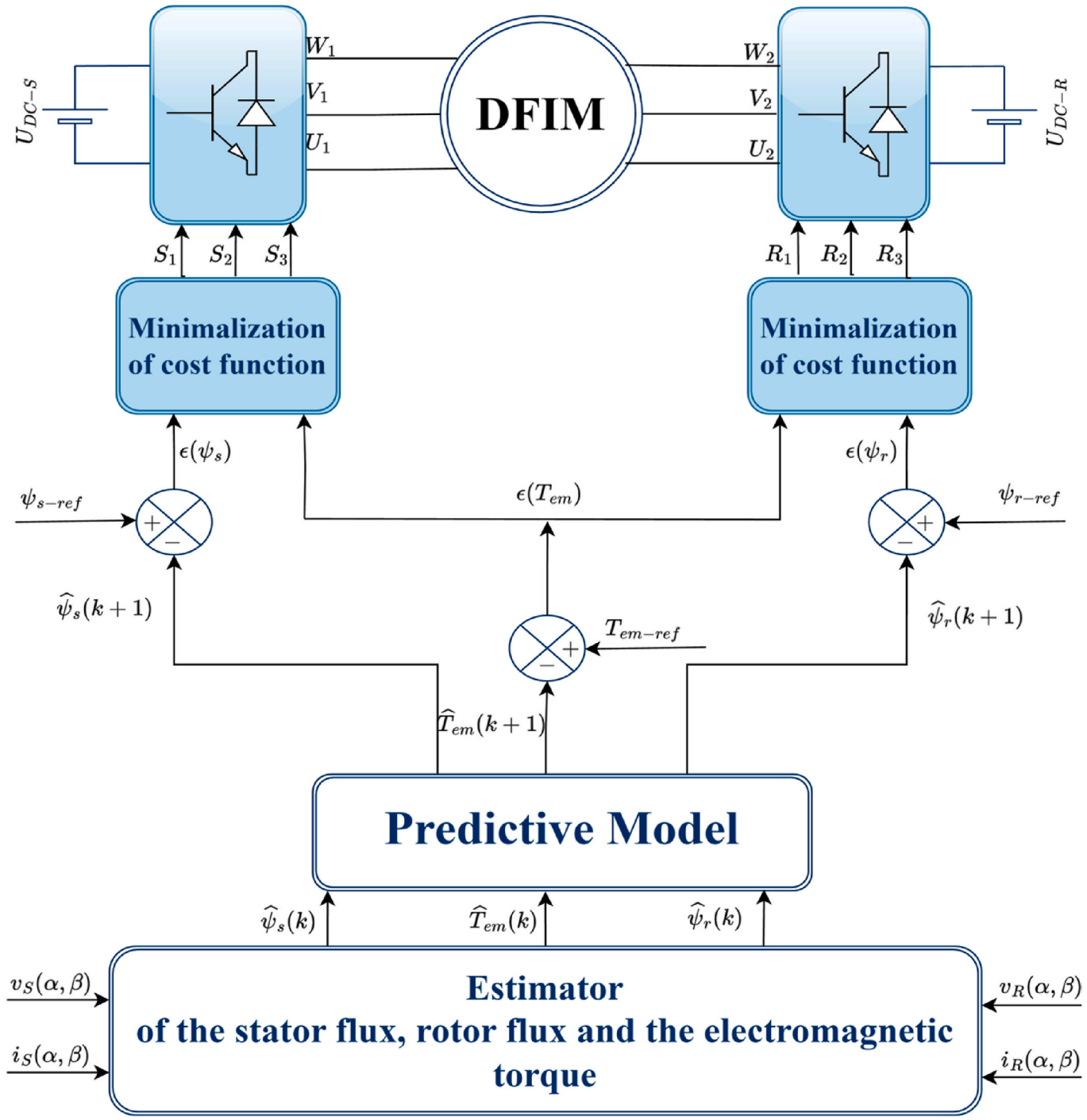

Fig. 39. Block diagram of the P-DTC.

At each sampling interval, new measurements are incorporated, and the process repeats to achieve closed-loop control. Feedback from these measurements guides the predictions and adjustments needed to minimize the cost function value (Wang et al., 2018), ('Performance Evaluation of DTC, 2024). The straightforward nature of the MPC concept makes it simple to implement, accommodating system constraints, nonlinearities, and multivariable systems ('[PDF] Model Predictive Direct Torque, 2024), ('M. Mossa and S). However, this control method requires more extensive online computation than traditional DTC.

Previous studies have introduced predictive control strategies that optimize a cost function over a specified horizon, enhancing disturbance rejection, robustness against parameter variations, and overall system efficiency. These strategies have significantly improved DTC's dynamic performance, delivering quick responses, reduced torque and flux ripples, and better current waveforms (Zeinaly et al., 2011), (Papafotiou et al., 2009), (Wang et al., 2018), ('Performance Evaluation of DTC, 2024), (Pacas and Weber, 2005).

5.27. Stator and rotor flux estimation

In the PTC approach, the estimation of stator and rotor fluxes at the current sampling step k is crucial. By employing the Euler method for derivative approximations along with necessary substitutions, the following equations are derived for flux estimations:

- The estimated stator flux at step k is given by:

$$\hat{\bar{\varphi}}_s(k) = \hat{\bar{\varphi}}_s(k-1) + T_s\bar{v}_s(k) - R_sT_s\bar{i}_s(k) \tag{79}$$

- The rotor flux estimation is updated using the relationship:

$$\hat{\bar{\varphi}}_r(k) = \frac{L_r}{L_m}\hat{\bar{\varphi}}_s(k) + \bar{i}_s(k)\left(L_m - \frac{L_sL_s}{L_m}\right) \tag{80}$$

5.28. Torque and flux prediction

An analysis of the electromagnetic torque T_s and the stator flux ψ_s for each voltage vector of a 2-level voltage source inverter (2L-VSI) is necessary. If the value of (**79**) has been modified at the subsequent sample moment $k+1$, the stator flux will be forecasted.

$$\bar{\varphi}_s^p(k+1) = \hat{\bar{\varphi}}_s(k) + T_s\bar{v}_s(k) - R_sT_s\bar{i}_s(k) \tag{81}$$

Torque prediction is based on the predicted values of stator flux and current:

$$T^p(k+1) = \frac{3}{2}pIm\left\{\bar{\varphi}_s^p(k+1)\bar{i}_s^p(k+1)\right\} \tag{82}$$

Prediction of the stator current for the subsequent instant $k+1$ utilizes the Euler method:

$$\bar{i}_s^p(k+1) = \left(1+\frac{T_s}{\tau_\sigma}\right)\bar{i}_s(k) + \frac{T_s}{\tau_\sigma + T_s}\left\{\frac{1}{R_\sigma}\left[\left(\frac{k_r}{\tau_r} - k_rj\omega\right)\hat{\bar{\varphi}}_r(k) + \bar{v}_s(k)\right]\right\} \tag{83}$$

5.29. Cost function optimization

With the stator flux expressed in terms of the inverter voltages $V_s(k)$, seven different predicted values of stator flux and torque are computed. These values are then evaluated using a Cost function to determine the optimal voltage vector:

$$g_h = |T^* - T^p(k+1)| + \lambda_\psi|\varphi_s^* - \bar{\varphi}_s^p(k+1)| \tag{84}$$

Where, λ_ψ is a weighting factor that prioritizes control objectives (Amiri et al., 2018).

8. Sliding Mode Control based Direct Torque Control (DTC-SMC)

Sliding Mode Control (SMC) falls under the umbrella of Variable Structure Control (VSC) and was initially developed by Utkin (Sliding mode control design principles, 2024; Sustainability Free Full; Systems Free Full; Tuning PID Controller for Inverted). It is particularly recognized for its resilience against both internal and external uncertainties, such as parameter variations within the machine and load-induced disturbances, as well as unaccounted phenomena in the model (Boubzizi et al., 2018), ('Sliding mode based DTC of, 2024). A distinctive feature of SMC is the altered control law, which is characterized by its discontinuous nature (Model Predictive Control; Modified vector controlled DFIG wind, 2024). Despite its advantages, SMC is not without its limitations. Notably, the discontinuity in the control can lead to a phenomenon known as chattering. This chattering effect can adversely impact the operational integrity of the machinery (Rodic and Jezernik, 2002). Moreover, the system demands constant and intensive control efforts to ensure it aligns with the desired trajectories, which can be impractical (see Fig. 40).

The control structure for a dual-feed induction machine utilizing the DTC-SMC, as illustrated in Fig. 41, is a cascade control that regulates electromagnetic torque, square-norm flux and speed. The control scheme employs steady-state control algorithms to adjust torque, flux and speed. The "estimator" block of this control scheme comprises a flux and torque estimator that utilizes solely stator and rotor voltage and

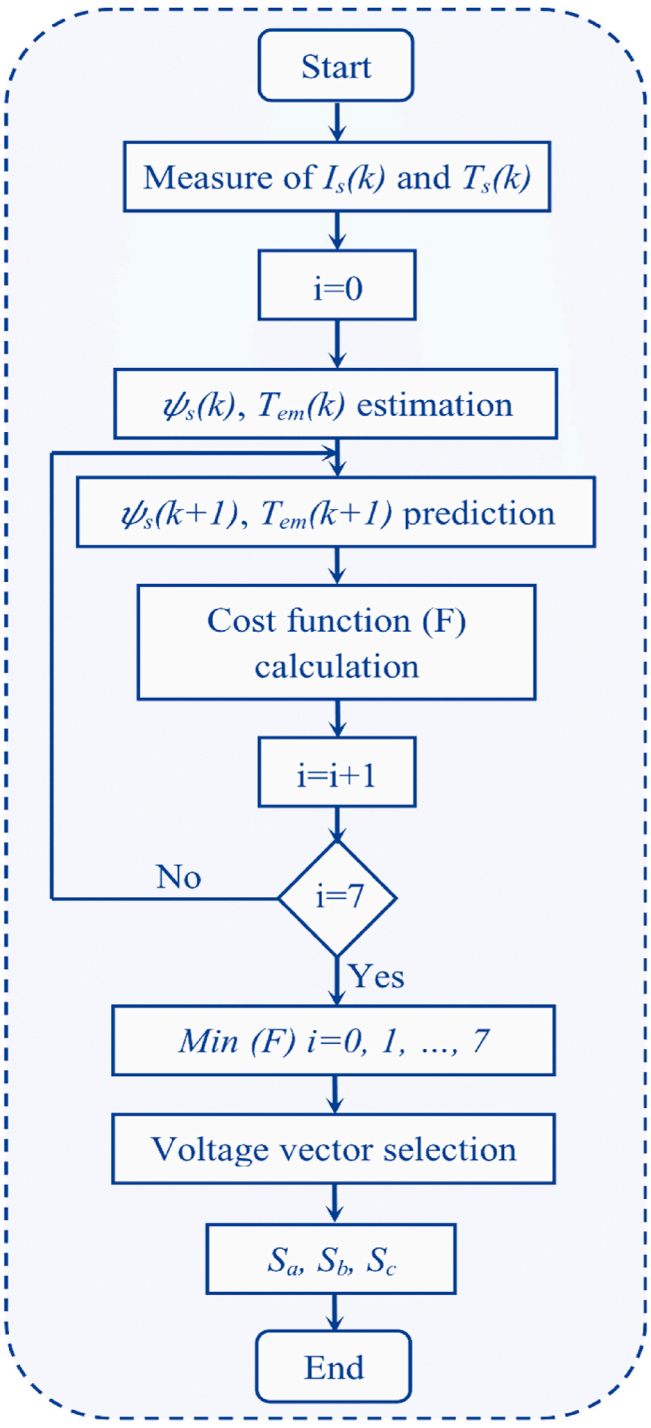

Fig. 40. Flowchart of the P-DTC.

current measurements in the reference frame (α,β). The aforementioned control scheme exhibits both rapid response times and robustness, although it may potentially generate undesirable oscillations in the controlled magnitude. To mitigate this issue, alternative research has employed the robust sliding-mode observer approach (Sun, 2010), which enhances flux estimation resilience to measurement noise.

5.30. Speed Sliding Mode Controller analysis

In this research, a first-order Sliding Mode Controller (SMC) is employed. The sliding surface, denoted as σ_s, is defined by the speed error e, which is calculated as follows (Bekakra et al., 2018):

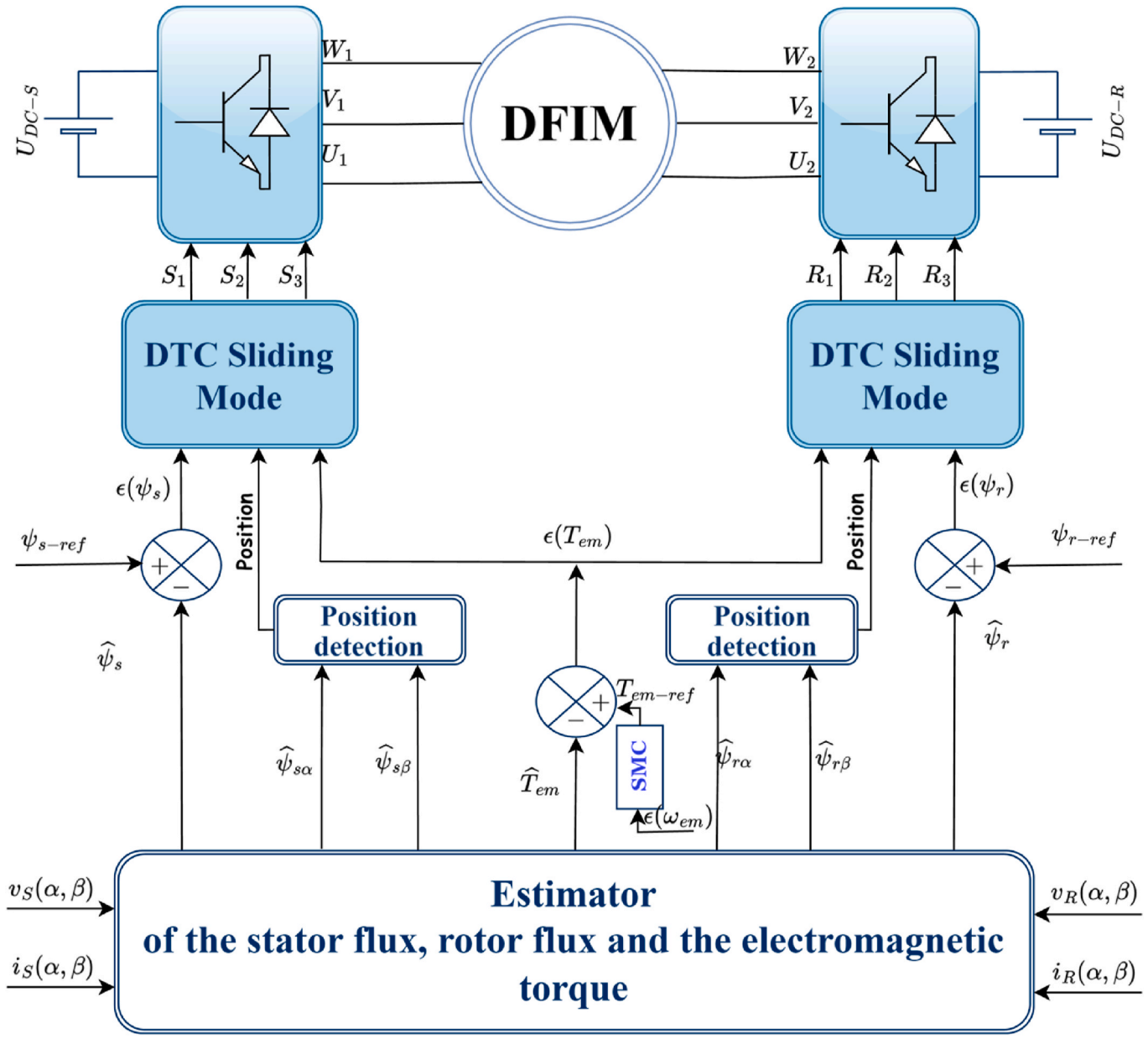

Fig. 41. Block diagram of the DTC-SMC.

$$e = \Omega_r^* - \Omega_r \tag{85}$$

The control surface for speed, $\sigma_s(\Omega_r)$, and its time derivative are derived as:

$$\sigma_s(\Omega_r) = e = \Omega_r^* - \Omega_r \tag{86}$$

$$\frac{d\sigma_s(\Omega_r)}{dt} = \frac{d\Omega_r^*}{dt} - \frac{d\Omega_r}{dt} \tag{87}$$

Given that $\varphi_{sq} = 0$ as per Equation. (9), post-Park transformation, the electromagnetic torque T_e is:

$$T_e = p\varphi_{sd} i_{sq} \tag{88}$$

Using the dynamics of rotor speed change from Equation. (10):

$$\frac{d\Omega_r}{dt} = \frac{1}{J}(T_e - T_L - f\Omega_r) \tag{89}$$

Inserting Equation. (88) into Equation. (89), the derivative of the sliding surface becomes:

$$\frac{d\sigma_s(\Omega_r)}{dt} = \frac{d\Omega^*}{dt} - \frac{1}{J}\left(p\varphi_{sd} \cdot i_{sq} - T_L - f\Omega_r\right) \tag{90}$$

In sliding mode, take:

$$i_{sq} = i_{sq}^{eq} + i_{sq}^{n} \tag{91}$$

with.

i_{sq}^{eq}: equivalent control,
i_{sq}^{n}: switching control,

Within the sliding mode, particularly in the transient state, the conditions are:

$$\sigma_s(\Omega_r) = 0, \frac{d\sigma_s(\Omega_r)}{dt} = 0 \text{ and } i_{sq}^{n} = 0 \tag{92}$$

Under these conditions, the equivalent control i_{sq}^{eq} is formulated as:

Table 6
Comparative analysis of enhancement strategies for direct torque control.

	Torque Ripple (Nm)	Flux Ripple (Stator/ Rotor) (Wb)	Current THD (Stator/ Rotor) (%)	Switching Frequency (kHz)	Parameter sensitivity	Switching loss	Dynamic at low speed	Algorithm complexity	Response Time (ms)	Precession
Conventional DTC (Ouanjli et al., 2017b), (El Ouanjli et al., 2019b)	2.445	0.05855/ 0.0122	7.82/11.7	Variable (1–8.66)	Sensitive	High	Poor	Simple	367.7	Low
SVM based DTC (Mahfoud et al., 2021a), (Kumar and Das, 2017)	1.64	0.051/ 0.012	4.87/5.2	Constant (5.62)	Sensitive	Medium	Good	Intermediate	16	Medium
SMC based DTC (Bekakra et al., 2018), (Ali et al., 2019),	1.8	0.00758/ 0.005	3.5/4.2	Slightly Variable (3.5–4)	Insensitive	Medium	Very good	More Complex	150.7	Medium
P-DTC (Venu Madhav et al., 2021), (Amiri et al., 2018)	0.58	0.0066/ 0.0024	3/4	Constant (1)	Insensitive	Low	Very good	Complex	48	High
Fuzzy based DTC (Ouanjli et al., 2018), (El Ouanjli et al., 2019c)	1.14	0.02/0.004	1.73/2.81	Variable (2–5)	Sensitive	Medium	Good	More complex	35	High
ANN based DTC (Mahfoud et al., 2022c), (Zemmit et al., 2016)	1.08	0.01827/ 0.00752	3.26/3.31	Variable (2–4)	Insensitive	Low	Very good	More complex	49.4	High
GA based DTC (Mahfoud et al., 2022e), (Mahfoud et al., 2021c)	1.76	0.04304/ 0.00893	4.8/7.54	Constant (3.5)	Insensitive	Low	Very good	Complex	18.2	High
ACO based DTC (Mahfoud et al., 2022b), (Mahfoud et al., 2022g)	1.91	0.04294/ 0.00983	4.82/7.98	Slightly Variable (4–5)	Sensitive	Medium	Good	Complex	25.6	Medium
RTO based DTC (Bekakra et al., 2021b), (Wadood et al., 2018)	2	0.035/0.01	5/6	Variable (2–4)	Insensitive	Medium	Good	Intermediate	156.1	Medium

$$i_{sq}^{eq} = \frac{1}{p \cdot \varphi_{sd}} \left(J \frac{d\Omega_r^*}{dt} + T_L + f\Omega_r \right) \tag{93}$$

Hence, the switching control i_{sq}^{n} is determined by:

$$i_{sq}^{n} = K \cdot sat\left(\sigma_s(\Omega_r)\right) \tag{94}$$

where, K: represents a positive gain, and *sat*: refers to the saturation function.

6. Critical analysis

Table 6 provides a comprehensive comparison of the various methods developed to improve DTC (direct torque control) performance in dual-fed induction machines, examining each approach on the basis of key performance parameters such as torque ripple, flux ripple, current THD, switching frequency, parameter sensitivity, switching losses, low-speed dynamic response and algorithm complexity. Each measurement was analyzed to highlight the strengths and weaknesses of each control technique. Although comparisons between techniques can be difficult due to variations in experimental set-ups, machine specifications and simulation parameters from one study to another, some general trends emerge. These trends offer valuable insights into the suitability of each method under specific operating conditions.

Conventional DTC, as shown in Table 6, benefits from a simpler structure than more advanced methods, resulting in lower switching frequencies but higher torque ripple - a known drawback of conventional DTC. While increasing sampling rates can reduce torque ripple, it also increases computational requirements. Recent advances, in particular AI-enhanced methods such as ANN-DTC and P-DTC, have shown promise in reducing torque ripple without excessively high sampling rates. However, these AI-Based approaches add algorithmic complexity, making them more suitable for high-precision, high-power applications. Other strategies, including space vector modulation (SVM) and sliding mode control (SMC), have also improved DTC performance, although each presents unique challenges. SVM-based DTC, for example, is more sensitive to parameter variations, while SMC-based DTC can introduce chattering effects, which can impact on smooth operation. Contrary to traditional assumptions, adaptive methods such as fuzzy logic and ANN-based DTC inherently exhibit variable switching frequencies. This adaptability, while advantageous for some applications, may require further optimization of the control algorithms to reduce the computational load on the microprocessor, which is crucial for real-time applications. One potential direction of optimization is the development of hybrid control schemes that integrate multiple techniques, capitalising on their individual strengths to achieve a balance between accuracy and computational efficiency. For example, combining AI-based methods with conventional approaches could enable a trade-off between performance and processing requirements. In essence, although each method offers distinct advantages, the choice of the best DTC strategy depends on the specific requirements of the application, such as minimizing torque ripple or improving robustness to parameter variations. Ultimately, Table 6 provides a structured framework for the evaluation of DTC methods, focusing on areas where further refinement and hybridisation could deliver significant performance improvements. This overview serves as a guide to choosing the most appropriate DTC approach according to the specific needs and constraints of the application.

7. Advanced DTC methods: simulation results from literature

Recent literature has reported several significant improvements in Direct Torque Control (DTC) through intelligent control approaches in

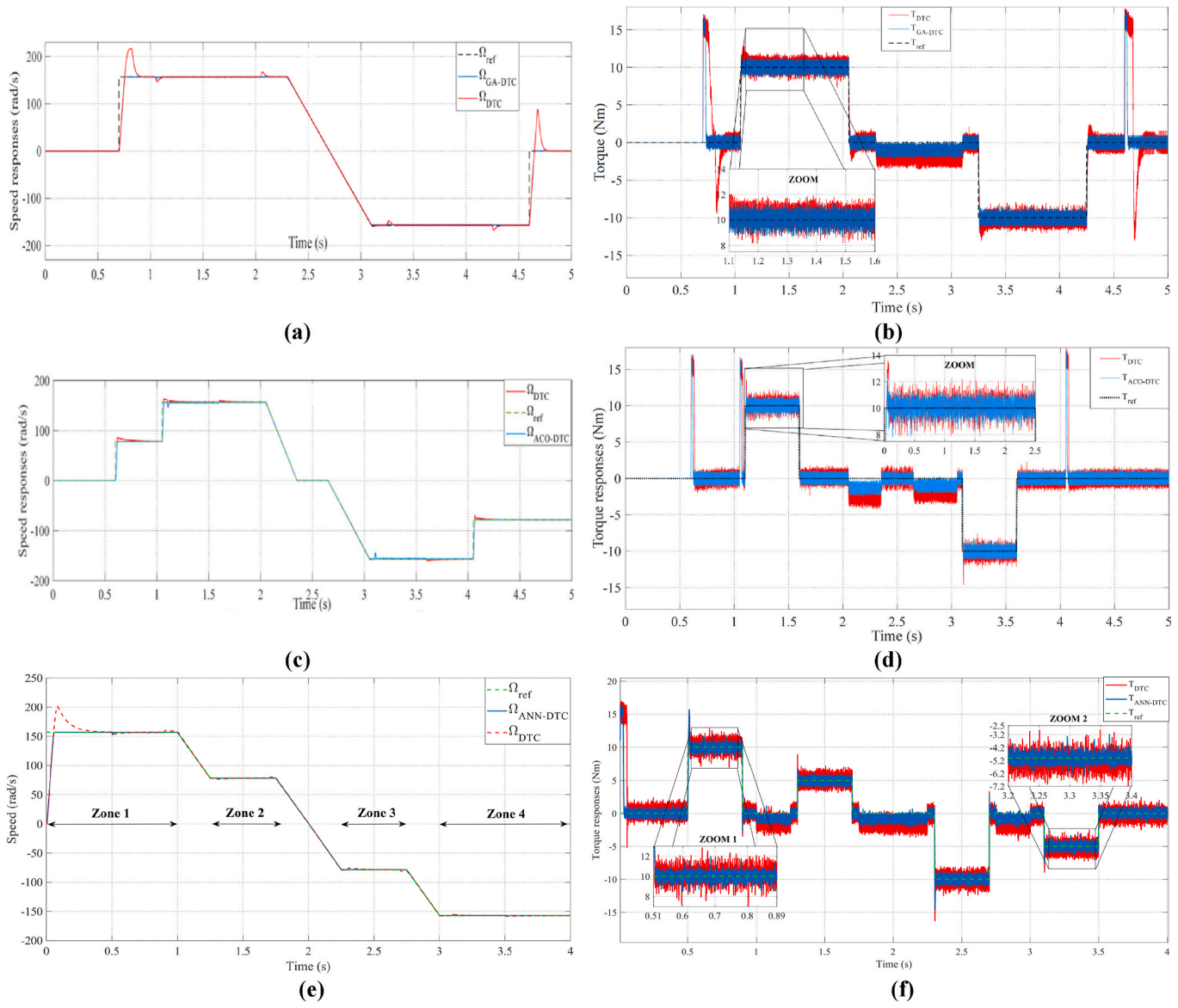

Fig. 42. DFIM speed and torque simulation results from literature: conventional DTC with GA DTC (a,b), ACO DTC (c,d), and ANN DTC (e,f).

DFIM systems. This section examines three representative examples from published research (Mahfoud et al., 2022b), (Mahfoud et al., 2022c), (Mahfoud et al., 2022e)., demonstrating the effectiveness of advanced DTC strategies. Using MATLAB/Simulink platform, these studies present comparative analyses between conventional DTC and intelligent control methods: GA-DTC (Mahfoud et al., 2022e), ACO-DTC (Mahfoud et al., 2022b), and ANN-DTC (Mahfoud et al., 2022c). Fig. 42 illustrates the comparative performance of these methods, with speed responses (a,c,e) and electromagnetic torque characteristics (b,d,f). Each method, as reported in these studies, undergoes rigorous testing under diverse operating conditions, including various speed references and load torque variations.

Fig. 42(a and b) presents the comparative test results between conventional DTC and GA-DTC strategies. Fig. 42 (a) illustrates the speed control behavior through a comprehensive operating profile including acceleration, steady-state operation, speed reversal, and deceleration phases, while Fig. 42 (b) shows the electromagnetic torque response. In (Mahfoud et al., 2022e), the control strategy was tested through various operating conditions, examining both speed variation and load torque fluctuation. Their results demonstrated that the GA-DTC approach substantially improved system performance compared to conventional DTC. The speed control exhibited perfect reference tracking without overshoot and eliminated static error across all operating conditions. The torque analysis showed significant reduction in ripples and improved dynamic response during transient conditions. The GA-DTC strategy demonstrated particular effectiveness in maintaining consistent performance during both loaded and unloaded operations, showing enhanced robustness throughout all operating modes.

Fig. 42(c and d) presents the comparative test results between conventional DTC and ACO-DTC strategies. Fig. 42 (c) illustrates the speed control performance through various operating modes, including forward and reverse operation, speed transitions, and different load conditions, while Fig. 42 (d) shows the electromagnetic torque behavior. In (Mahfoud et al., 2022b), the authors evaluated their strategy through a comprehensive speed profile including acceleration, steady state, speed reversal, and deceleration phases, with sudden load torque variations. Their results showed that the ACO-DTC significantly enhanced the system's performance compared to conventional DTC. The speed control demonstrated improved characteristics with elimination of overshoot and notable reductions in response time, rejection time, and undershoot. The torque analysis revealed considerable reduction in ripples while maintaining excellent reference tracking during load variations. The

ACO-DTC strategy proved particularly effective in maintaining stable performance during speed transitions and load disturbances, demonstrating enhanced robustness across all operating conditions.

Fig. 42(e and f) presents the comparative test results between conventional DTC and ANN-DTC strategies. Fig. 42 (e) shows the speed response through a complete operating profile, including acceleration, steady state operation, speed reversal, and deceleration phases, while Fig. 42 (f) demonstrates the corresponding electromagnetic torque behavior. In (Mahfoud et al., 2022c), the authors carried out various operating conditions in MATLAB/Simulink, testing both low and high-speed ranges with sudden changes in load torque. Their results demonstrated that the ANN-DTC approach significantly improved the system's dynamic performance compared to conventional DTC. The speed control showed marked improvement in undershoot reduction and faster disturbance rejection. The torque analysis revealed considerable reduction in ripple while maintaining precise reference tracking throughout all operating phases. Notably, the ANN-DTC maintained consistent performance during both acceleration and deceleration phases, demonstrating enhanced robustness during speed transitions and load variations.

Based on these simulation results from literature, all three intelligent control methods demonstrate significant improvements over conventional DTC for DFIM systems. The presented investigations clearly highlight the advantages of each approach: GA DTC offers excellent speed tracking and torque ripple reduction, ACO DTC provides enhanced dynamic response with minimal overshoots, and ANN DTC achieves superior disturbance rejection capabilities. These detailed performance assessments provide valuable guidelines for selecting the most suitable control strategy according to specific application requirements in industrial DFIM drives.

8. Conclusion

This study presents an in-depth analysis of advanced strategies for improving direct torque control (DTC) in dual-feed induction machines (DFIMs), focusing on overcoming the limitations of traditional DTC methods. The results indicate that each advanced DTC technique offers distinct benefits tailored to specific operational requirements. Both DTC-SVM and DTC-ANN demonstrate superior performance in minimizing torque and flux ripples, making them particularly well suited to high-precision applications, such as manufacturing systems and industrial drives requiring constant torque output. In contrast, DTC-FL (fuzzy logic) and DTC-SMC (sliding mode control) are more robust to parameter variations and disturbances, making them ideal for industrial environments where operating conditions can fluctuate unpredictably. For applications where energy efficiency and switching loss reduction are priorities-such as heavy machinery and energy-intensive systems-optimization-based methods, including DTC-GA (genetic algorithm), DTC-ACO (ant colony optimization) and DTC-RTO (rooted tree optimization), are recommended, with DTC-RTO showing particular effectiveness in real-time environments. For applications requiring fast dynamic response and accurate speed tracking, such as electric vehicles and aerospace systems, Predictive DTC (DTC-P) is particularly advantageous due to its ability to adapt quickly to changes in speed and load. The choice of the most suitable DTC enhancement method depends on the specific requirements of each application. DTC-SVM and DTC-ANN are recommended for tasks requiring high precision, while DTC-FL and DTC-SMC are better suited to robust environments. Optimization-based methods such as DTC-GA, DTC-ACO, and DTC-RTO are beneficial for applications focused on maximising energy efficiency, while DTC-P is optimal for those requiring fast response times. This study provides a structured decision-making framework that helps engineers and researchers select the most appropriate DTC approach by aligning specific performance metrics and practical constraints, including computing resources and budget considerations, with the unique requirements of their applications.

CRediT authorship contribution statement

Zakariae Sakhri: Writing – original draft, Investigation, Formal analysis, Data curation, Conceptualization. **El-Houssine Bekkour:** Writing – original draft, Formal analysis, Data curation, Conceptualization. **Badre Bossoufi:** Supervision, Resources, Project administration, Methodology, Investigation. **Nicu Bizon:** Resources, Methodology, Investigation. **Mishari Metab Almalki:** Resources, Methodology, Investigation. **Thamer A.H. Alghamdi:** Validation, Software, Resources. **Mohammed Alenezi:** Visualization, Validation, Supervision.

Declaration of competing interest

The authors declare that they have no known competing financial interests or personal relationships that could have appeared to influence the work reported in this paper.

Data availability

Data will be made available on request.

References

A. Colorni, M. Dorigo, V. Maniezzo, Distributed Optimization by Ant Colonies.
Aarniovuori, L., Laurila, L.I.E., Niemela, M., Pyrhonen, J.J., 2012. Measurements and simulations of DTC voltage source converter and induction motor losses. IEEE Trans. Ind. Electron. 59 (5), 2277–2287. https://doi.org/10.1109/TIE.2011.2161061.
Abad, G., Rodriguez, M.A., Poza, J., 2006. Predictive direct torque control of the doubly fed induction machine with reduced torque and flux ripples at low constant switching frequency. In: IECON 2006 - 32nd Annual Conference on IEEE Industrial Electronics. IEEE, Paris, France, pp. 1000–1005. https://doi.org/10.1109/IECON.2006.347349.
Abad, G., Rodriguez, M.A., Poza, J., 2008. Two-level VSC based predictive direct torque control of the doubly fed induction machine with reduced torque and flux ripples at low constant switching frequency. IEEE Trans. Power Electron. 23 (3), 1050–1061. https://doi.org/10.1109/TPEL.2008.921160.
Abdul Kadir, M.N., Mekhilef, S., Wooi Ping, Hew, 2007. Direct torque control permanent magnet synchronous motor drive with asymmetrical multilevel inverter supply. In: *2007 7th Internatonal Conference On Power Electronics*, Daegu, South Korea. IEEE, pp. 1196–1201. https://doi.org/10.1109/ICPE.2007.4692567.
Abu-Rub, H., Stando, D., Kazmierkowski, M.P., 2013. Simple speed sensorless DTC-SVM scheme for induction motor drives. Bull. Pol. Acad. Sci. Tech. Sci. 61 (2), 301–307. https://doi.org/10.2478/bpasts-2013-0028.
Aghasi, M., Faraji, V., Behnia, H., Khaburi, D.A., Banadaki, A.D., 2012. Predictive DTC-ISVM for doubly-fed induction machine system fed by indirect matrix converter, 5 (2).
Agustin, C.A., Yu, J., Lin, C.-K., Fu, X.-Y., 2019. A modulated model predictive current controller for interior permanent-magnet synchronous motors. Energies 12 (15), 2885. https://doi.org/10.3390/en12152885.
Ahmed, D., Mokhtar, B., Aek, B., 2020a. DTC-ANN-2-level hybrid by neuronal hysteresis with mechanical sensorless induction motor drive using KUBOTA observer. IJPEDS 11 (1), 34. https://doi.org/10.11591/ijpeds.v11.i1.pp34-44.
Ahmed, D., Mokhtar, B., Aek, B., 2020b. DTC-ANN-2-level hybrid by neuronal hysteresis with mechanical sensorless induction motor drive using KUBOTA observer. IJPEDS 11 (1), 34. https://doi.org/10.11591/ijpeds.v11.i1.pp34-44.
Akın, E., Kaya, M., Karakose, M., 2003. A robust integrator algorithm with genetic based fuzzy controller feedback for direct vector control. Comput. Electr. Eng. 29 (3), 379–394. https://doi.org/10.1016/S0045-7906(01)00041-6.
Ali, M.M., Xu, W., Elmorshedy, M.F., Liu, Y., Allam, S.M., Dong, M., 2019. 'Sliding Mode Speed Regulation of Linear Induction Motors Based on Direct Thrust Control with Space-Vector Modulation Strategy'.
Amiri, M., Milimonfared, J., khaburi, D.A., 2018. Predictive torque control implementation for induction motors based on discrete space vector modulation. IEEE Trans. Ind. Electron. 1. https://doi.org/10.1109/TIE.2018.2795589, 1.
Amirjanov, A., 2015. The parameters setting of a changing range genetic algorithm. Nat. Comput. 14 (2), 331–338. https://doi.org/10.1007/s11047-014-9420-2.
Aroussi, H.A., Ziani, E., Bouderbala, M., Bossoufi, B., 2020. Improvement of direct torque control applied to doubly fed induction motor under variable speed. Int. J. Power Electron. Drive Syst. 11 (1), 97–106. https://doi.org/10.11591/ijpeds.v11.i1.pp97-106.
Bakou, Y., Abid, M., Harrouz, A., Yaichi, I., Colak, I., Kayisli, K., Aissaoui, A., 2019. DTC control of the DFIG, application to the production of electrical energy. In: 2019 8th International Conference on Renewable Energy Research and Applications (ICRERA). IEEE, pp. 910–915.
Baliga, B.J., 2010. Fundamentals of Power Semiconductor Devices. Springer Science & Business Media [Online]. Available: https://books.google.fr/books?hl=en&lr=&id=UiqrUWrYZXkC&oi=fnd&pg=PR7&dq=Baliga,+B.+J.+(2008).+Fundamentals+of+power+semiconductor+devices.+Springer+Science+%26+Business+

Media&ots=1EwkHDpkXE&sig=phu5OntZqyTHN1ychliT4Q0CxYI. (Accessed 13 March 2024).
Bascetta, L., Magnani, G., Rocco, P., Zanchettin, A.M., 2010. Performance limitations in field-oriented control for asynchronous machines with low resolution position sensing. IEEE Trans. Control Syst. Technol. 18 (3), 559–573. https://doi.org/10.1109/TCST.2009.2024300.
Bekakra, Y., Lammouchi, Z., Serhoud, H., 2018. Improved speed and torque performance for DTC of DFIM using sliding mode speed controller. In: *2018 International Conference On Communications And Electrical Engineering (ICCEE)*, El Oued, Algeria. IEEE, pp. 1–6. https://doi.org/10.1109/CCEE.2018.8634538.
Bekakra, Y., Attous, D.B., Tir, Z., Malik, O., 2020. 'IMPROVEMENT IN SPEED PERFORMANCE OF AN INDUCTION MOTOR WITH SLIDING MODE CONTROLLER AND ANN FOR DTC'.
Bekakra, Y., Labbi, Y., Ben Attous, D., Malik, O.P., 2021a. Rooted tree optimization algorithm to improve DTC response of DFIM. Journal of Electrical Engineering and Technology 16 (5), 2463–2483. https://doi.org/10.1007/s42835-021-00796-4.
Bekakra, Y., Labbi, Y., Ben Attous, D., Malik, O.P., 2021b. Rooted tree optimization algorithm to improve DTC response of DFIM. J. Electr. Eng. Technol. 16 (5), 2463–2483. https://doi.org/10.1007/s42835-021-00796-4.
Bekakra, Y., Labbi, Y., Ben Attous, D., Malik, O.P., 2021c. Rooted tree optimization algorithm to improve DTC response of DFIM. J. Electr. Eng. Technol. 16 (5), 2463–2483. https://doi.org/10.1007/s42835-021-00796-4.
Belay, A., Salau, A.O., Kassahun, H.E., Eneh, J.N., 2024. Stator flux estimation and hybrid sliding mode torque control of an induction motor. Int J Syst Assur Eng Manag 15 (6), 2541–2553. https://doi.org/10.1007/s13198-024-02275-1.
Bose, B.K., 2009. Power electronics and motor drives recent progress and perspective. IEEE Trans. Ind. Electron. 56 (2), 581–588. https://doi.org/10.1109/TIE.2008.2002726.
Boubzizi, S., Abid, H., El Hajjaji, A., Chaabane, M., 2018. Comparative study of three types of controllers for DFIG in wind energy conversion system. Prot Control Mod Power Syst 3 (1), 21. https://doi.org/10.1186/s41601-018-0096-y.
Bouhoune, K., Yazid, K., Boucherit, M.S., Menaa, M., 2017. Fuzzy logic-based direct torque control for induction machine drive. In: 2017 25th Mediterranean Conference on Control and Automation (MED). IEEE, Valletta, Malta, pp. 577–582. https://doi.org/10.1109/MED.2017.7984179.
Boukadida, S., Gdaim, S., Mtibaa, A., 2014. A novel direct torque control for induction machine drive system with low torque and flux ripples using XSG. Int. J. Power Electron. Drive Syst. 4 (4), 517–527. https://doi.org/10.11591/ijpeds.v4i4.6374.
Boumaraf, F., Boutabba, T., Belkacem, S., 2021. Dual direct torque control of doubly fed induction machine using second order sliding mode control. J. meas. eng. 9 (1), 1–12. https://doi.org/10.21595/jme.2021.21432.
Brahim, D., Mokhtar, B., Salah, L., 2020. Improvement of adaptive fuzzy control to adjust speed for a doubly fed induction motor drive (DFIM). Int. J. Power Electron. Drive Syst. 11 (1), 496–504. https://doi.org/10.11591/ijpeds.v11.i1.pp496-504.
Camacho, E.F., 1993. Constrained generalized predictive control. IEEE Trans. Automat. Control 38 (2), 327–332. https://doi.org/10.1109/9.250485.
Casadei, D., Serra, G., Tani, K., 2000. Implementation of a direct control algorithm for induction motors based on discrete space vector modulation. IEEE Trans. Power Electron. 15 (4), 769–777. https://doi.org/10.1109/63.849048.
Chegwidden, W.R., Watts, D.C., 1975. Kinetic studies and effects of anions on creatine phosphokinase from skeletal muscle of rhesus monkey (Macaca mulatta). Biochim. Biophys. Acta 410 (1), 99–114. https://doi.org/10.1016/0005-2744(75)90210-7.
Cherifi, D., Miloud, Y., 2018. Robust speed-sensorless vector control of doubly fed induction motor drive using sliding mode rotor flux observer. IJAPE 7 (3), 235. https://doi.org/10.11591/ijape.v7.i3.pp235-250.
Chiha, I., Liouane, N., Borne, P., 2012. Tuning PID controller using multiobjective ant colony optimization. Applied Computational Intelligence and Soft Computing 2012, e536326. https://doi.org/10.1155/2012/536326.
Daraban, S., Petreus, D., Morel, C., 2014. A novel MPPT (maximum power point tracking) algorithm based on a modified genetic algorithm specialized on tracking the global maximum power point in photovoltaic systems affected by partial shading. Energy 74, 374–388. https://doi.org/10.1016/j.energy.2014.07.001.
Department of Electrical Engineering, El-Oued University Center, Attous, D.B., Bekakra, Y., Department of Electrical Engineering, El-Oued University Center, 2010a. 'Speed control of a doubly fed induction motor using fuzzy logic techniques'. ijeei 2 (3), 179–191. https://doi.org/10.15676/ijeei.2010.2.3.2.
Department of Electrical Engineering, El-Oued University Center, Attous, D.B., Bekakra, Y., Department of Electrical Engineering, El-Oued University Center, 2010b. 'Speed control of a doubly fed induction motor using fuzzy logic techniques'. ijeei 2 (3), 179–191. https://doi.org/10.15676/ijeei.2010.2.3.2.
Depenbrock, M., 1988. Direct self-control (DSC) of inverter-fed induction machine. IEEE Trans. Power Electron. 3 (4), 420–429. https://doi.org/10.1109/63.17963.
El Mahfoud, M., Bossoufi, B., El Ouanjli, N., Mahfoud, S., Yessef, M., Taoussi, M., 2021a. Speed sensorless direct torque control of doubly fed induction motor using model reference adaptive system. In: Motahhir, S., Bossoufi, B. (Eds.), Digital Technologies and Applications. Springer International Publishing, Cham, pp. 1821–1830. https://doi.org/10.1007/978-3-030-73882-2_165.
El Mahfoud, M., Bossoufi, B., El Ouanjli, N., Mahfoud, S., Yessef, M., Taoussi, M., 2021b. 'Speed sensorless direct torque control of doubly fed induction motor using model reference adaptive system', in digital technologies and applications. In: Motahhir, S., Bossoufi, B. (Eds.), Lecture Notes in Networks and Systems, vol. 211. Springer International Publishing, Cham, pp. 1821–1830. https://doi.org/10.1007/978-3-030-73882-2_165, 211.
El Ouanjli, N., Derouich, A., ghzizal Abdelaziz, el, Ali, C., Taoussi, M., 2017a. A Comparative Study between FOC and DTC Controls of the Doubly Fed Induction Motor (DFIM), p. 6. https://doi.org/10.1109/EITech.2017.8255302.
El Ouanjli, N., Derouich, A., El Ghzizal, A., Chebabhi, A., Taoussi, M., 2017b. A comparative study between FOC and DTC control of the doubly fed induction motor (DFIM). In: 2017 International Conference on Electrical and Information Technologies (ICEIT), pp. 1–6. https://doi.org/10.1109/EITech.2017.8255302.
El Ouanjli, N., Motahhir, S., Derouich, A., El Ghzizal, A., Chebabhi, A., Taoussi, M., 2019a. Improved DTC strategy of doubly fed induction motor using fuzzy logic controller. Energy Rep. 5, 271–279. https://doi.org/10.1016/j.egyr.2019.02.001.
El Ouanjli, N., et al., 2019b. Direct torque control of doubly fed induction motor using three-level NPC inverter. Protection and Control of Modern Power Systems 4 (1). https://doi.org/10.1186/s41601-019-0131-7.
El Ouanjli, N., Motahhir, S., Derouich, A., El Ghzizal, A., Chebabhi, A., Taoussi, M., 2019c. Improved DTC strategy of doubly fed induction motor using fuzzy logic controller. Energy Rep. 5, 271–279. https://doi.org/10.1016/j.egyr.2019.02.001.
El Ouanjli, N., et al., 2019d. Modern improvement techniques of direct torque control for induction motor drives - a review. Prot Control Mod Power Syst 4 (1), 11. https://doi.org/10.1186/s41601-019-0125-5.
El Ouanjli, N., et al., 2019e. Direct torque control of doubly fed induction motor using three-level NPC inverter. Protection and Control of Modern Power Systems 4 (1), 17. https://doi.org/10.1186/s41601-019-0131-7.
Esen, H., Inalli, M., Sengur, A., Esen, M., 2008. Artificial neural networks and adaptive neuro-fuzzy assessments for ground-coupled heat pump system. Energy Build. 40 (6), 1074–1083. https://doi.org/10.1016/j.enbuild.2007.10.002.
Esen, H., Ozgen, F., Esen, M., Sengur, A., 2009. Artificial neural network and wavelet neural network approaches for modelling of a solar air heater. Expert Syst. Appl. 36 (8), 11240–11248. https://doi.org/10.1016/j.eswa.2009.02.073.
Esen, H., Esen, M., Ozsolak, O., 2017. Modelling and experimental performance analysis of solar-assisted ground source heat pump system. J. Exp. Theor. Artif. Intell. 29 (1), 1–17. https://doi.org/10.1080/0952813X.2015.1056242.
Evangelista, C., Puleston, P., Valenciaga, F., 2010. Wind turbine efficiency optimization. Comparative study of controllers based on second order sliding modes. Int. J. Hydrogen Energy 35 (11), 5934–5939. https://doi.org/10.1016/j.ijhydene.2009.12.104.
Fuzzy gain scheduling of PID controllers, 2024. IEEE Journals & Magazine | IEEE Xplore [Online]. Available, vol 34. https://ieeexplore.ieee.org/document/260670.
gai Ye, L., Yuan-bin, H., Yan, L., Dong, L., 2017. Genetic algorithm's application for optimization of PID parameters in dynamic positioning vessel. MATEC Web Conf. 139, 00153. https://doi.org/10.1051/matecconf/201713900153.
Gupta, N., Swarnkar, A., Niazi, K.R., 2014. Distribution network reconfiguration for power quality and reliability improvement using Genetic Algorithms. Int. J. Electr. Power Energy Syst. 54, 664–671. https://doi.org/10.1016/j.ijepes.2013.08.016.
Habetler, T.G., Profumo, F., Pastorelli, M., Tolbert, L.M., 1992. Direct torque control of induction machines using space vector modulation. IEEE Trans. Ind. Appl. 28 (5), 1045–1053. https://doi.org/10.1109/28.158828.
Hamidia, F., Boucherit, M.S., Larabi, A., 2013. Artifiacial neural network controlled PMSM, DFIM and IM drives. J. Electr. Eng. 13 (4), 23–28.
Hannan, M.A., Ali, J.A., Mohamed, A., Hussain, A., 2018. Optimization techniques to enhance the performance of induction motor drives: a review. Renew. Sustain. Energy Rev. 81, 1611–1626. https://doi.org/10.1016/j.rser.2017.05.240.
Herizi, A., Rouabhi, R., Zemmit, A., 2023. Speed control of doubly fed induction motor using backstepping control with interval type-2 fuzzy controller. Diagnostyka 24 (3), 1–8. https://doi.org/10.29354/diag/166460.
Hiba, H., Ali, H., Othmen, H., 2013. DTC-SVM control for three phase induction motors. In: *2013 International Conference On Electrical Engineering And Software Applications*, Hammamet, Tunisia. IEEE, pp. 1–7. https://doi.org/10.1109/ICEESA.2013.6578421.
Holmes, D.G., Lipo, T.A., 2003. Pulse width modulation for power converters. IEEE. https://doi.org/10.1109/9780470546284.
Idris, N.R.N., Yatim, A.H.M., 2002. An improved stator flux estimation in steady-state operation for direct torque control of induction machines. IEEE Trans. Ind. Appl. 38 (1), 110–116. https://doi.org/10.1109/28.980364.
Irshad, M., Khalid, S., Hussain, M.Z., Sarfraz, M., 2016. Outline capturing using rational functions with the help of genetic algorithm. Appl. Math. Comput. 274, 661–678. https://doi.org/10.1016/j.amc.2015.10.014.
Jaladi, K.K., 2019. Experimental validation of SMC-based DTC-VC for DFIG-WECS. Electr. Eng. 101 (2), 587–598. https://doi.org/10.1007/s00202-019-00809-6.
Jayachitra, A., Vinodha, R., 2014. Genetic algorithm based PID controller tuning approach for continuous stirred tank reactor. Advances in Artificial Intelligence 2014, e791230. https://doi.org/10.1155/2014/791230.
Kanojiya, R.G., Meshram, P.M., 2012. Optimal tuning of PI controller for speed control of DC motor drive using particle swarm optimization. In: 2012 International Conference on Advances in Power Conversion and Energy Technologies (APCET), pp. 1–6. https://doi.org/10.1109/APCET.2012.6302000.
Kati, O., 2011. PENGENDALI sliding mode control (SMC) motor INDUKSI 3 phasa dengan metode direct torque control (DTC) MENGGUNAKAN ALGORITMA GENETIKA, 5 (3).
Kaźmierkowski, M.P., Krishnan, R., Blaabjerg, F., . Control in Power Electronics: Selected Problems. Academic press [Online]. Available: https://books.google.fr/books?hl=en&lr=&id=cHuYj49Ivt4C&oi=fnd&pg=PR7&dq=Kazmierkowski,+M.+P.,+Krishnan,+R.,+%26+Blaabjerg,+F.+(2002).+Control+in+power+electronics:+selected+problems.+Academic+press.&ots=r2VZmiXA2b&sig=wmnNYYmfmxi_3aLbdi5vHIYGZgI. (Accessed 13 March 2024).
Kim, J.-S., Sul, S.-K., 1996. A novel voltage modulation technique of the space vector PWM. IEEJ Trans. IA 116 (8), 820–825. https://doi.org/10.1541/ieejias.116.820.
Kouro, S., et al., 2010. Recent advances and industrial applications of multilevel converters. IEEE Trans. Ind. Electron. 57 (8), 2553–2580. https://doi.org/10.1109/TIE.2010.2049719.

Krieger, A.W., Salmon, J.C., 2005. Hysteresis-based current control at fixed frequency, with a resonating integrator to eliminate the steady state error. In: Canadian Conference on Electrical and Computer Engineering, pp. 512–516. https://doi.org/10.1109/CCECE.2005.1556982. May 2005.

Kruselj, D., 2017. Methods for direct torque control of induction machines. In: 2017 19th International Conference on Electrical Drives and Power Electronics (EDPE). Dubrovnik: IEEE, pp. 218–225. https://doi.org/10.1109/EDPE.2017.8123236.

Kumar, R., Das, S., 2017. Sensorless DTC-SVM strategy for doubly-fed induction machine drive using model reference adaptive system. In: *2017 14th IEEE India Council International Conference (INDICON)*, Roorkee. IEEE, pp. 1–6. https://doi.org/10.1109/INDICON.2017.8487924.

Kumar, B., Gupta, R., Kumar, R., 2006. 12-Sector methodology of torque ripple reduction in a direct torque controlled induction motor drive. In: *2006 SICE-ICASE International Joint Conference*, Busan Exhibition & Convention Center-BEXCO. IEEE, Busan, Korea, pp. 3587–3592. https://doi.org/10.1109/SICE.2006.314746.

Labbi, Y., Attous, D.B., Gabbar, H.A., Mahdad, B., Zidan, A., 2016. A new rooted tree optimization algorithm for economic dispatch with valve-point effect. Int. J. Electr. Power Energy Syst. 79, 298–311. https://doi.org/10.1016/j.ijepes.2016.01.028.

Lee, K.-B., Huh, S.-H., Yoo, J.-Y., Blaabjerg, F., 2005. Performance improvement of DTC for induction motor-fed by three-level inverter with an uncertainty observer using RBFN. IEEE Trans. Energy Convers. 20 (2), 276–283. https://doi.org/10.1109/TEC.2005.845542.

Lequin, O., Gevers, M., Mossberg, M., Bosmans, E., Triest, L., 2003. Iterative feedback tuning of PID parameters: comparison with classical tuning rules. Control Eng. Pract. 11 (9), 1023–1033. https://doi.org/10.1016/S0967-0661(02)00303-9.

Li, S., Wei, Y., Liu, X., Zhu, H., Yu, Z., 2022. A new fast ant colony optimization algorithm: the saltatory evolution ant colony optimization algorithm. Mathematics 10 (6), 925. https://doi.org/10.3390/math10060925.

Lin, F.-J., Yu, J.-C., Tzeng, M.-S., 2001. Sensorless induction spindle motor drive using fuzzy neural network speed controller. Elec. Power Syst. Res. 58 (3), 187–196. https://doi.org/10.1016/S0378-7796(01)00133-X.

Lyu, X., Lin, Z., 2022. Design of PID control for planar uncertain nonlinear systems with input delay. Int. J. Robust Nonlinear Control 32 (18), 9407–9420. https://doi.org/10.1002/rnc.5577.

Mahfoud, M.E., Bossoufi, B., Ouanjli, N.E., Said, M., Taoussi, M., 2021a. Improved direct torque control of doubly fed induction motor using space vector modulation. International Journal of Intelligent Engineering and Systems 14 (3), 177–188. https://doi.org/10.22266/ijies2021.0630.16.

Mahfoud, S., Derouich, A., El Ouanjli, N., El Mahfoud, M., Taoussi, M., 2021b. A new strategy-based PID controller optimized by genetic algorithm for DTC of the doubly fed induction motor. Systems 9 (2), 37. https://doi.org/10.3390/systems9020037.

Mahfoud, S., Derouich, A., El Ouanjli, N., El Mahfoud, M., Taoussi, M., 2021c. A new strategy-based PID controller optimized by genetic algorithm for DTC of the doubly fed induction motor. Systems 9 (2), 37. https://doi.org/10.3390/systems9020037.

Mahfoud, S., Derouich, A., El Ouanjli, N., 2022a. Performance improvement of DTC for doubly fed induction motor by using artificial neuron network. Lecture Notes in Networks and Systems 455 (LNNS), 32–42. https://doi.org/10.1007/978-3-031-02447-4_4.

Mahfoud, S., Derouich, A., Iqbal, A., El Ouanjli, N., 2022b. ANT-colony optimization-direct torque control for a doubly fed induction motor : an experimental validation. Energy Rep. 8, 81–98. https://doi.org/10.1016/j.egyr.2021.11.239.

Mahfoud, S., Derouich, A., Ouanjli, N.E., Mahfoud, M.E., 2022c. Enhancement of the direct torque control by using artificial neuron network for a doubly fed induction motor. Intelligent Systems with Applications 13, 200060. https://doi.org/10.1016/j.iswa.2022.200060.

Mahfoud, S., Derouich, A., El Ouanjli, N., 2022d. 'Performance improvement of DTC for doubly fed induction motor by using artificial neuron network', in digital technologies and applications. In: Motahhir, S., Bossoufi, B. (Eds.), Lecture Notes in Networks and Systems, vol. 455. Springer International Publishing, Cham, pp. 32–42. https://doi.org/10.1007/978-3-031-02447-4_4, 455.

Mahfoud, S., et al., 2022e. A new robust direct torque control based on a genetic algorithm for a doubly-fed induction motor: experimental validation. Energies 15 (15). https://doi.org/10.3390/en15155384.

Mahfoud, S., et al., 2022f. Comparative study between cost functions of genetic algorithm used in direct torque control of a doubly fed induction motor. Appl. Sci. 12 (17), 8717. https://doi.org/10.3390/app12178717.

Mahfoud, S., Derouich, A., El Ouanjli, N., Quynh, N.V., Mossa, M.A., 2022g. A new hybrid ant colony optimization based PID of the direct torque control for a doubly fed induction motor. WE! 13 (5), 78. https://doi.org/10.3390/wevj13050078.

Mahfoud, S., et al., 2022h. Comparative study between cost functions of genetic algorithm used in direct torque control of a doubly fed induction motor. Appl. Sci. 12 (17), 8717. https://doi.org/10.3390/app12178717.

Matraji, I., Ahmed, F.S., Laghrouche, S., Wack, M., 2015. Comparison of robust and adaptive second order sliding mode control in PEMFC air-feed systems. Int. J. Hydrogen Energy 40 (30), 9491–9504. https://doi.org/10.1016/j.ijhydene.2015.05.090.

Meena, D.C., Devanshu, A., 2017. Genetic algorithm tuned PID controller for process control. In: 2017 International Conference on Inventive Systems and Control (ICISC), pp. 1–6. https://doi.org/10.1109/ICISC.2017.8068639.

Menghal, P.M., Laxmi, A.J., 2018. Real time control of induction motor using neural network. In: 2018 International Conference on Communication Information and Computing Technology (ICCICT). IEEE, Mumbai, pp. 1–6. https://doi.org/10.1109/ICCICT.2018.8325873.

Mohammed, E.M., et al., 2022. 'Predictive torque and direct torque controls for doubly fed induction motor: a comparative study', in digital technologies and applications. In: Motahhir, S., Bossoufi, B. (Eds.), Lecture Notes in Networks and Systems, vol. 454. Cham: Springer International Publishing, pp. 825–835. https://doi.org/10.1007/978-3-031-01942-5_82, 454.

Mondal, S.K., Pinto, J.O.P., Bose, B.K., 2002a. A neural-network-based space-vector PWM controller for a three-level voltage-fed inverter induction motor drive. IEEE Trans. Ind. Appl. 38 (3), 660–669. https://doi.org/10.1109/TIA.2002.1003415.

Mondal, S.K., Pinto, J.O.P., Bose, B.K., 2002b. A neural-network-based space-vector PWM controller for a three-level voltage-fed inverter induction motor drive. IEEE Trans. Ind. Appl. 38 (3), 660–669. https://doi.org/10.1109/TIA.2002.1003415.

Moussaoui, A., Benbouhenni, H., Attous, D.B., 2021. 24 sectors DTC control with fuzzy hysteresis comparators for DFIM fed by the three-level NPC inverter. WSEAS Trans. Electron. 12, 141–154. https://doi.org/10.37394/232017.2021.12.19.

Ouanjli, N.E., Derouich, A., Ghzizal, A.E., Mourabit, Y.E., Bossoufi, B., Taoussi, M., 2017a. Contribution to the performance improvement of doubly fed induction machine functioning in motor mode by the DTC control. Int. J. Power Electron. Drive Syst. 8 (3), 1117–1127. https://doi.org/10.11591/ijpeds.v8i3.pp1117-1127.

Ouanjli, N.E., Derouich, A., Ghzizal, A.E., Mourabit, Y.E., Bossoufi, B., Taoussi, M., 2017b. Contribution to the performance improvement of doubly fed induction machine functioning in motor mode by the DTC control, 8 (3).

Ouanjli, N.E., Taoussi, M., Derouich, A., Chebabhi, A., Ghzizal, A.E., Bossoufi, B., 2018. 'High Performance Direct Torque Control of Doubly Fed Induction Motor Using Fuzzy Logic'.

Ozkop, E., Okumus, H.I., 2008. Direct torque control of induction motor using space vector modulation (SVM-DTC). In: *2008 12th International Middle-East Power System Conference*, Aswan, Egypt. IEEE, pp. 368–372. https://doi.org/10.1109/MEPCON.2008.4562350.

Pacas, M., Weber, J., 2005. Predictive direct torque control for the PM synchronous machine. IEEE Trans. Ind. Electron. 52 (5), 1350–1356. https://doi.org/10.1109/TIE.2005.855662.

Papafotiou, G., Kley, J., Papadopoulos, K.G., Bohren, P., Morari, M., 2009. Model predictive direct torque control - Part II: implementation and experimental evaluation. IEEE Trans. Ind. Electron. 56 (6), 1906–1915. https://doi.org/10.1109/TIE.2008.2007032.

Rafajlovski, G., Digalovski, M., 2018. Controlling induction motors [Online]. Available: https://www.semanticscholar.org/paper/CONTROLLING-INDUCTION-MOTORS-Rafajlovski-Digalovski/7a6c04ac2d4fdfd02457004ad2c44d1f9a0cfc29. (Accessed 12 March 2024).

Reza, C.M.F.S., Mekhilef, S., 2013. Online stator resistance estimation using artificial neural network for direct torque controlled induction motor drive. In: *2013 IEEE 8th Conference On Industrial Electronics And Applications (ICIEA)*, Melbourne, VIC. IEEE, pp. 1486–1491. https://doi.org/10.1109/ICIEA.2013.6566602.

Reza, C.M.F.S., Islam, Md D., Mekhilef, S., 2014. A review of reliable and energy efficient direct torque controlled induction motor drives. Renew. Sustain. Energy Rev. 37, 919–932. https://doi.org/10.1016/j.rser.2014.05.067.

Rezvanian, A., Mehdi Vahidipour, S., Sadollah, A., 2023. An overview of ant colony optimization algorithms for dynamic optimization problems. In: Ant Colony Optimization - Recent Variants, Application and Perspectives [Working Title]. IntechOpen. https://doi.org/10.5772/intechopen.111839.

Rodic, M., Jezernik, K., 2002. Speed-sensorless sliding-mode torque control of an induction motor. IEEE Trans. Ind. Electron. 49 (1), 87–95. https://doi.org/10.1109/41.982252.

Rodriguez, J., Lai, Jih-Sheng, Peng, Fang Zheng, 2002. Multilevel inverters: a survey of topologies, controls, and applications. IEEE Trans. Ind. Electron. 49 (4), 724–738. https://doi.org/10.1109/TIE.2002.801052.

Sami, I., Ullah, S., Basit, A., Ullah, N., Ro, J.-S., 2020. Integral super twisting sliding mode based sensorless predictive torque control of induction motor. IEEE Access 8, 186740–186755. https://doi.org/10.1109/ACCESS.2020.3028845.

Shukla, A.K., Singh, P., Vardhan, M., 2019. A new hybrid feature subset selection framework based on binary genetic algorithm and information theory. Int. J. Comput. Intell. Appl. 18 (3), 1950020. https://doi.org/10.1142/S1469026819500202.

Singh, B., Mukherjee, V., Tiwari, P., 2016. Genetic algorithm for impact assessment of optimally placed distributed generations with different load models from minimum total MVA intake viewpoint of main substation. Renew. Sustain. Energy Rev. 57, 1611–1636. https://doi.org/10.1016/j.rser.2015.12.204.

Skackauskas, J., Kalganova, T., Dear, I., Janakiram, M., 2022. Dynamic impact for ant colony optimization algorithm. Swarm Evol. Comput. 69, 100993. https://doi.org/10.1016/j.swevo.2021.100993.

Soleimani, H., Kannan, G., 2015. A hybrid particle swarm optimization and genetic algorithm for closed-loop supply chain network design in large-scale networks. Appl. Math. Model. 39 (14), 3990–4012. https://doi.org/10.1016/j.apm.2014.12.016.

Stein, J.M., 1975. The effect of adrenaline and of alpha- and beta-adrenergic blocking agents on ATP concentration and on incorporation of 32Pi into ATP in rat fat cells. Biochem. Pharmacol. 24 (18), 1659–1662. https://doi.org/10.1016/0006-2952(75)90002-7.

Storti, G.L., Paschero, M., Rizzi, A., Frattale Mascioli, F.M., 2015. Comparison between time-constrained and time-unconstrained optimization for power losses minimization in Smart Grids using genetic algorithms. Neurocomputing 170, 353–367. https://doi.org/10.1016/j.neucom.2015.02.088.

Sun, D., 2010. Sliding mode direct torque control for induction motor with robust stator flux observer. In: 2010 International Conference on Intelligent Computation Technology and Automation, pp. 348–351. https://doi.org/10.1109/ICICTA.2010.580.

Sutikno, T., Idris, N.R.N., Jidin, A., 2014. A review of direct torque control of induction motors for sustainable reliability and energy efficient drives. Renew. Sustain. Energy Rev. 32, 548–558. https://doi.org/10.1016/j.rser.2014.01.040.

Tabassum, M., 2014. The society of digital information and wireless communication, 'A genetic algorithm analysis towards optimization solutions'. IJDIWC 4 (1), 124–142. https://doi.org/10.17781/P001091.
Takahashi, I., Noguchi, T., 1986. A new quick-response and high-efficiency control strategy of an induction motor. IEEE Trans. Ind. Appl. IA-22 (5), 820–827. https://doi.org/10.1109/TIA.1986.4504799.
Tripathi, A., Khambadkone, A.M., Panda, S.K., 2004. Stator flux based space-vector modulation and closed loop control of the stator flux vector in overmodulation into six-step mode. IEEE Trans. Power Electron. 19 (3), 775–782. https://doi.org/10.1109/TPEL.2004.826507.
V.M. Aparanji, U.V. Wali, and R. Aparna, Multi-Layer Auto Resonance Network for Robotic Motion Control.
Varol, H.A., Bingul, Z., 2004. A new PID tuning technique using ant algorithm. In: Proceedings of the 2004 American Control Conference, vol. 3. IEEE, Boston, MA, USA, pp. 2154–2159. https://doi.org/10.23919/ACC.2004.1383780.
Venu Madhav, G., Obulesu, Y.P., 2021. Predictive direct torque control strategy for doubly fed induction machine for torque and flux ripple minimization. In: Ben Salem, F. (Ed.), Direct Torque Control Strategies of Electrical Machines. IntechOpen. https://doi.org/10.5772/intechopen.89979.
Wadood, A., et al., 2018. An optimized protection coordination scheme for the optimal coordination of overcurrent relays using a nature-inspired root tree algorithm. Appl. Sci. 8, 1664. https://doi.org/10.3390/app8091664.
Wang, F., Zhang, Z., Mei, X., Rodríguez, J., Kennel, R., 2018. Advanced control strategies of induction machine: field oriented control, direct torque control and model predictive control. Energies 11 (1). https://doi.org/10.3390/en11010120. Art. no. 1.
Wang, L., Luo, Y., Yan, H., 2023. Ant colony optimization-based adjusted PID parameters: a proposed method. PeerJ Computer Science 9. https://doi.org/10.7717/peerj-cs.1660.
Whitley, D., 1994. A genetic algorithm tutorial. Stat. Comput. 4 (2). https://doi.org/10.1007/BF00175354.
Zaid, M.M., Ro, J.-S., 2019. Switch ladder modified H-bridge multilevel inverter with novel pulse width modulation technique. IEEE Access 7, 102073–102086. https://doi.org/10.1109/ACCESS.2019.2930720.
Zamfirache, I.A., Precup, R.-E., Roman, R.-C., Petriu, E.M., 2022. Reinforcement Learning-based control using Q-learning and gravitational search algorithm with experimental validation on a nonlinear servo system. Inf. Sci. 583, 99–120. https://doi.org/10.1016/j.ins.2021.10.070.
Zarean Shahraki, N., Kazemi, H., 2012. A New DTC Control Method of Doubly Fed Induction Generator for Wind Turbine. https://doi.org/10.1109/ICREDG.2012.6190471.
Zeinaly, Y., Geyer, T., Egardt, B., 2011. Trajectory extension methods for model predictive direct torque control. In: 2011 Twenty-Sixth Annual IEEE Applied Power Electronics Conference and Exposition (APEC), pp. 1667–1674. https://doi.org/10.1109/APEC.2011.5744819.
Zemmit, A., Messalti, S., Harrag, A., 2016. 'Innovative Improved Direct Torque Control of Doubly Fed Induction Machine (DFIM) Using Artificial Neural Network (ANN-DTC)', vol. 11, 16.
Zemmit, A., Messalti, S., Harrag, A., 2018. A new improved DTC of doubly fed induction machine using GA-based PI controller. Ain Shams Eng. J. 9 (4), 1877–1885. https://doi.org/10.1016/j.asej.2016.10.011.
Zhang, Y., Li, Z., Wang, T., Hu, J., Zhu, J., 2011. Predictive direct torque and flux control of doubly fed induction generator with switching frequency reduction for wind energy applications. In: 2011 International Conference on Electrical Machines and Systems. IEEE, Beijing, China, pp. 1–6. https://doi.org/10.1109/ICEMS.2011.6073721.
A novel optimal PID controller autotuning design based on the SLP algorithm - pongfai - 2020 - expert Systems - wiley Online Library [Online]. Available: https://onlinelibrary.wiley.com/doi/10.1111/exsy.12489. (Accessed 8 July 2024).
A novel rooted tree optimization apply in the high order sliding mode control using super-twisting algorithm based on DTC scheme for DFIG - ScienceDirect [Online]. Available: https://www.sciencedirect.com/science/article/abs/pii/S0142061518305635. (Accessed 8 July 2024).
A numerical algorithm for stability testing of fractional delay systems - ScienceDirect [Online]. Available: https://www.sciencedirect.com/science/article/abs/pii/S0005109806000586. (Accessed 8 July 2024).
A review on Direct Torque Control (DTC) of induction motor: with applications of fuzzy. In: IEEE Conference Publication, 2024. IEEE Xplore' [Online]. Available: https://ieeexplore.ieee.org/abstract/document/7755579.
An Enhanced ACO and PSO Based Fault Identification and Rectification Approaches for FACTS Devices - Devasahayam - 2017 - International Transactions on Electrical Energy Systems, 2024. Wiley Online Library [Online]. Available: https://onlinelibrary.wiley.com/doi/abs/10.1002/etep.2344.
Comparison of Proportional-Integral (P-I) and Integral-Proportional (I-P) controllers for speed control in vector controlled induction Motor drive. In: IEEE Conference Publication, 2024. IEEE Xplore' [Online]. Available: https://ieeexplore.ieee.org/document/6508089.
Comparison of the error-integral performance indexes in a GA-tuned PID controlling system of a PWR-type nuclear reactor point-kinetics model - ScienceDirect [Online]. Available: https://www.sciencedirect.com/science/article/abs/pii/S0149197020303504?via%3Dihub. (Accessed 7 July 2024).
Controller design for direct torque controlled space vector modulated (DTC-SVM) induction motor drives. In: IEEE Conference Publication, 2024. IEEE Xplore [Online]. Available: https://ieeexplore.ieee.org/document/1529052.
Direct torque control versus indirect field-oriented control of induction motors for electric vehicle applications - ScienceDirect [Online]. Available: https://www.sciencedirect.com/science/article/pii/S2215098619326734. (Accessed 31 May 2024).
Energies | free full-text | A new robust direct torque control based on a genetic algorithm for a doubly-fed induction motor: experimental validation [Online]. Available: https://www.mdpi.com/1996-1073/15/15/5384. (Accessed 8 July 2024).
Five-phase induction motor DTC-SVM scheme with PI controller and ANN controller - ScienceDirect [Online]. Available: https://www.sciencedirect.com/science/article/pii/S221201731630531X. (Accessed 6 July 2024).
Improving the search pattern of Rooted Tree Optimisation algorithm to solve complex problems - ScienceDirect [Online]. Available: https://www.sciencedirect.com/science/article/pii/S2666720721000096?via%3Dihub. (Accessed 30 June 2024).
M. Mossa and S. Bolognani, Model Predictive Direct Torque Control, Doubly Fed Induction Motor as a Case Study, Chapter 6.
Model predictive control | SpringerLink [Online]. Available: https://link.springer.com/book/10.1007/978-0-85729-398-5. (Accessed 9 July 2024).
Modified vector controlled DFIG wind energy system based on barrier function adaptive sliding mode control | Protection and Control of Modern Power Systems | Full Text [Online]. Available: https://pcmp.springeropen.com/articles/10.1186/s41601-019-0119-3.
Optimization of PID Tuning Using Genetic Algorithm, 2021. Journal of Applied Science & Process Engineering [Online]. Available: https://publisher.unimas.my/ojs/index.php/JASPE/article/view/168. (Accessed 26 March 2024).
Particle swarm optimization (PSO) and ant colony optimization (ACO) for optimizing PID parameters on autonomous underwater vehicle (AUV) control system - IOPscience [Online]. Available: https://iopscience.iop.org/article/10.1088/1742-6596/1211/1/012039. (Accessed 8 July 2024).
[PDF] model predictive direct torque control—Part I: concept, algorithm, and analysis | semantic scholar [Online]. Available: https://www.semanticscholar.org/paper/Model-Predictive-Direct-Torque-Control%E2%80%94Part-I%3A-and-Geyer-Papafotiou/113decaa3ab70046a6b26969aad577f9190b6699.
Performance evaluation of DTC, MPDTC and DDTC methods for drive of a SPMSM | semantic scholar [Online]. Available: https://www.semanticscholar.org/paper/Performance-Evaluation-of-DTC%2C-MPDTC-and-DDTC-for-a-Ezeonwumelu-Shinde/b682c81a1ed15795a09e2b774e48decd1b165d22.
Sliding mode based DTC of three-level inverter fed induction motor using switching vector table | Semantic Scholar [Online]. Available: https://www.semanticscholar.org/paper/Sliding-mode-based-DTC-of-three-level-inverter-fed-Ahammad-Beig/2540219316cf4ff934e0a3665ff9dba6be943ccc.
Sliding Mode Control Design Principles and Applications to Electric Drives | IEEE Journals & Magazine, 2024. IEEE Xplore [Online]. Available: https://ieeexplore.ieee.org/document/184818.
Sustainability | free full-text | multiobjective genetic algorithm-based optimization of PID controller parameters for fuel cell voltage and fuel utilization [Online]. Available: https://www.mdpi.com/2071-1050/11/12/3290. (Accessed 7 July 2024).
Systems | free full-text | combining a genetic algorithm and a fuzzy system to optimize user centricity in autonomous vehicle concept development [Online]. Available: https://www.mdpi.com/2079-8954/9/2/25. (Accessed 7 July 2024).
Tuning PID controller for inverted pendulum using genetic algorithm | SpringerLink [Online]. Available: https://link.springer.com/chapter/10.1007/978-981-10-4762-6_38. (Accessed 8 July 2024).